AD-A187 576 FINITE ELEMENT MODELLING OF LARGE PLASTIC STRAINS IN A ROLLING CONTACT ME..(U) PENNSYLVANIA STATE UNIV STATE COLLEGE APPLIED RESEARCH LAB S N KHER ET AL. AUG 87 TR-87-004 F/G 20/11 NL

1/2

UNCLASSIFIED

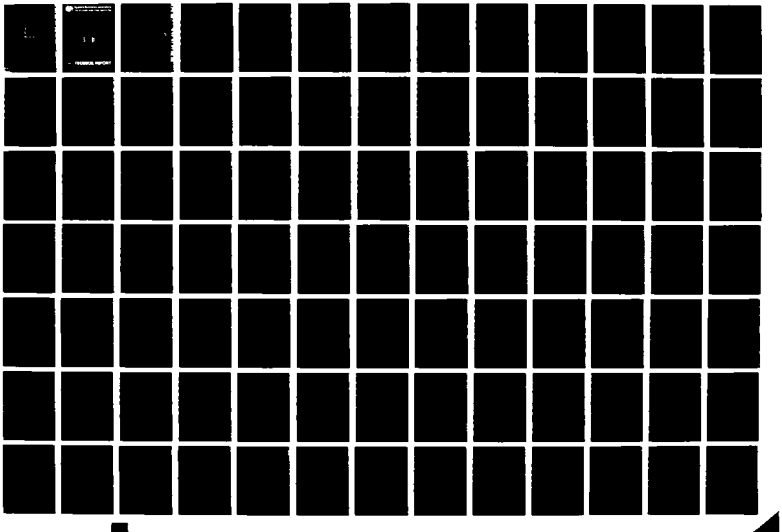

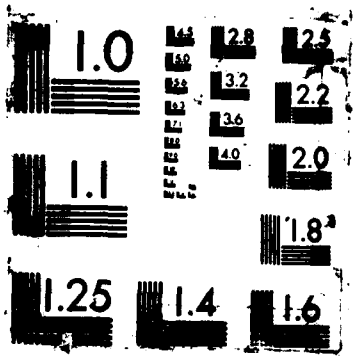
1.0
1.1
1.25
1.4
1.6
1.8
2.0
2.2
2.5
2.8
3.2
3.6
4.0

Applied Research Laboratory
The Pennsylvania State University

(12)

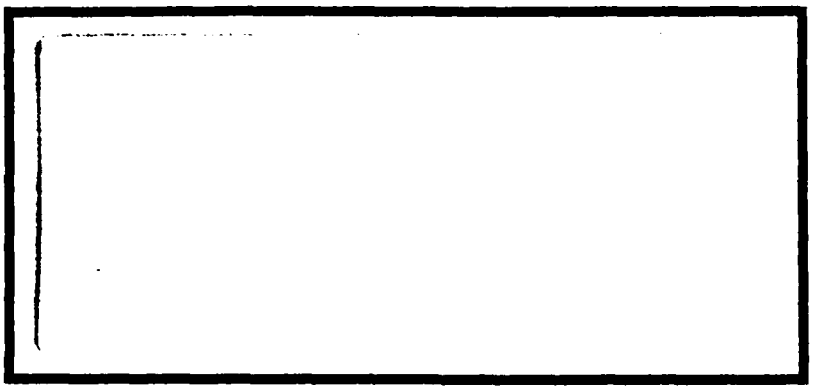

TECHNICAL REPORT

The Pennsylvania State University
APPLIED RESEARCH LABORATORY
P. O. Box 30
State College, PA 16804

(12)

FINITE ELEMENT MODELLING OF LARGE PLASTIC STRAINS IN A ROLLING CONTACT METAL FORMING PROCESS

by

S. N. Kher and M. F. Amateau

Technical Report No. TR-87-004
August 1987

Supported by :
Naval Sea Systems Command

L. R. Hettche, Director
Applied Research Laboratory

Approved for public release; distribution unlimited

Unclassified
SECURITY CLASSIFICATION OF THIS PAGE

REPORT DOCUMENTATION PAGE

1a. REPORT SECURITY CLASSIFICATION Unclassified	1b. RESTRICTIVE MARKINGS
2a. SECURITY CLASSIFICATION AUTHORITY	3. DISTRIBUTION/AVAILABILITY OF REPORT Unlimited
2b. DECLASSIFICATION/DOWNGRADING SCHEDULE	
4 PERFORMING ORGANIZATION REPORT NUMBER(S)	5. MONITORING ORGANIZATION REPORT NUMBER(S)
6a NAME OF PERFORMING ORGANIZATION Applied Research Laboratory Penn State University 6b. OFFICE SYMBOL (*If applicable*) ARL	7a. NAME OF MONITORING ORGANIZATION Naval Sea Systems Command Department of the Navy
6c ADDRESS (*City, State, and ZIP Code*) P.O. Box 30 State College, PA 16804	7b. ADDRESS (*City, State, and ZIP Code*) Washington, DC 20362
8a. NAME OF FUNDING/SPONSORING ORGANIZATION Naval Sea Systems Command 8b. OFFICE SYMBOL (*If applicable*) NAVSEA	9. PROCUREMENT INSTRUMENT IDENTIFICATION NUMBER
8c ADDRESS (*City, State, and ZIP Code*) Department of the Navy Washington, DC 20362	10. SOURCE OF FUNDING NUMBERS PROGRAM ELEMENT NO. / PROJECT NO. / TASK NO. / WORK UNIT ACCESSION NO

11 TITLE (*Include Security Classification*)
Finite Element Modelling of Large Plastic Strains in a Rolling Contact Metal Forming Process

12 PERSONAL AUTHOR(S)
S. N. Kher and M. F. Amateau

13a TYPE OF REPORT	13b TIME COVERED	14. DATE OF REPORT (*Year, Month, Day*)	15. PAGE COUNT
Ph.D. Thesis	FROM _____ TO _____	August 1987	163

16 SUPPLEMENTARY NOTATION

17 COSATI CODES			18 SUBJECT TERMS (*Continue on reverse if necessary and identify by block number*)
FIELD	GROUP	SUB-GROUP	Ausrolling, Numerical Modelling, Finite Element Analysis, Plastic Strain

19 ABSTRACT (*Continue on reverse if necessary and identify by block number*)

A numerical model to simulate the deformations in gear teeth subjected to rolling loads as in the ausrolling process has been developed. Ausrolling involves applying rolling loads to the gear when it is in the metastable austenitic state. A model of the process must consider material, geometric and surface non-linearities as well as changes in temperature and material properties with time and rolling loads in three dimensions. Only some of these requirements, namely, the elastic-

20 DISTRIBUTION/AVAILABILITY OF ABSTRACT	21 ABSTRACT SECURITY CLASSIFICATION	
☒ UNCLASSIFIED/UNLIMITED ☐ SAME AS RPT ☐ DTIC USERS	Unclassified	
22a NAME OF RESPONSIBLE INDIVIDUAL	22b TELEPHONE (*Include Area Code*) 814-865-6344	22c OFFICE SYMBOL

DD FORM 1473, 84 MAR 83 APR edition may be used until exhausted
All other editions are obsolete

SECURITY CLASSIFICATION OF THIS PAGE

cont'd

plastic flow; geometric non-linearities due to large deformations; frictional contact conditions at the die-workpiece interface; and the travelling loads due to rolling, have been considered here to be of primary importance. The objective of this thesis is, accordingly, to satisfactorily establish the forementioned features in the non-linear finite element analysis program (NOFEAP). The theoretical aspects of the non-linear formulations have beer briefly described and the model of the rolling process has been outlined here. The implemented non-linear formulations have been compared, individually and in various combinations, with existing analytical, numerical and experimental solutions. Since no such results are availiabie in the literature to compare the response of the rolling model, several experiments have been conducted on aluminum 6061 disks. The experimental results and their numerical counterparts have been included with discussion on the similarities and differences in the two. Finally, the applicability of NOFEAP to modelling the deformations in gear rolling has been demonstrated by modelling the deformations in the approach and the trailing sides of a gear tooth when rolled against a hard die. These deformation plots and stress contours are also given in this thesis.

Keywords:

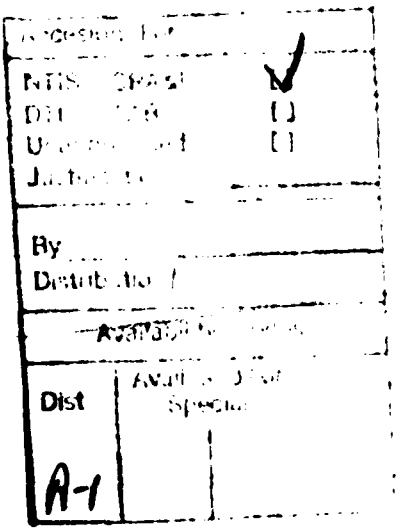

ABSTRACT

A numerical model to simulate the deformations in gear teeth subjected to rolling loads as in the ausrolling process has been developed. Ausrolling involves applying rolling loads to the gear when it is in the metastable austenitic state. A model of the process must consider material, geometric and surface non-linearities as well as changes in temperature and material properties with time and rolling loads in three dimensions. Only some of these requirements, namely, the elastic-plastic flow; geometric non-linearities due to large deformations; frictional contact conditions at the die-workpiece interface; and the travelling loads due to rolling, have been considered here to be of primary importance. The objective of this thesis is, accordingly, to satisfactorily establish the forementioned features in the non-linear finite element analysis program (NOFEAP). The theoretical aspects of the non-linear formulations have been briefly described and the model of the rolling process has been outlined here. The implemented non-linear formulations have been compared, individually and in various combinations, with existing analytical, numerical and experimental solutions. Since no such results are available in the literature to compare the response of the rolling model, several experiments have been conducted on aluminum 6061 disks. The experimental results and their numerical counterparts have been included with discussion on the similarities and differences in the two. Finally, the applicability of NOFEAP to modelling the deformations in gear rolling has been demonstrated by modelling the deformations in the approach and the trailing sides of a gear tooth when rolled against a hard die. These deformation plots and stress contours are also given in this thesis.

TABLE OF CONTENTS

TABLE OF CONTENTS (continued)

LIST OF FIGURES

LIST OF FIGURES (continued)

LIST OF FIGURES (continued)

LIST OF FIGURES (continued)

LIST OF FIGURES (continued)

NOMENCLATURE

The following symbols have been used in tensor notation in this thesis.

a	flow vector
A	a constant
D	elastic constitutive tensor
$d\_$	increment of quantity
dt	increment of time
D^T	transpose of D
D^{-1}	inverse of constitutive matrix
D_{ep}	elastic-plastic constitutive matrix
e_{ij}	components of linear strain increments
E_{ij}	components of engineering strain tensor
f	yield function
f_i^b	components of external body forces
f_i^s	components of external surface forces
F	alternate definition of yield function, or external loads
ΔF	test load increment
H'	slope of hardening curve
J_2'	second deviatoric stress invariant
K	hardening function, or stiffness matrix
l_i	components of relative displacements
n	subscript denoting normal direction
Q	plastic potential
$\Delta Q'$	incremental contact forces or relative displacements

NOMENCLATURE (Continued)

R	reactions at contact surface, or radius of gears
$\mathcal{R}$	external virtual work
S_{ij}	components of 2^{nd} Piola Kirchoff stresses
t	subscript denoting tangential direction
u_i	components of displacement vector
V	volume of the body
x_i	value of i^{th} coordinate
X	determinant of deformation gradient
α_k	load increment ratio
β	a scaling parameter
Δ_	increment in quantity
δ_	variation in a quantity
δ_c	initial gaps between nodal pairs
δ_n	normal gap
ϵ	engineering strain
ϵ_{ij}	components of Green-Lagrange strain tensor
η_{ij}	components of non-linear strain increments
θ	angle of rotation
κ	hardening parameter
λ	plastic multiplier
μ	coefficient of static friction
σ	engineering stress

NOMENCLATURE (Continued)

σ_{ij}	components of engineering stress tensor
σ^t_{ij}	components of Truesdell stress tensor
τ_{ij}	components of Cauchy stress tensor
$\mathring{\tau}_{ij}$	components of Jaumann rate of Cauchy stresses
Ω	speed of rotation of gears
Ω_{ij}	components of spin tensor
∂_-	partial of quantity
$*$	used to denote multiplication

ACKNOWLEDGEMENTS

I am sincerely grateful to Professor Maurice F. Amateau for giving me the opportunity to work on this project. It has truly been a fruitful and rewarding experience. His encouragement and advice through this research have been invaluable and I thank him for the same. I am indebted to Professor Nicholas J. Salamon for the discussions on the formulation aspects of the project which frequently have led to the successful solution of the obstructing problems.

I wish to thank my committee members, Professors Vernon H. Neubert, Jaan Kiusalaas, Richard A. Queeney and Goong Chen. Thanks are also due to various members of the Engineering Materials Department at the Applied Research Laboratory, especially to Mr. Dwayne Kidwell, Mr. Charles Stull and Mr. Michael Anderson, for their suggestions and help in conducting the experimental analysis and to Mr. William Saylor for performing these tests. I deeply appreciate the intangible contributions of my friends and family towards a successful completion of this project.

This work has been supported by the Naval Sea Systems Command and the Applied Research Laboratory Exploratory and Foundational Research Program. Their financial support is gratefully acknowledged.

Chapter 1
INTRODUCTION

A low temperature thermomechanical process is being developed by the author and coworkers for finishing precision machine elements. This process is being applied to the finishing of gears by working the surface layers of the teeth by a combination of rolling, swaging and shearing operations. This process is referred to as "ausrolling" and results in a significant saving in time and processing costs over conventional finishing operation such as grinding. Ausrolling also results in a fine grained martensitic structure and high compressive stresses in the carburized surface which improves the fatigue life of the machine elements. One key to the success of ausrolling is the ability to reliably and accurately predict the finished dimensions of the machine components. Such an estimate can be obtained by numerically analyzing the process. This thesis presents a non-linear finite element model used to study the ausrolling process which is described next.

1.1 The Ausrolling Process

Most mechanical systems contain a few precision machine elements which must possess superior mechanical properties to improve performance, and they must be precisely finished to minimize noise and vibration. These requirements are satisfied by a number of manufacturing steps, as shown in Figure 1.1. Unfortunately, some of these steps may annul one or more of the desirable characteristics introduced by the preceding operations. Moreover, as the specifications for the mechanical properties and dimensional tolerances become more stringent, the cost of processing can be significantly higher. These detrimental aspects of the conventional finishing processes can be neutralized if some of the operations can be

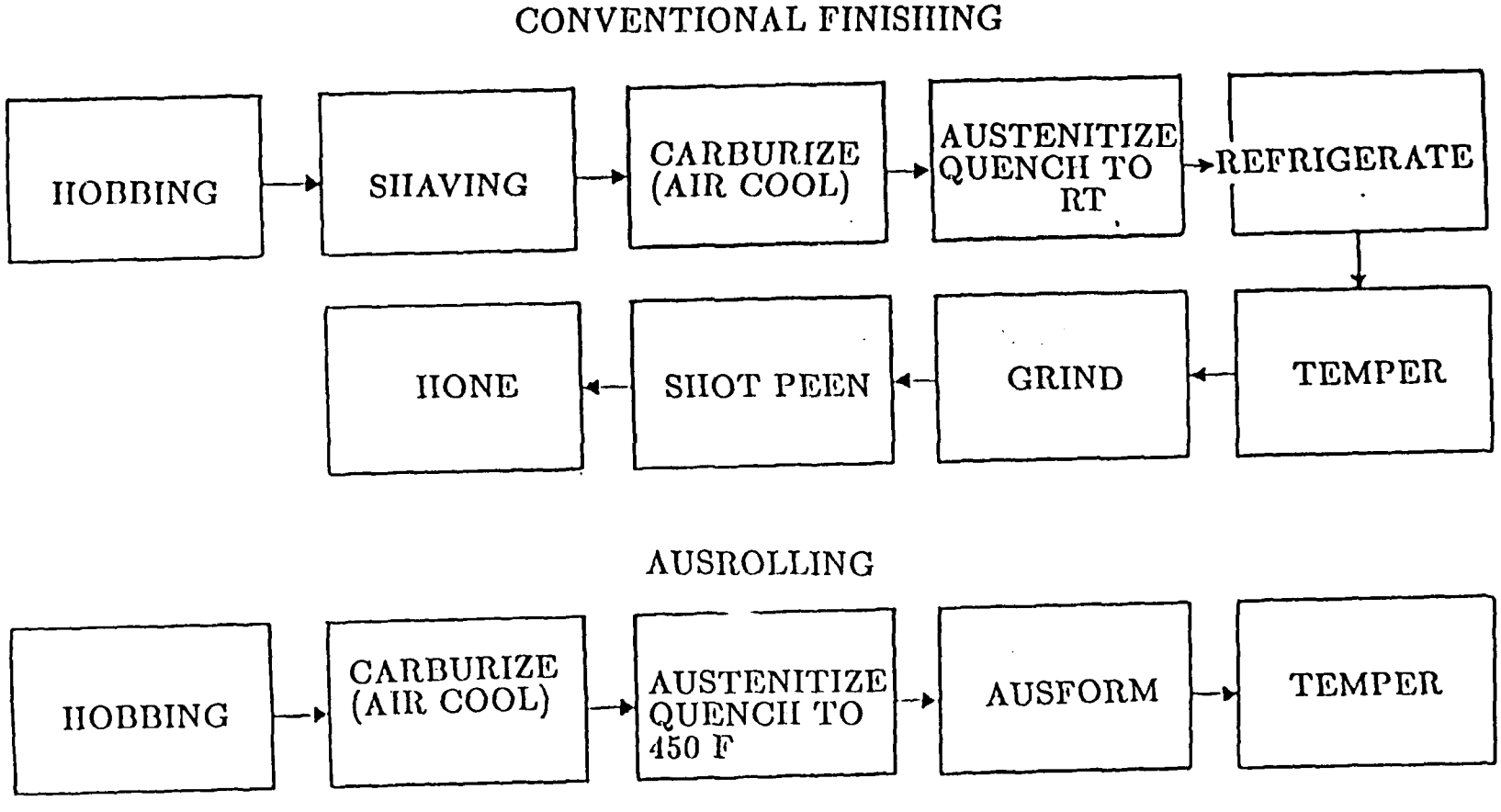

Figure 1.1 STEPS IN CONVENTIONAL FINISHING AND AUSROLLING PROCESSES

merged into a single process. Such a combination of steps has been accomplished in the ausrolling process (Figure 1.1).

Since the plastic deformations are introduced by ausrolling in the machine component while the component is in metastable austinitic state, the time-temperature-transformation (TTT) diagram of the material plays an important role in the operation. There are two essential requirements of a steel to be effective in an ausforming operation: presence of some carbide forming elements and a deep austenite bay region in the TTT curve. The carburized 9310 steel (1.0C-1.2Cr-3.25Ni-0.13Mo), which has been successfully surface-ausformed, follows the TTT-diagram shown in Figure 1.2. The mechanical system used for ausforming is described next.

Ausrolling, applied to gears [1], is a modified form of the conventional gear rolling operation, where the die gear (A) is powered and drives the softer workpiece gear (B), as shown in Figure 1.3. The workpiece, henceforth referred to as the gear, is fed into the die by a combination of horizontal and vertical movements. This operation, where the gear is simultaneously worked along the circumferential surface and the thickness, is called the swage-rolling process. The slide (C) on which the gear is mounted and the rear column (D) are connected to electrohydraulically operated actuators. The vertical feed is achieved by lowering the front ram, thus moving the gear across the die. The horizontal feed is obtained by translating the vertical motion of the rear ram into a horizontal motion by the use of a 40:1 tapered column (D) between the rear plate (E) and a block (F) wedged against the middle plate (G). An indexing gear (H) may be used to enforce pure rolling at desired radius and to assure smooth entry into the die. The whole assembly is immersed into a hot oil tank to maintain temperature and lubrication conditions. The loading conditions range from pure rolling at the pitch-line to

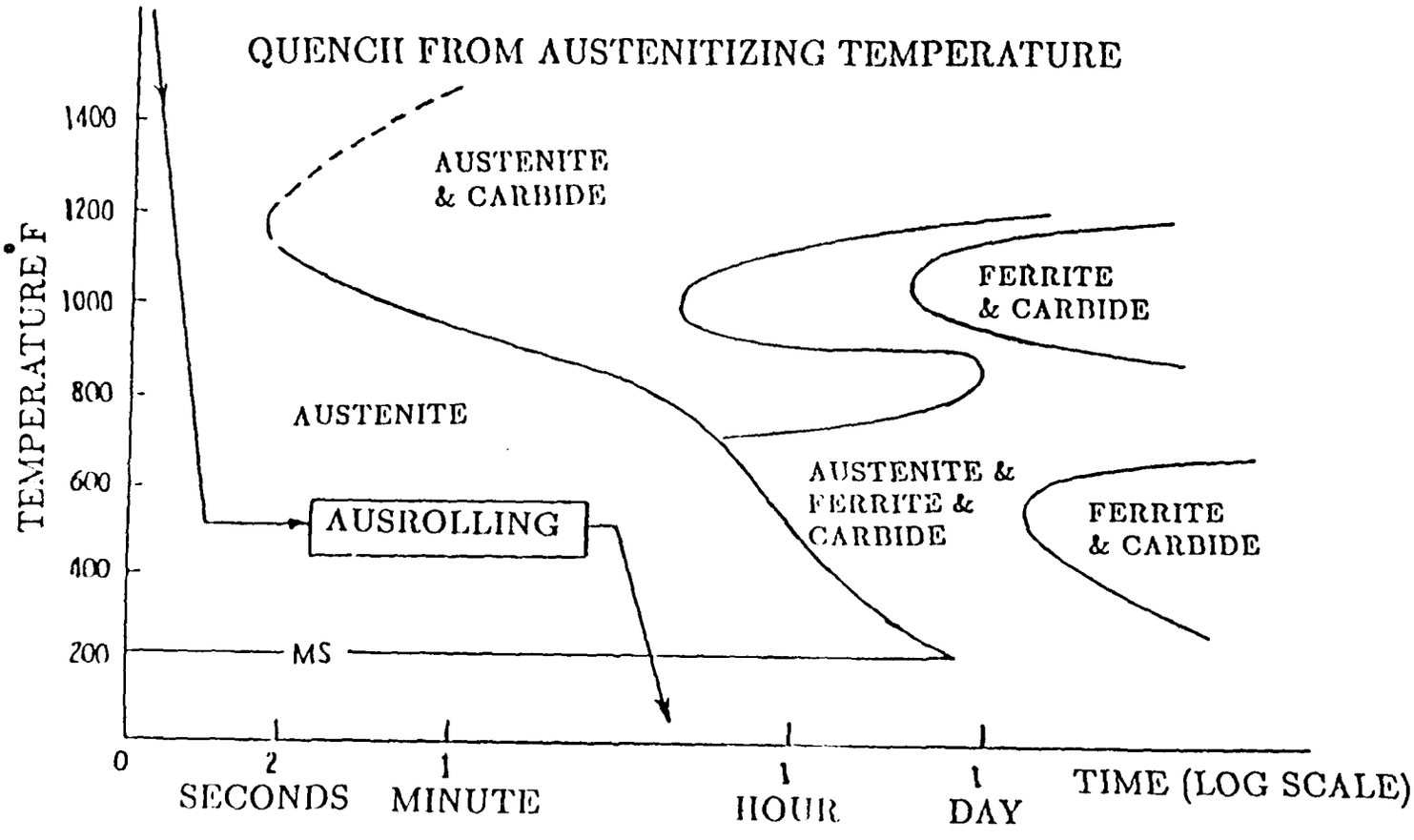

Figure 1.2 SCHEMATIC ILLUSTRATION OF TTT-DIAGRAM FOR AUSROLLING

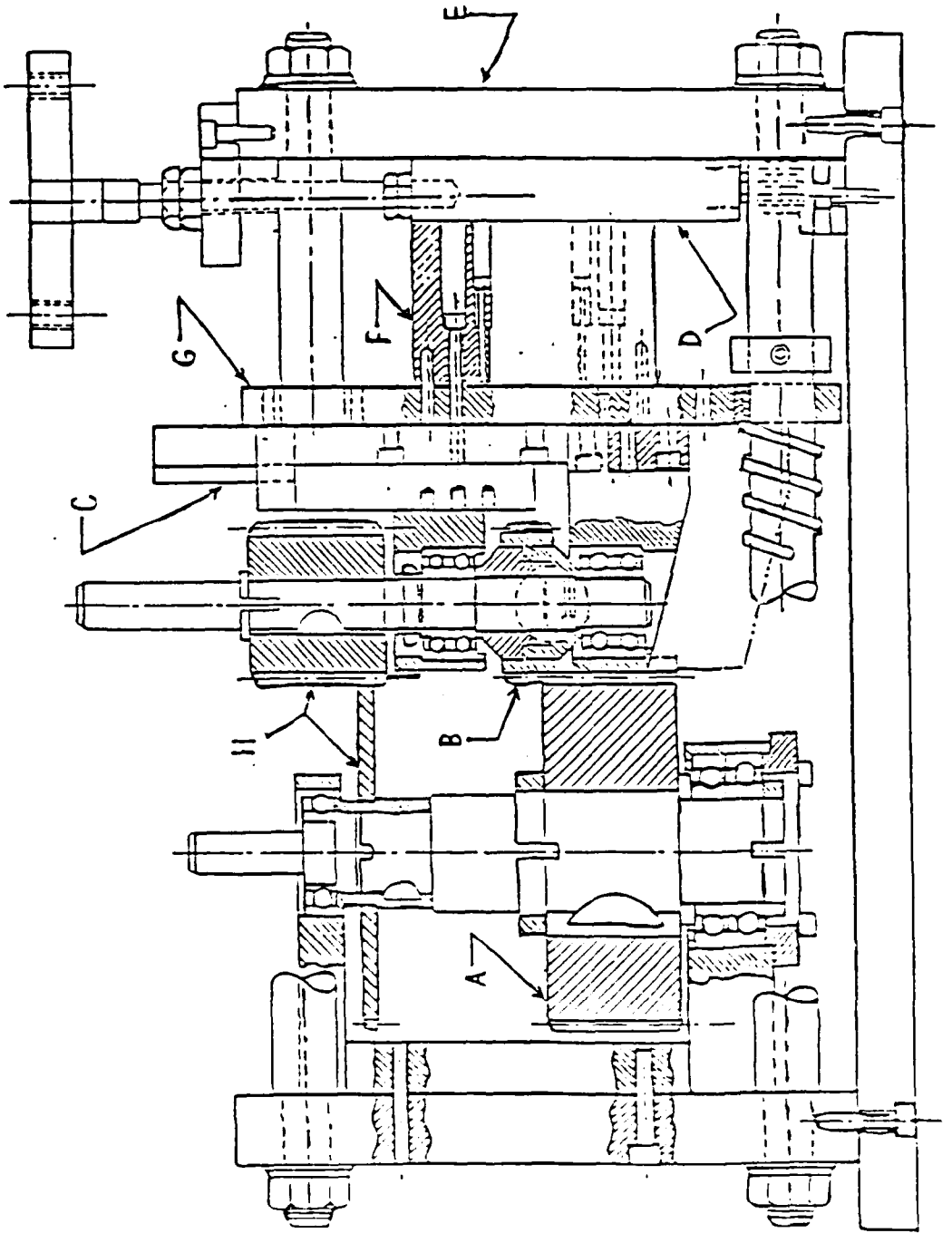

Figure 1.3 SCHEMATIC DIAGRAM OF BASIC FIXTURING FOR AUSROLLING

combined rolling and sliding away from the pitch-line. Thus the state of stress changes radically along the active profile of the involute gear surface. Material on the approach side of the workpiece gear is displaced toward the pitch-line while it is displaced in the opposite direction on the trailing side as shown in Figure 1.4.

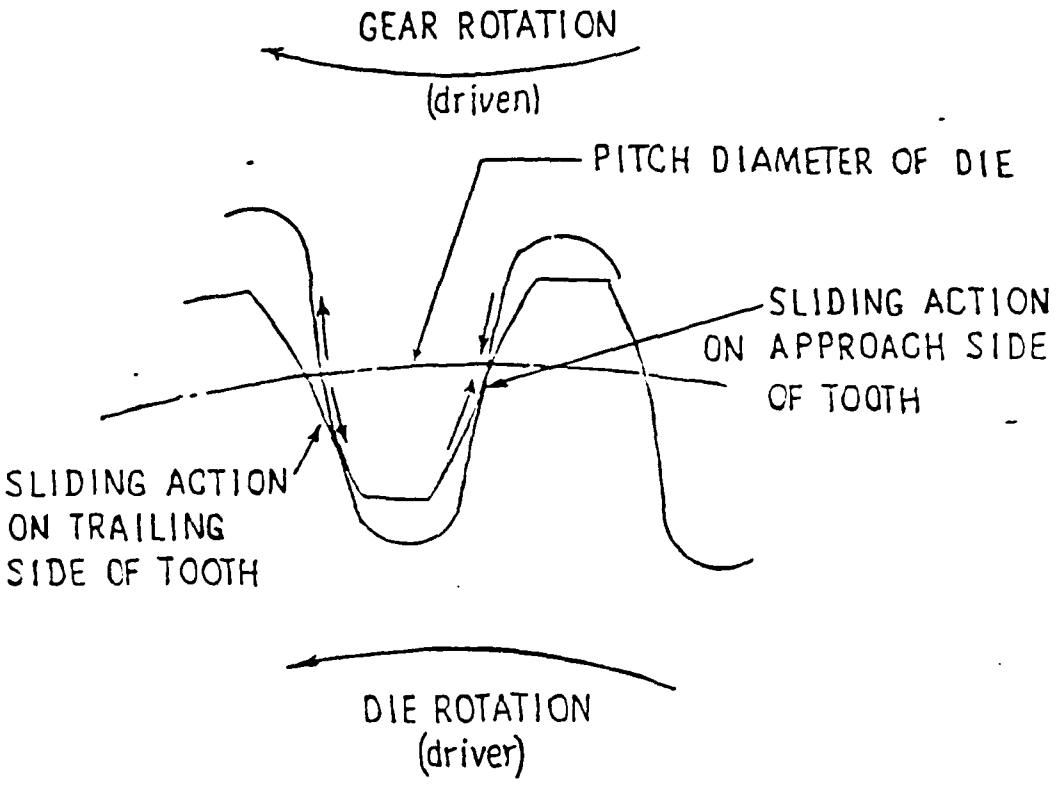

Figure 1.4 RELATIVE SLIDING BETWEEN GEAR TEETH IN MESH

In addition to stress gradients on the surface of the tooth being worked there are also compositional and thermal gradients in the direction normal to the surface. The compositional gradients are due to the carburized condition while the thermal gradients are a result of the quenching to the metastable austenitic state just prior to and during working. Significant dynamic-hardening is also characteristic of the process since working takes place below the recrystallization temperature and under conditions that promote rapid dislocation network pinning. When this

process is applied to spur gears a specially tapered lead geometry is provided in the die (Figure 1.5) to produce a swaging action on the teeth during forming. The lead in the die being used in the experiments also contains a hollow section to produce a crown contour in the gear.

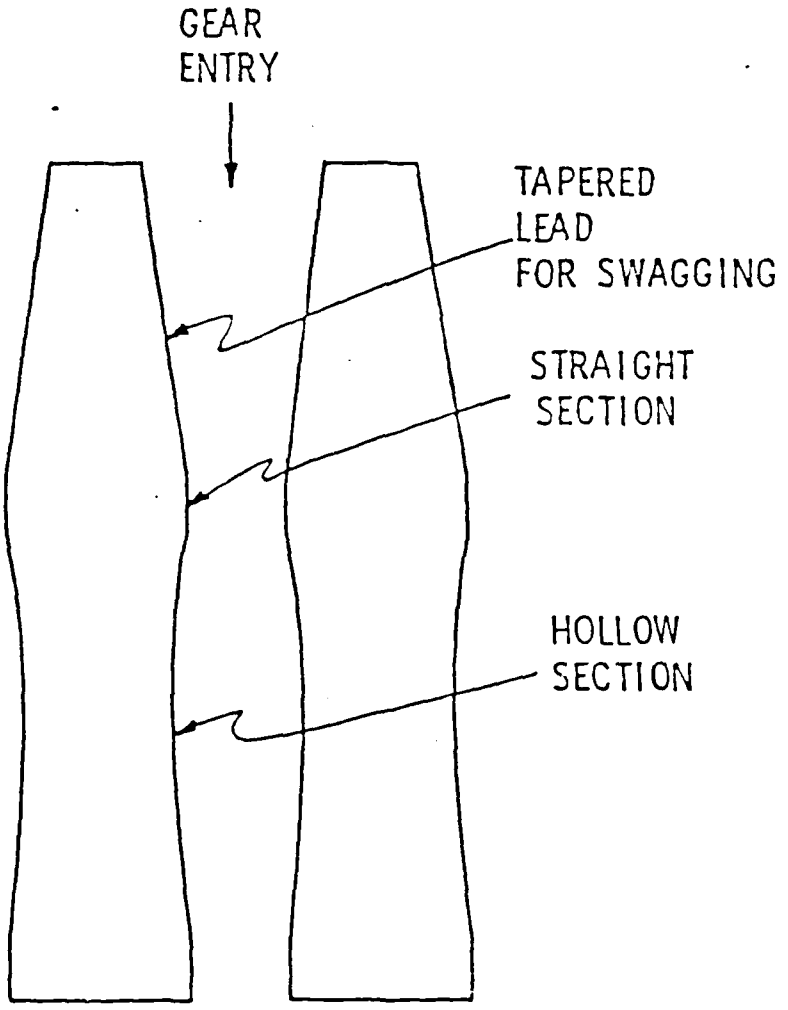

Figure 1.5 LEAD PROFILE FOR GEAR DIE

1.2 Scope and Outline of the Thesis

A numerical model which adequately simulates forming processes must account for material, geometric and surface non-linearities depending on the application. Formulations of these non-linearities abound in the literature [2-4]. The objective of the thesis is to combine these non-linearities in one algorithm so that the resulting model can be used to study the ausrolling process.

Important steps of the non-linear formulations are described in Chapter 2. Each formulation is preceded by a review of the available literature on the subject. Material non-linearities are modelled by an elastic-plastic formulation [5]. Geometric non-linearities are formulated by using the total and the updated Lagrangian formulations [3]. The surface non-linearities are incorporated into the model by using a frictional contact formulation [6]. The transformation of these formulations into the finite element matrix equations [7] and a brief description of the non-linear finite element analysis program (NOFEAP) [8] which combines these models into a computer code are also presented in Chapter 2. The implementation of each of these non-linear formulations has been verified by solving a number of benchmark problems using NOFEAP. The results of these verification excercises are presented in Chapter 3.

The most unique feature of the ausrolling process is that the deformation in the workpiece is introduced by rolling the gear against a hard die. The rolling process has not been widely modelled in existing finite element codes. Mori [9] has used rigid-plastic finite element method to study the rolling of sheet metal by approximating the tractions at the roll-strip interface and also the velocity of the roll relative to the strip at its neutral region. Elastic-plastic rolling contact has been studied by Bhargava [10,11] who simulates the rolling conditions by

translating a semi-elliptic Hertzian pressure distribution along the surface of a flat workpiece. These methods which assume a pressure distribution have severe drawbacks when applied to rolling cylinders or gears. A model of the rolling process developed using geometric and kinematic considerations is used in NOFEAP. The details of this model and its application to the study of rolling cylinders and gear teeth are presented in Chapter 4. The conclusions of this thesis are discussed in Chapter 5.

1.3 Review of Literature

There is a vast amount of literature on non-linear finite element analysis. For the sake of organized presentation the literature review is divided into various sections. This section only summarizes the research on combined non-linear formulations with special emphasis on applications to metal forming processes. The literature dealing with specific non-linearities is covered in Chapter 2 in discussions of these non-linearities.

The rigid-plastic finite element method (FEM) proposed by Lee and Kobayashi [12] has been popularly used to model several metal forming processes. This method uses a Lagrange multiplier to enforce the incompressibility condition in pure plastic flow. The solution scheme in the method is based on using an initial guess of the velocity vector with small perturbation in the velocity field in subsequent iterations to obtain the solution as a function of time. The rate of convergence of this solution, therefore, depends on the proximity of the initial guess to the exact solution. The rigid-plastic model is perhaps locally valid for large plastic flow where the solution is only applied to regions with unrestricted plastic flow. Keeping these characteristics of the rigid-plastic method in mind, the application of the method to modelling processes such as cold forging [13,14], extrusion [15], strip-rolling [9], and ring-compression [16] is quite acceptable.

The rigid-viscoplastic finite element method originated from the rigid-plastic method due to the work of Oh who later used it to model forming processes with dies of general shape [17] and for hot-forging of an alloyed engine disk [18].

Although finite strains have been used in rigid-plastic (or viscoplastic) analysis [19,20], the large strain formulations have been more commonly used with the elastic-plastic (or viscoplastic) material model by a number of researchers. Prominent among these are the works of Wifi [21] and Yamada [22,23]. The elasto-plastic FEM has been compared to the rigid-plastic FEM by Bõer [24] for upsetting of cylinders. Interestingly, Bõer's solutions favor the rigid-plastic FEM for the 4-node isoparametric elements. However, the elastic-plastic FEM should not be condemned on this evidence alone, since the upsetting process predominantly produces areas of large plastic flow. Secondly, the 4-node element may not be the proper element to use in large strain applications, where the "4CST-element" (a rectangular element divided into four constant strain triangular elements by joining the nodes on the diagonals) has been shown to have a more accurate response [25,26].

The next step towards a more accurate modelling of metal forming processes involves the representation of friction along the die-workpiece interface. Wifi [21] accounted for friction by assuming a fully sticking contact along the interface. Hartley [27] modelled the frictional loading condition by including a layer of interfacial elements. However, no definite criterion for establishing the properties of these elements is forwarded in the paper. More realistic models of the frictional contact conditions are used by Yamada [22] and Kikuchi [28]. The latter uses a microscopic definition of contact, similar to the one proposed by Fredriksson [29]. However, the parameters used in the microscopic model do not seem to have significant physical properties associated with them.

Thermal stresses have also been coupled with large plastic deformations by several authors to analyze forming processes such as upsetting and extrusion problems [30,31]. However, inspite of the extensive literature on analysis of forming processes, no paper presents a convenient large strain formulation with realistic representation of frictional contact in one package. This thesis uses a combination of conventional large deformation elastic-plastic formulation with a simple yet effective frictional contact model.

While most of the works mentioned previously have been oriented towards some industrial application, several authors have directed their attention to developing combined non-linear formulations capable of both analyzing metal forming processes and solving structural mechanics problems. Two popular approaches have emerged from the efforts of Lee [32] and Marcal [33]. Lee proposed the theory that finite strain components are non-linear expressions in the displacements and hence may not be additive in nature. His theory using multiplicative decomposition of the deformation gradient has been followed by Kleiber [34,35] among others. However, the additive decomposition of the strains into elastic and plastic parts has been more commonly used in literature and has been followed in this thesis. Following Marcal's formulation of geometric and material non-linearities, several other formulations have been forwarded. Among these formulations, the popular ones are due to Hibbit [36], Bathe [37], McMeeking [38], and Yamada [39]. These formulations are based on the Prandtl-Reuss equations [40] coupled to geometric non-linearities by either a Lagrangian or an Eulerian formulation using energetically conjugate stress and strain tensors. Relevent details of these formulations are given with references in Chapter 2.

The formulations mentioned in the preceding paragraphs can be used to model a number of metal forming processes, including the ausrolling process. However, the

unique features of the ausrolling process cannot be modelled by existing software packages. Hence, using the existing non-linear formulations as a starting block, a non-linear finite element analysis program (NOFEAP) has been developed by the author. All the characteristics of ausrolling have not been modelled in the program. This thesis describes the non-linear formulations and the model of the rolling process included in NOFEAP. Various benchmark and sample problems solved using NOFEAP are also included in the thesis.

Chapter 2

NON-LINEAR FORMULATIONS

As stated in the previous chapter, the ausrolling process has several characteristics which must be reflected in the numerical model. Keeping these characteristics in mind, the model must account for the following: (1) non-linear material behavior due to plastic flow; (2) non-linear geometric behavior due to large strains; (3) frictional contact conditions at the die-workpiece interface; (4) rolling, shearing and swaging operations; (5) temperature effects on stress distribution and material properties; and (6) three-dimensional analysis capability. Of these features, the first three features and a model of the rolling process have been implemented in the computer program NOFEAP. Shearing and swaging operations, which are part of the extension to three dimensions, and the thermal effects have not yet been included in the program.

This chapter describes the non-linear formulations used in the program. Description of each form of non-linearity is preceded by a review of the relevent literature on the subject. The finite element formulation of these non-linearities, to obtain the matrix equations, follows their description. A concise narrative of the NOFEAP computer program is presented at the end of this chapter.

2.1 Elastic-plastic Material Behavior

In the following sections, discussion of formulations and relevent references is restricted to the solution of plasticity problems by the finite element method. The obvious reason for such a limitation is that the earlier techniques, such as slip-line theory, mathematical and theoretical approaches, etc., have been completely overwhelmed by the numerical approach.

2.1.1 Review of Literature

Plasticity is one of the fields which has greatly benefited by the development of the finite element method. Initial approach to solving the plasticity problems used either the direct stiffness, or the initial strain method. The latter was initially formulated using the finite difference method, but resulted in an unstable solution. It was later adopted by Gallagher [41] to the finite element method. Simultaneously, the tangent stiffness method was being developed by Pope [42] and Marcal [2] to solve the elastic-plastic problem. This method is essentially a piece-wise solution to the non-linear problem. A summary of these early developments in numerical solution of elastic-plastic problems has been given by Marcal [43] and Yamada [44]. Yamada [45] also introduced a plastic stress-strain matrix obtained from the Prandtl-Reuss relations. The use of this and other matrix formulations has since been popular in the non-linear solutions. Zienkiewicz and coworkers [46-48] introduced the "initial stress" approach which includes a general development of the elastic-plastic constitutive tensor.

The formulation used in this thesis is similar to the one given by Zienkiewicz and is described by Owen [5]. The basic assumptions in the mathematical theory of plasticity and the associated expressions are outlined in the following sections. A complete treatment of the mathematics is given by Hill [49].

2.1.2 Mathematical Formulation

A general formulation of the elastic-plastic problem is given in this section. The problem of elastic-plastic flow is characterized by a yield criterion given as

$$f(\vec{\sigma}) = K(\kappa) \tag{1a}$$

or,

$$F(\vec{\sigma}, \kappa) = f(\vec{\sigma}) - K(\kappa) = 0 \tag{1b}$$

The right hand side of (1a) is a function of the work hardening parameter κ. The following derivation assumes isotropic expansion of the yield surface. Similar derivation for kinematic hardening has been given by Dogui [50], and for mixed hardening by Axelsson [51,52].

The elastic behavior of the material is represented by $f < K$, while for plastic flow $f = K$. At a plastic state, the incremental change in the yield function due to an increment in stress is given by the following:

$$df = \frac{\partial f}{\partial \vec{\sigma}} d\vec{\sigma} \tag{2}$$

Then if $df < 0$, elastic unloading occurs, and the stress point returns inside the yield surface; if $df = 0$, neutral loading occurs, and the stress point remains on the current yield surface; and if $df > 0$, plastic loading occurs with the stress point moving to the envelope of an expanding yield surface.

Following initial yielding of material, an increment of strain is assumed to be the sum of an elastic and a plastic increment.

$$d\vec{\epsilon} = d\vec{\epsilon^e} + d\vec{\epsilon^p} \tag{3}$$

A contrasting theory for large strains, based on the decomposition of the deformation gradient into elastic and plastic parts, has been forwarded by Lee [32,53]. A discussion of this controversy is also provided by Lee [54].

In order to derive a relationship between the plastic strains and the stress increments, the plastic strains are assumed to be proportional to the stress gradient of the plastic potential Q.

$$d\vec{\epsilon^p} = \lambda \frac{\partial Q}{\partial \vec{\sigma}} \tag{4}$$

Here λ is a proportionality constant called the plastic multiplier. Using the yield function, F, for the plastic potential leads to the associated theory of plasticity

which has been used in this derivation. In such a case, equation (4) can be rewritten as follows:

$$d\vec{\epsilon}^{P} = \lambda \frac{\partial F}{\partial \vec{\sigma}} \tag{5}$$

Defining the flow vector, $\vec{a}$, by

$$\vec{a} = \frac{\partial F}{\partial \vec{\sigma}} \tag{6}$$

a differential of equation (1b) can be written in the following form:

$$dF = \frac{\partial F}{\partial \vec{\sigma}} d\vec{\sigma} + \frac{\partial F}{\partial \kappa} d\kappa = 0 \tag{7a}$$

or,

$$\vec{a}^{T} d\vec{\sigma} - A\lambda = 0 \tag{7b}$$

Here A is defined by

$$A = -\frac{1}{\lambda} \frac{\partial F}{\partial \kappa} d\kappa \tag{8}$$

For the von Mises criterion, $f = J_2^{'}$ the second deviatoric stress invariant, and equation (5) reduces to the familiar Prandtl-Reuss relations. Since the elastic strain increments can be related to the stress increments using the constitutive matrix D, equation (3) can be rewritten as follows:

$$d\vec{\epsilon} = [D]^{-1} d\vec{\sigma} + \lambda \frac{\partial F}{\partial \vec{\sigma}} \tag{9}$$

Using (9) and (7b), the following expression for λ is obtained:

$$\lambda = \frac{\vec{a}^{T}[D] d\vec{\epsilon}}{A + \vec{a}^{T}[D]\vec{a}} \tag{10}$$

Substutiting (10) in (9) yields the complete elastic-plastic stress-strain relation as given next.

$$d\vec{\sigma} = [D_{ep}] d\vec{\epsilon} \tag{11}$$

with

$$[D_{ep}] = [D] - \frac{[D]\vec{a}\vec{a}^{T}[D]}{A + \vec{a}^{T}[D]\vec{a}} \tag{12}$$

For the work hardening hypothesis, the constant A is seen to be equal to the slope (H') of the hardening curve [5]. The elastic-plastic constitutive matrix, given by (12), has to be corrected for large rotations as explained in the following sections.

2.2 Geometrically Non-linear Behavior

The following sections review the formulations defining geometrically non-linear behavior and present the total and the updated Lagrangian formulations.

2.2.1 Review of Literature

Large displacement analysis was initially of interest to structural engineers in solving bending and buckling problems. Marcal [33] presented one of the first formulations combining the non-linear material behavior with large displacements. He has also given a historical development of the large displacement formulations. At the same time Lee [32] proposed that for finite elastic-plastic strains, the total strain may not be the sum of the elastic and plastic components due to the dilatational nature of the strains. However, the additive decomposition of the finite strains is still popularly used and has been followed here. Hibbit [36] introduced the load correction terms for the first time in large deformation analysis. Hofmeister [55] presented another version of this formulation and used it to analyze large displacements of structural components. Bathe [37] provided a complete description of the total Lagrangian formulation, which, similar to the approach of Marcal [33], uses the initial state as the reference configuration. Bathe also introduced the updated Lagrangian formulation which employs the last updated position as the reference. Many authors erroneously refer to the updated Lagrangian method as the Eulerian method. The subtle difference between the two is explained by Gadala [56]. Bathe used these formulations for static and dynamic, large deformation analyses of structures [57-59]. Osias [60] and McMeeking [38]

forwarded Eulerian formulations using relative velocities as independent variables and using rate equilibrium equations.

The rate formulation became quite popular in applications involving high speed operations, especially metal forming processes. Yamada [39] has presented a comprehensive description of the rate formulation with explanation of various stress-rates and the load correction matrices. This formulation has been used to analyze large flow processes such as extrusion [23,39], upsetting and stretch-forming [21,22]. Several authors have since used various formulations to analyze different metal forming processes [28,37,61].

Although a number of formulations have been forwarded [36,38,39,59,62,63], as yet there is no universal agreement on a best approach to solve a particular problem. A comprehensive survey of the available formulations is given by Gadala [56,64]. Of these numerous formulations, the total and updated Lagrangian formulations have been incorporated in the program NOFEAP. Salient features of these formulations are given in the next section, the details being available in the book written by Bathe [3].

2.2.2 Mathematical Formulations

In the analysis, the motion of a body is considered in a stationary Cartesian coordinate system, as shown in Fig 2.1. All kinematic and static variables are measured in this coordinate system. Tensor notation is followed in this section.

The basic equation to be solved is given by (13), which expresses the equilibrium of a general body at time $t + dt$.

$$\int_{{}^2V} {}^2\sigma_{ij} \quad \delta_2 E_{ij} \quad {}^2dV \quad = \quad {}^2\mathcal{R} \tag{13}$$

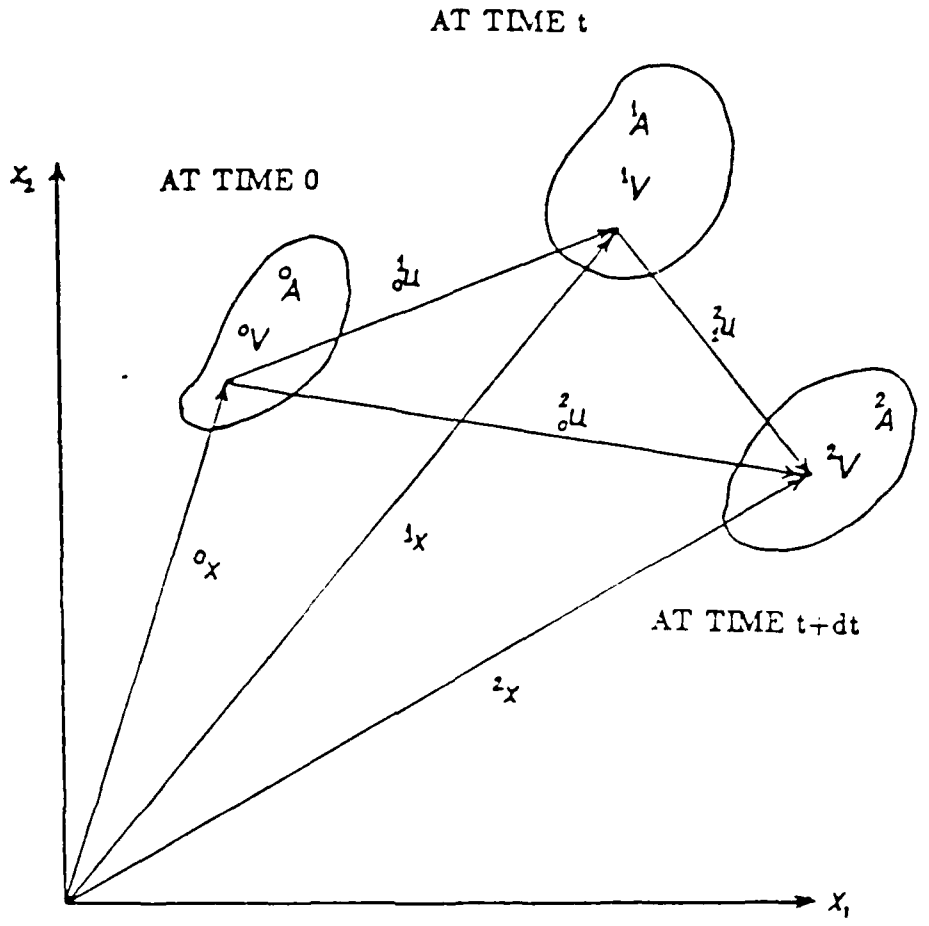

Figure 2.1 MOTION OF A BODY IN STATIONARY CARTESIAN SYSTEM

Here σ_{ij} and E_{ij} denote the engineering stress and strain tensors respectively. With the standard tensor notation, a left subscript is used to indicate the reference coordinate axes and a left superscript to denote the configuration of the body. If a quantity occurs in the same configuration in which it is also measured, the left subscript is dropped. Also, an incremental quantity is denoted by dropping the left superscript. For instance, the term ${}^{2}_{0}u_i$ indicates the i^{th} component of the displacement vector at time $t + dt$, measured with respect to the configuration at time 0; the quantity ${}^{1}u_i$ denotes the component at time t with respect to an updated configuration, also at time t; and ${}_{0}u_i$ indicates incremental displacement component at the current state measured with respect to the initial state.

The following sections describe the derivation of the final form of equilibrium equations for the total Lagrangian formulation. The equations for the updated Lagrangian formulation are presented without proof since these can be obtained simply by following the steps given in the next section.

2.2.2.1 Total Lagrangian Formulation

The stress and strain tensors selected for the total Lagrangian (TL) formulation are the 2^{nd} Piola-Kirchoff stress tensor, S_{ij}, and the Green-Lagrange strain tensor, ϵ_{ij}, respectively. The equilibrium equation (13) takes the following form using these tensors with the initial configuration used as the reference.

$$\int_{{}^{0}V} {}^{2}_{0}S_{ij} \quad \delta {}^{2}_{0}\epsilon_{ij} \quad {}^{0}dV \quad = \quad {}^{2}\mathcal{R} \tag{14}$$

In equation (14), the Green-Lagrange strains are defined by the following:

$${}^{1}_{0}\epsilon_{ij} = \frac{1}{2}\left[{}^{1}_{0}u_{i,j} + {}^{1}_{0}u_{j,i} + {}^{1}_{0}u_{k,i} * {}^{1}_{0}u_{k,j}\right] \tag{15}$$

where,

$${}^{1}_{0}u_{i,j} = \frac{\partial {}^{1}u_i}{\partial {}^{0}x_j} \tag{16}$$

The stresses and strains are decomposed as follows:

$$ {}^{2}_{0}S_{ij} = {}^{1}_{0}S_{ij} + {}_{0}S_{ij} \tag{17a} $$

and

$$ {}^{2}_{0}\epsilon_{ij} = {}^{1}_{0}\epsilon_{ij} + {}_{0}\epsilon_{ij} \tag{17b} $$

The incremental strains are further assumed to be the sum of linear and non-linear parts as given next:

$$ {}_{0}\epsilon_{ij} = {}_{0}e_{ij} + {}_{0}\eta_{ij} \tag{18} $$

where,

$$ {}_{0}e_{ij} = \frac{1}{2}\left({}_{0}u_{i,j} + {}_{0}u_{j,i} + {}_{0}u_{k,i} * {}^{1}_{0}u_{k,j} + {}^{1}_{0}u_{k,i} * {}_{0}u_{k,i}\right) \tag{19a} $$

and

$$ {}_{0}\eta_{ij} = \frac{1}{2}{}_{0}u_{k,i} * {}_{0}u_{k,j} \tag{19b} $$

Equation (14) can now be expanded to the following form:

$$ \int_{{}^{0}V} {}_{0}S_{ij} \quad \delta {}_{0}e_{ij} \quad {}^{0}dV \quad + \quad \int_{{}^{0}V} {}^{1}_{0}S_{ij} \quad \delta {}_{0}\eta_{ij} \quad {}^{0}dV = $$

$$ {}^{2}\mathcal{R} - \int_{{}^{0}V} {}^{1}_{0}S_{ij} \quad \delta {}_{0}e_{ij} \quad {}^{0}dV \tag{20} $$

Equation (20) is used with a constitutive law and is converted to a matrix form to be solved iteratively. The external virtual work, ${}^{2}\mathcal{R}$, is given by the following:

$$ {}^{2}\mathcal{R} = \int_{{}^{0}V} {}^{2}f_{i}^{b} \quad \delta u_{i} \quad {}^{0}dV + \int_{{}^{0}A} {}^{2}f_{i}^{s} \quad \delta u_{i} \quad {}^{0}dA \tag{21} $$

Here f_i^b and f_i^s denote the components of body forces and surface tractions respectively.

2.2.2.2 Updated Lagrangian Formulation

In this formulation, the Cauchy stress tensor, τ_{ij}, is used with the following strain definition:

$$ {}_{1}\epsilon_{ij} = {}^{2}_{1}\epsilon_{ij} = {}_{1}e_{ij} + {}_{1}\eta_{ij} \tag{22a} $$

where,

$$ {}_1e_{ij} = \frac{1}{2}({}_1u_{i,j} + {}_1u_{j,i}) \tag{22b} $$

The equilibrium equation (13) is written as follows, using the configuration at time t as reference.

$$ \int_{{}^1V} {}^2_1S_{ij} \quad \delta^2_1\epsilon_{ij} \quad {}^1dV = {}^2\mathcal{R} \tag{23} $$

Using the steps outlined in the previous section, equation (23) can be converted to the following form:

$$ \int_{{}^1V} {}_1S_{ij} \quad \delta_1e_{ij} \quad {}^1dV \quad + \quad \int_{{}^1V} {}^1\tau_{ij} \quad \delta_1\eta_{ij} \quad {}^1dV = $$

$$ {}^2\mathcal{R} - \int_{{}^1V} {}^1\tau_{ij} \quad \delta_1e_{ij} \quad {}^1dV \tag{24} $$

The external virtual work is given by the following:

$$ {}^2\mathcal{R} = \int_{{}^1V} {}^2f^b_i \quad \delta u_i {}^1dV + \int_{{}^1A} {}^2f^s_i \quad \delta u_i {}^1dA \tag{25} $$

In equation (20), ${}_0S_{ij}$ is replaced by $\{{}_0D_{ijrs} \quad {}_0e_{rs}\}$ and in (24), ${}_1S_{ij}$ is replaced by $\{{}_1D_{ijrs} \quad {}_1e_{rs}\}$ using appropriate incremental constitutive tensor D_{ijrs} at time t referred to the initial and updated configurations respectively. The next section describes the relation of the constitutive tensor to the elastic (or elastic-plastic) constitutive matrix described in section 2.1.

2.2.3 Use of Constitutive Relations

In order to obtain a sensible solution to a given problem, it is imperative that the employed formulation contains appropriate model of both the kinematic and constitutive description. The kinematics of the formulations have been discussed in the previous sections. This section outlines the use of constitutive relations [3] for the total and the updated Lagrangian formulations.

2.2.3.1 Elastoplasticity With Total Lagrangian Formulation

The kinematic description of this formulation, as described in section 2.2.2.1, permits large displacements, rotations and strains. However, the formulation is most effective for large displacements and rotations, but small strain analysis of elastic-plastic materials [3]. Such a model is directly obtained by substituting the 2^{nd} Piola-Kirchoff stresses and Green-Lagrange strains for engineering stresses and strains in the elastic-plastic formulation. The yield function is written as

$$ {}^1F({}^1_0S_{ij}, {}^1\kappa) = 0 \tag{26} $$

and the flow rule relates an increment in the Green-Lagrange strains to the 2^{nd} Piola-Kirchoff stress-gradient of the yield function.

$$ d\epsilon^p_{ij} = {}^1\lambda \frac{\partial {}^1F}{\partial {}^1_0S_{ij}} \tag{27} $$

The stress-strain relation takes the following form:

$$ dS_{ij} = {}_0D_{ijrs}(d\epsilon_{rs} - d\epsilon^p_{rs}) \tag{28} $$

and an expression for elastic-plastic constitutive matrix, similar to equation (12), is obtained.

2.2.3.2 Elastoplasticity With Updated Lagrangian Formulation

For large displacement, rotation and strain analysis of elastic-plastic materials, the updated Lagrangian method with Jaumann stress rate, $\hat{\tau}_{ij}$, (ULJ) formulation has been used in the program NOFEAP. The yield function is now a function of Cauchy stresses and can be expressed as follows:

$$ {}^1F({}^1\tau_{ij}, {}^1\kappa) = 0 \tag{29} $$

The flow rule relates the plastic strain increment to the Cauchy stress derivative of the yield function.

$$d\epsilon_{ij}^{p} = {}^{1}\lambda \frac{\partial {}^{1}F}{\partial {}^{1}\tau_{ij}} \tag{30}$$

The stress-strain equation (31) relates an increment in the Jaumann stresses to an elastic strain increment.

$${}^{1}\hat{\tau}_{ij}dt = {}_{1}D_{ijrs}(de_{rs} - de_{rs}^{p}) \tag{31}$$

In (31), de_{ij} are increments of the deformation tensor and are the linear components of the Euler or Almansi strain tensor [65]. The Cauchy stress increments are computed from the Jaumann stresses using the following expression:

$${}_{1}\tau_{ij} = {}^{1}\hat{\tau}_{ij}dt + {}^{1}\tau_{ip}\,{}^{1}\Omega_{pj}dt + {}^{1}\tau_{jp}\,{}^{1}\Omega_{pi}dt \tag{32}$$

where ${}^{1}\Omega_{ij}$ are components of the spin tensor.

$${}^{1}\Omega_{ij} = \frac{1}{2}\left(\frac{\partial {}^{1}\dot{u}_{j}}{\partial {}^{1}x_{i}} - \frac{\partial {}^{1}\dot{u}_{i}}{\partial {}^{1}x_{j}}\right) \tag{33}$$

Equations (31-33) are used to compute the Cauchy stresses at each increment. In order to obtain the constitutive matrix relating the 2^{nd} Piola-Kirchoff stress increment, ${}_{1}S_{ij}$, to an increment of deformation tensor, $d\epsilon_{ij}$, a relation between the 2^{nd} Piola-Kirchoff stresses and the Truesdell stresses, $d\sigma_{mn}^{t}$, is used [36].

$$dS_{ij} = \left|{}_{0}^{1}X\right| \frac{\partial {}^{0}x_{i}}{\partial {}^{1}x_{m}} \frac{\partial {}^{0}x_{j}}{\partial {}^{1}x_{n}} d\sigma_{mn}^{t} \tag{34}$$

where $\left|{}_{0}^{1}X\right|$ is the determinant of the deformation gradient. The Truesdell stress increments are related to the Jaumann stresses by the following relation:

$$\hat{\tau}_{ij}dt = d\sigma_{mn}^{t} + {}^{1}\tau_{mp}de_{pn} + {}^{1}\tau_{np}de_{pm} - {}^{1}\tau_{mn}de_{pp} \tag{35}$$

Equation (31), (34) and (35) provide the desired constitutive relation. The term ${}^{1}\tau_{mn}de_{pp}$ contributes an unsymmetric matrix to the stiffness matrix. However,

de_{pp} denotes the volumetric strain which is small for large plastic flow. Also, the ratio of ${}^{1}\tau_{mn}$ to the elastic modulus is within the order of elastic strain and is generally negligible in finite strain analysis. Therefore, this term may be dropped from the relation without significantly affecting the solution while saving considerable computational effort.

The external virtual work contains contributions due to body and surface forces, as given in equations (21) and (25). Some of the surface loads may be applied by a die penetrating the workpiece. A treatment of such contact loads is given in the next section.

2.3 Surface Non-linearities

The next section includes a review of the formulations used to numerically solve a contact problem. A discussion of the formulation used in NOFEAP follows.

2.3.1 Review of Literature

Although the analysis of contact problems has been an area of investigation since Signorini [66] first applied a variational method to it in 1959, numerical methods were not actively used in the field for more than a decade. The finite element method was introduced into the realm of contact problems by Chan [4] in 1971. Chan interpolated the stiffness at the point of contact, which was permitted to be between any two nodes, from the stiffnesses at these nodes. The procedure was developed for linear triangular elements. Similar approach for higher order elements seems complicated and has not been followed in subsequent research. Since 1971, a number of formulations and algorithms [6,29,67-71] have been presented. Most of these formulations use interface or bond elements on the contact surface. An entirely different approach has been taken by Fredriksson [29,72], who developed a formulation similar to the theory

of plasticity. He introduced a yield criterion and a flow rule into contact problem definition. This formulation has been adopted by Kikuchi [28] and Cheng [31]. Both Fredriksson [73] and Cheng [31] have presented experimental means of determining the frictional properties. However, some of the parameters used in this micromechanical formulation seem to lack physical significance.

These algorithms have been used to analyze a variety of problems, ranging from indentation [29] and contact in machine elements [72,74] to dynamic contact [70,75,76]. The method used in this thesis is developed by Okamoto [6] and is described next.

2.3.2 Mathematical Formulation

In this formulation [6], a contact element is used at the surface. The stiffness matrix and load vector of the element are generated using the equilibrium equations and continuity conditions imposed on the force and displacement increments, as given next.

Let u_i^A, R_i^A and u_i^B, R_i^B denote the displacements and reactions at the contact surfaces of bodies A and B respectively, defined along the local normal and tangential coordinates (Fig 2.2). A prefixed Δ denotes an increment in the quantity. The constraints for various contact conditions are the following:

1. Open contact condition:

$$\Delta R_i^A = -\Delta R_i^B = 0 \tag{36a}$$

$$\Delta u_i^A - \Delta u_i^B = \Delta l_i \tag{36b}$$

2. Sticking contact condition:

$$\Delta R_i^A = -\Delta R_i^B = \Delta R_i \tag{37a}$$

$$\Delta u_n^A - \Delta u_n^B = \delta_n \tag{37b}$$

$$\Delta u_t^A - \Delta u_t^B = 0 \tag{37c}$$

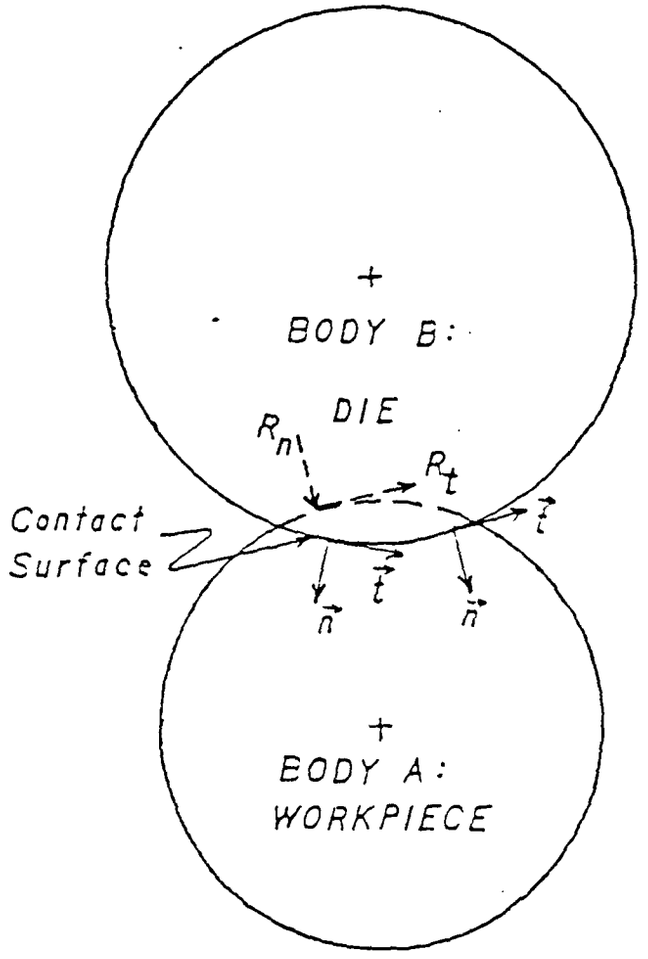

Figure 2.2 LOCAL COORDINATE SYSTEM AT THE CONTACT SURFACE

3. Sliding contact condition:

$$\Delta R_n^A = -\Delta R_n^B = \Delta R_n \tag{38a}$$

$$\Delta R_t^A = -\Delta R_t^B = \pm\mu\Delta R_n \tag{38b}$$

$$\Delta u_n^A - \Delta u_n^B = \delta_n \tag{38c}$$

$$\Delta u_t^A - \Delta u_t^B = \Delta l_t \tag{38d}$$

The nodal unknowns are the incremental displacements and the relative increments Δl_i, whenever the motion along the i^{th} direction is permitted, or the incremental contact forces, if no such motion is allowed. Thus, although there are six variables associated with each contact element, compared to four in commonly used elements, the nodal reactions and relative increments are obtained as part of the solution.

The nodal displacement increments Δu_i and the contact force increments ΔR_i under the known contact conditions C_n and a test load increment ΔF are obtained by solving the combined matrix equation. This system of simultaneous equations is obtained by assembling the structural stiffness matrices and load vectors with the contact stiffness matrices and load vectors. The solution vectors are used to calculate the load increment ratio α_k at the k^{th} step as given by

$$\Delta F_i^{'} = \alpha_k * \Delta F_i \tag{39a}$$

and

$$\Delta u_i^{'} = \alpha_k * \Delta u_i \tag{39b}$$

The factor α_k is the smallest fraction of the load required to cause a change in the contact statuses of one contact element. A discussion of the load factor computation scheme is given by Okamoto [6], whose work has been extended by Salamon [77]. Expressions for these load factors are presented in Appendix A.

2.4 Finite Element Formulation

The equations (20) and (24) are coupled with elastic-plastic constitutive laws and constraint equations at contact surface. Both in elastic-plastic solution and large deformation analysis, the out of balance virtual work is reduced by performing iterations until the difference between the external and internal virtual work is negligible within a certain convergence criterion. For the total Lagrangian formulation, equation (20) is rewritten as follows and is solved for an iteration step k.

$$\int_{{}^0V} {}_0D_{ijrs} \;\; {}_0e_{rs}^{(k)} \;\; \delta_0 e_{ij} \;\; {}^0dV + \int_{{}^0V} {}_0^1S_{ij} \;\; \delta_0\eta_{ij} \;\; {}^0dV \;\; =$$

$${}^2\mathcal{R} - \int_{{}^0V} {}_0^1S_{ij}^{(k-1)} \;\; \delta_0\epsilon_{ij}^{(k-1)} \;\; {}^0dV \qquad (40)$$

Equation (24) for the updated Lagrangian formulation is written in the following form:

$$\int_{{}^1V} {}_1D_{ijrs} \;\; {}_1e_{rs}^{(k)} \;\; \delta_1 e_{ij} \;\; {}^1dV + \int_{{}^1V} {}^1\tau_{ij} \;\; \delta_1\eta_{ij} \;\; {}^1dV \;\; =$$

$${}^2\mathcal{R} - \int_{{}^2V^{(k-1)}} {}^2\tau_{ij}^{(k-1)} \;\; \delta_2\epsilon_{ij}^{(k-1)} \;\; {}^2dV \qquad (41)$$

where the constitutive matrices ${}_0D_{ijrs}$ and ${}_1D_{ijrs}$ are obtained using the method outlined in section 2.2.3. The following development is only for the total Lagrangian formulation. Similar expressions can be obtained for the updated Lagrangian method by following these steps. Using the standard finite element discretization technique [7], equation (40) can be converted to the following matrix equation:

$$\Big[[K_L] + [K_{NL}]\Big]\Big\{\Delta u\Big\} = \Big\{{}_0^2R\Big\} - \Big\{{}_0^2F^{(k-1)}\Big\} \qquad (42a)$$

or,

$$\Big[[K_L] + [K_{NL}]\Big]\Big\{\Delta u\Big\} = \Big\{{}^2\Delta R^{(k)}\Big\} \tag{42b}$$

where,

$[K_L]$ = linear stiffness matrix = $[K_S] + [K_G]$;

$[K_S]$ = small displacement stiffness matrix;

$$[K_S]\{\Delta u\}\delta\{\Delta u\} = \int_{{}^0V} {}_0e^L_{rs} \;\; {}_0D_{ijrs} \;\; \delta\, {}_0e^L_{ij} \;\; {}^0dV \quad . \tag{43}$$

$[K_G]$ = geometric stiffness matrix;

$$[K_G]\{\Delta u\}\delta\{\Delta u\} = \int_{{}^0V} {}_0e^L_{rs} \;\; {}_0D_{ijrs} \;\; \delta\, {}_0e^{NL}_{ij} \;\; {}^0dV +$$

$$\int_{{}^0V} {}_0e^{NL}_{rs} \;\; {}_0D_{ijrs} \;\; \delta\, {}_0e^L_{ij} \;\; {}^0dV + \int_{{}^0V} {}_0e^{NL}_{rs} \;\; {}_0D_{ijrs} \;\; \delta\, {}_0e^{NL}_{ij} \;\; {}^0dV \tag{44}$$

$[K_{NL}]$ = non-linear (initial stress) stiffness matrix;

$$[K_{NL}]\{\Delta u\}\delta\{\Delta u\} = \int_{{}^0V} {}^1_0S_{ij}\,\delta\, {}_0\eta_{ij}\, {}^0dV \tag{45}$$

$\{{}^2_0R\}$ = total external virtual work at time $t + dt$;

$\{{}^2_0F^{(k-1)}\}$ = total internal work at time $t + dt$, but at previous iteration step;

$\{{}^2\Delta R^{(k)}\}$ = increment in external virtual work at time $t + dt$ and at k^{th} step.

In (43) and (44), the quantities ${}_0e^L_{ij}$ and ${}_0e^{NL}_{ij}$ are defined as follows:

$${}_0e^L_{ij} = \frac{1}{2}({}_0u_{i,j} + {}_0u_{j,i}) \tag{46a}$$

$${}_0e^{NL}_{ij} = \frac{1}{2}({}^1_0u_{k,i} * {}_0u_{k,j} + {}_0u_{k,i} * {}^1_0u_{k,j}) \tag{46b}$$

The non-linear strain increments, ${}_0\eta_{ij}$, are defined by equation (19b). The expressions for updated Lagrangian formulation are similar to the ones given here except for the absence of the geometric stiffness matrix. Equation (42b) can be expressed as

$$[K]\{\Delta u\} = \Big\{{}^2\Delta R^{(k)}\Big\} \quad \equiv \quad \{\Delta R\} \tag{47}$$

with the incremental virtual work $\{\Delta R\}$ given by the following:

$$\{\Delta R\}\delta\{\Delta u\} = \int_{{}^{0}V} \Delta f_i^b \delta u_i {}^{0}dV + \int_{{}^{0}A} \Delta f_i^s \delta u_i {}^{0}dA \tag{48}$$

If the contact surface of the body is separated from the remaining surface, the incremental virtual work may be broken up as follows:

$$\{\Delta R\} = \{\Delta R^{sb}\} + \{\Delta R^{c}\} \tag{49}$$

Here $\{\Delta R^{c}\}$ contains the work of the unknown contact forces, and $\{\Delta R^{sb}\}$ includes the contributions of the body forces and known surface tractions. For two contacting bodies, A and B, equations (47) and (49) are written as

$$[K_A]\{\Delta u_A\} = \{\Delta R_A^{sb}\} + \{\Delta R_A^{c}\} \tag{50a}$$

and,

$$[K_B]\{\Delta u_B\} = \{\Delta R_B^{sb}\} + \{\Delta R_B^{c}\} \tag{50b}$$

with

$$\{\Delta R_B^{c}\} = -\{\Delta R_A^{c}\} \tag{50c}$$

Equations (50) can be combined to yield a single matrix equation as follows [6]:

$$\begin{pmatrix} K_A & 0 & K_{AC} \\ 0 & K_B & K_{BC} \\ K_{CA} & K_{CB} & K_{CC} \end{pmatrix} \begin{pmatrix} \Delta u_A \\ \Delta u_B \\ \Delta Q' \end{pmatrix} = \begin{pmatrix} \Delta R_A^{sb} \\ \Delta R_B^{sb} \\ \delta_c \end{pmatrix} \tag{51}$$

where, K_{AC}, K_{BC}, K_{CA}, K_{CB}, and K_{CC} are contact stiffness matrices obtained from constraint equations (36-38). $\Delta Q'$ are incremental vectors of contact forces or relative displacements and δ_c are vectors of initial gaps between nodal pairs along the contact surface.

Equation (51) includes non-linearities due to large deformations in the structural stiffness matrices, K_A and K_B; due to contact conditions in establishing the contact statuses at each step; and due to plastic flow in the stiffness and stress

computations. This can be expected to lead to convergence problems. Programs with conventional algorithms may lack the flexibility required to solve such problems. A macro programming language [7] overcomes this difficulty by letting the user control the solution algorithm. A brief description of this feature is given in the next section.

2.5 Program Features

The non-linear formulations presented in previous sections have been used to develop a non-linear finite element analysis program (NOFEAP). The program has been designed as a flexible tool for research, educational, or applications environments, which demand frequent modifications to meet each new problem's requirements. The program has been developed on a VAX 11/782 running under VMS version 4.3 operating system, and is also operational on a Data General Eclipse MV/10000 with AOS/VS 7.54 operating system. The program consists of several general modules: (1) Problem control; (2) Problem definition and mesh input; (3) Element library; (4) Problem solution; and (5) Graphics outputs.

The problem solution module is centered around a unique macro programming language [7] concept in which the solution algorithm is written by the user. There are sufficient macro instructions included in the system for many applications in structural mechanics; however, each user may modify the program by adding new language features to meet the user's specific application's requirements.

The NOFEAP system includes a general element library. Elements are currently available to model linear and non-linear problems in structural mechanics. Included in the existing library are elements for solving linear elasticity problems in plane stress, plane strain, or axisymmetric analysis. Non-linear elements are available for an elastic-plastic solution of planar problems using a variety of yield

criteria. The total and the updated Lagrangian formulations are modelled in elements for geometrically non-linear analysis of planar elements. Surface non-linearities have been modelled by including the contact problem formulation described in the previous section.

External loads can be applied in the problems by prescribing the forces or displacements as well as by rigid body translation or rotation of contacting bodies. The rolling process has not been modelled in any existing commercial program, although some programs do approximate the rolling process by assuming the pressure distributions along the contact surface [10,11]. The features of NOFEAP and descriptions of the available macro commands are given in the NOFEAP Users' Manual [8].

The program NOFEAP has been used to analyze the deformations in a cylinder when it is rolled against a hard cylinder. The plastic flow and stress distribution in a gear tooth, when the gear is rolled against a rigid die, has also been studied. These results are presented in Chapter 4. The implementation of each of the non-linear formulations in NOFEAP has been verified by solving a number of benchmark problems – problems which have been solved both analytically and numerically by various authors. Some of the problems have also been solved experimentally by different authors. The results of some of these verification exercises are presented in the next chapter.

Chapter 3

ANALYSIS OF SOME NON-LINEAR PROBLEMS

The non-linear formulations in NOFEAP have been checked for accuracy by solving a number of benchmark examples. These problems have been selected to test the formulations both individually and in various combinations. Results of some of these exercises are given in this chapter.

The program NOFEAP is capable of using a number of planar isoparametric elements, namely, three through nine node elements. The analysis can be carried out for plane strain, plane stress or axisymmetric bodies. The elastic-plastic analysis can be performed for materials obeying either Tresca, von Mises, Drucker-Prager or Mohr-Coulomb criterion for yielding. However, the results are only included for von Mises material since this model is to be used to study the gear-rolling process.

3.1 Thick Cylinder Under Internal Pressure

The first example, analysis of a thick cylinder subjected to an internal pressure, provides a simple means of comparing the numerical results with analytical ones. This problem has been solved by several authors [5,47,78] and the stress distributions are also available in the literature.

The finite element mesh used in the analysis, consisting of 12 eight-node elements, is shown in Figure 3.1. Only a quadrant of the cross-section needs to be modelled due to symmetry about both coordinate axes. The material properties are assumed to be the following:

modulus of elasticity, E $= 0.210E+06 N/mm^2$;

yield stress, σ_y $= 240.00 N/mm^2$;

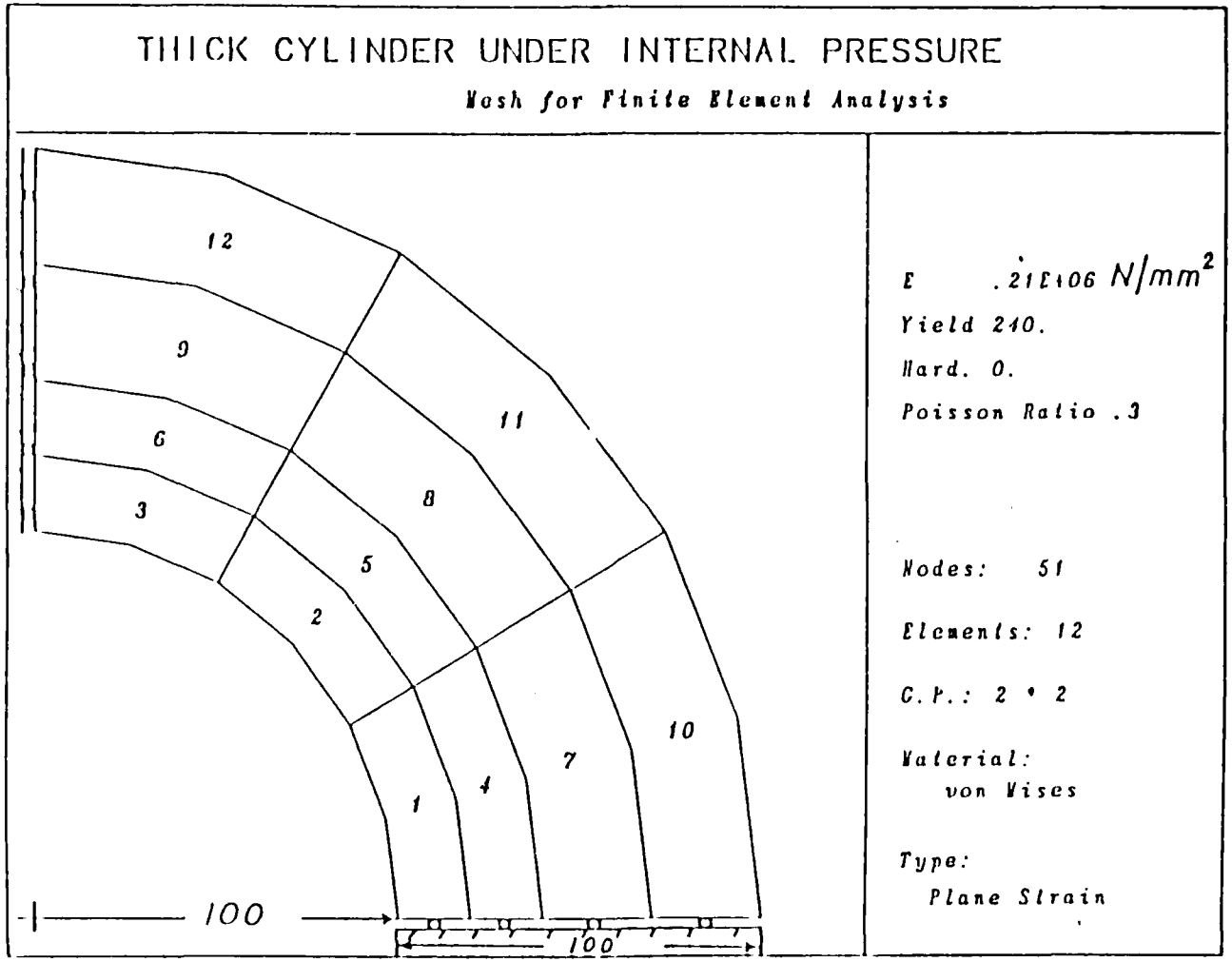

Figure 3.1 THICK CYLINDER UNDER INTERNAL PRESSURE:
Mesh for Finite Element Analysis

slope of hardening curve, $H^{'}$(=A) $= 0.00 N/mm^2$;

Poisson's ratio, ν $= 0.30$.

Figure 3.1 also displays the number of nodes and elements along with the number of integration points (G.P.) used in the problem. The cylinder is subjected to an internal pressure of $80 N/mm^2$, which is then doubled in steps of $20 N/mm^2$. Non-dimensionalized curves obtained from the analysis are presented in Fig 3.2-3.4. The computed stresses referred to in this thesis imply the stresses at Gauss points unless otherwise noted. The distances and displacements are normalized by the inner radius, r(a), while the pressure and stresses are normalized by the yield stress, σ_y. The shear modulus of the material is denoted by G.

The loading curve of the problem is given in Fig 3.2 along with the numerical solution of Nayak [47] and the analytical solution of Hodge [78]. The solution obtained by NOFEAP exactly matches the analytical solution while differing slightly from the numerical results of Nayak. The slight variation between the two numerical solutions may be attributed to a difference in convergence tolerance or criterion, numerical formulation and finite element mesh. However, the agreement of NOFEAP solution with the analytical results indicate the accuracy of the elastic-plastic formulation.

The hoop stress distribution across the thickness of the cylinder is presented in Fig 3.3. The results of NOFEAP compare exceedingly well with the analytical ones while again deviating from Nayak's solutions. Finally, the stress distributions for various steps are presented in Fig 3.4. The behavior of the curves is as expected with the maximum hoop stress shifting away from the inner surface with increasing plastic flow while the radial stresses maintain a traction free outer surface.

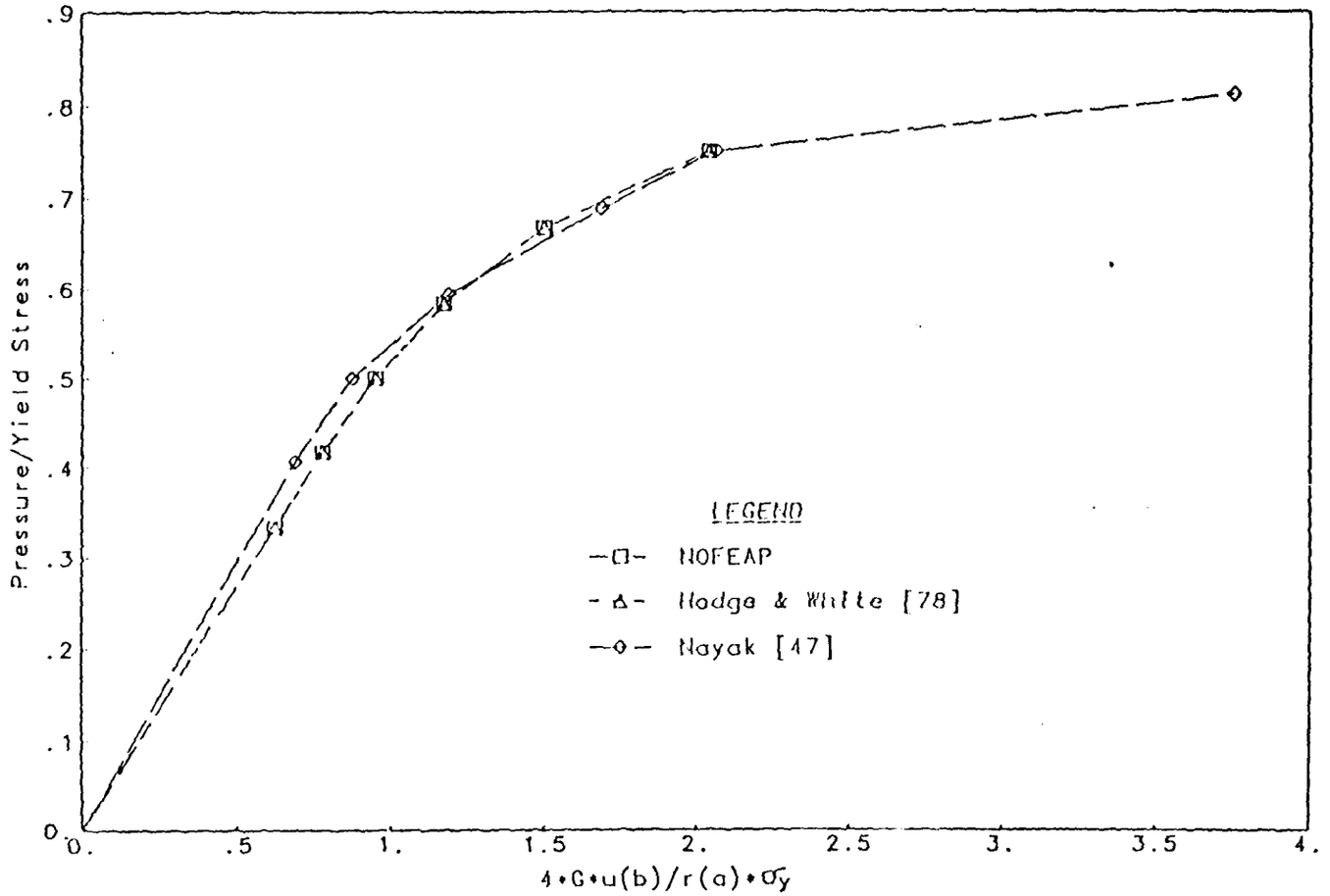

Figure 3.2 PRESSURE VERSUS DISPLACEMENT CURVE FOR THICK CYLINDER

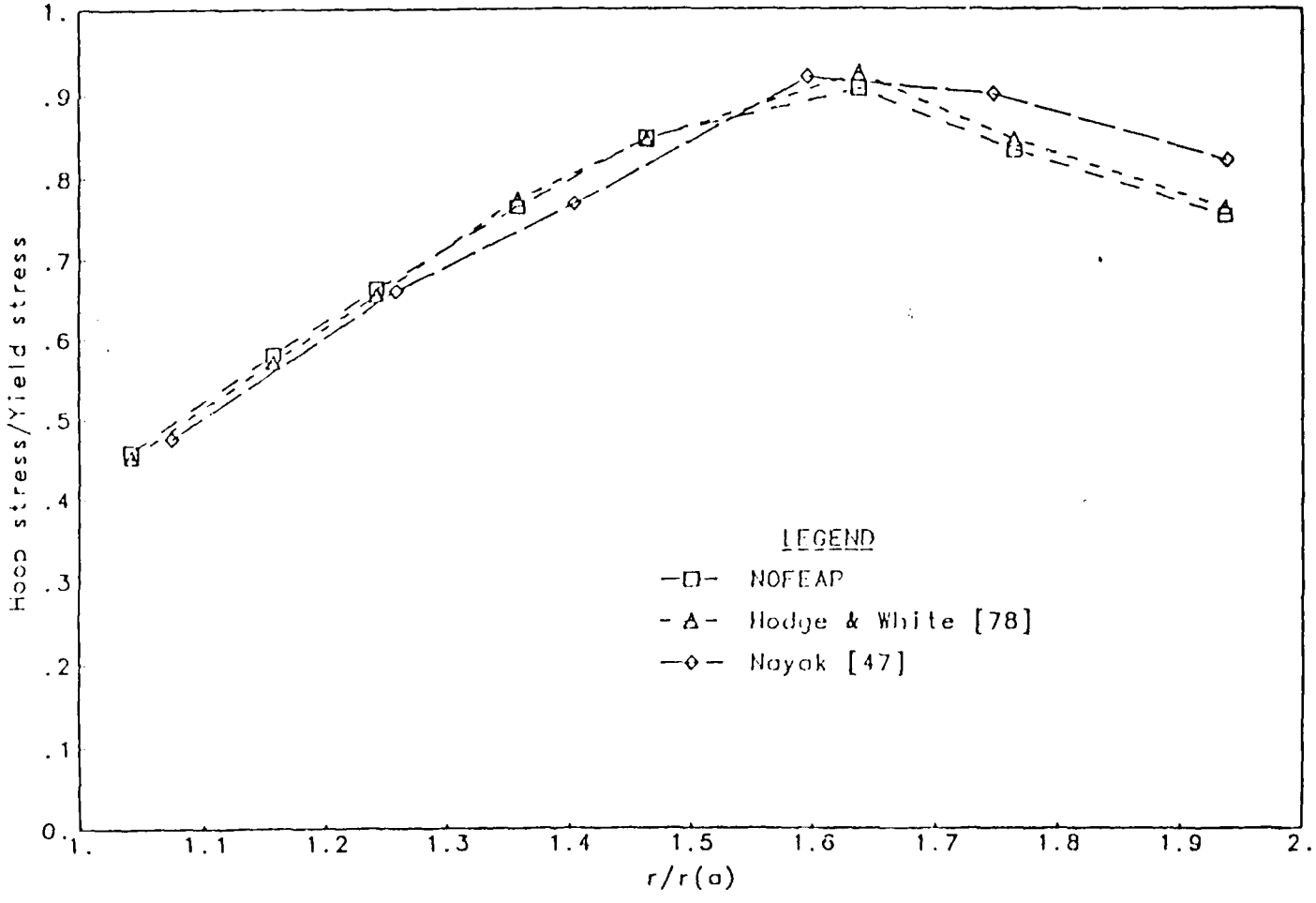

Figure 3.3 HOOP STRESS DISTRIBUTION FOR THICK CYLINDER UNDER PRESSURE

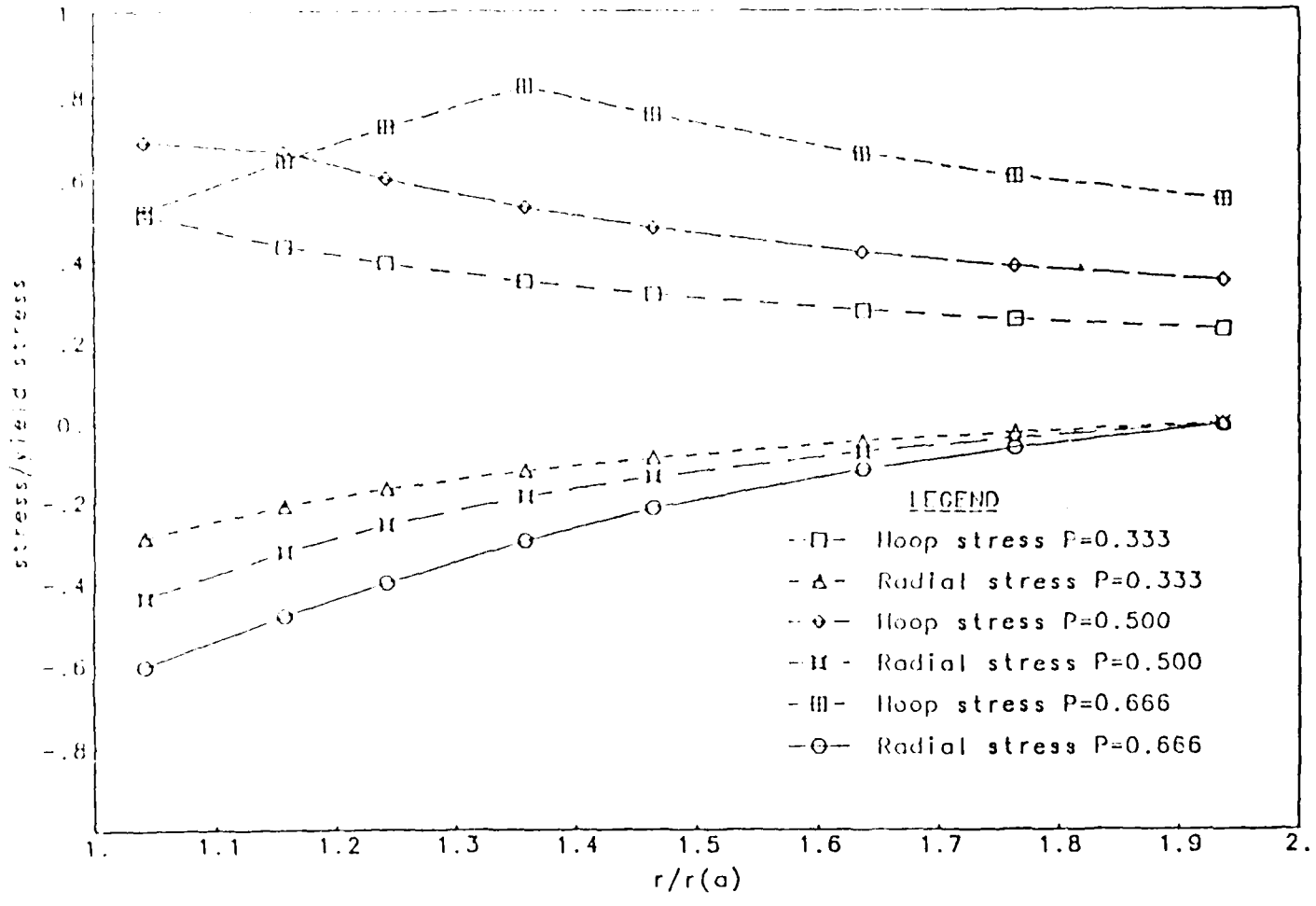

Figure 3.4 STRESSES WITH INCREASING PRESSURE IN THICK CYLINDER

3.2 Small Strain Extrusion

This example demonstrates the application of the elastic-plastic analysis to a practical problem: the extrusion process. The actual process has been simplified by assuming a frictionless die and small plastic strains so that large deformation formulations and frictional contact conditions do not have to be included in the analysis. This problem has also been solved by Nayak and Zienkiewicz [47] who have compared their solutions to an experimental study.

The finite element mesh (Fig 3.5) employs four-node plane strain elements in the analysis. Symmetry of the die about the vertical axis in the figure permits the use of half the section. An elastic, but perfectly plastic material is considered in the extrusion process with an elastic modulus of 68,950 MPa, a yield stress of 68.95 MPa and a Poisson's ratio of 0.3. Forward extrusion is carried out by steadily forcing the die into the wider end. Since only small strain analysis is performed; the final displacement of the die, approximately 0.762 mm, is negligible compared to that in a typical process. However, the analysis does produce results which can be compared to both numerical and experimental results.

The contours of effective stress are shown in Fig 3.6. These contours are indicative of the progress in the deformation of the material since they point to the origin and the direction of plastic flow. These contours do agree with those of Nayak [47] which could not be reproduced here. The largest amount of flow (Fig 3.7) occurs at the corners near the bend in the die, as can be expected. The load versus deflection curve of NOFEAP analysis has been compared to that of Nayak in Fig 3.8. The pressure, P, is computed by summing the reactions at the penetrating punch and dividing the sum by the width at the die. As can be seen in Fig 3.8, the two results are in excelled agreement.

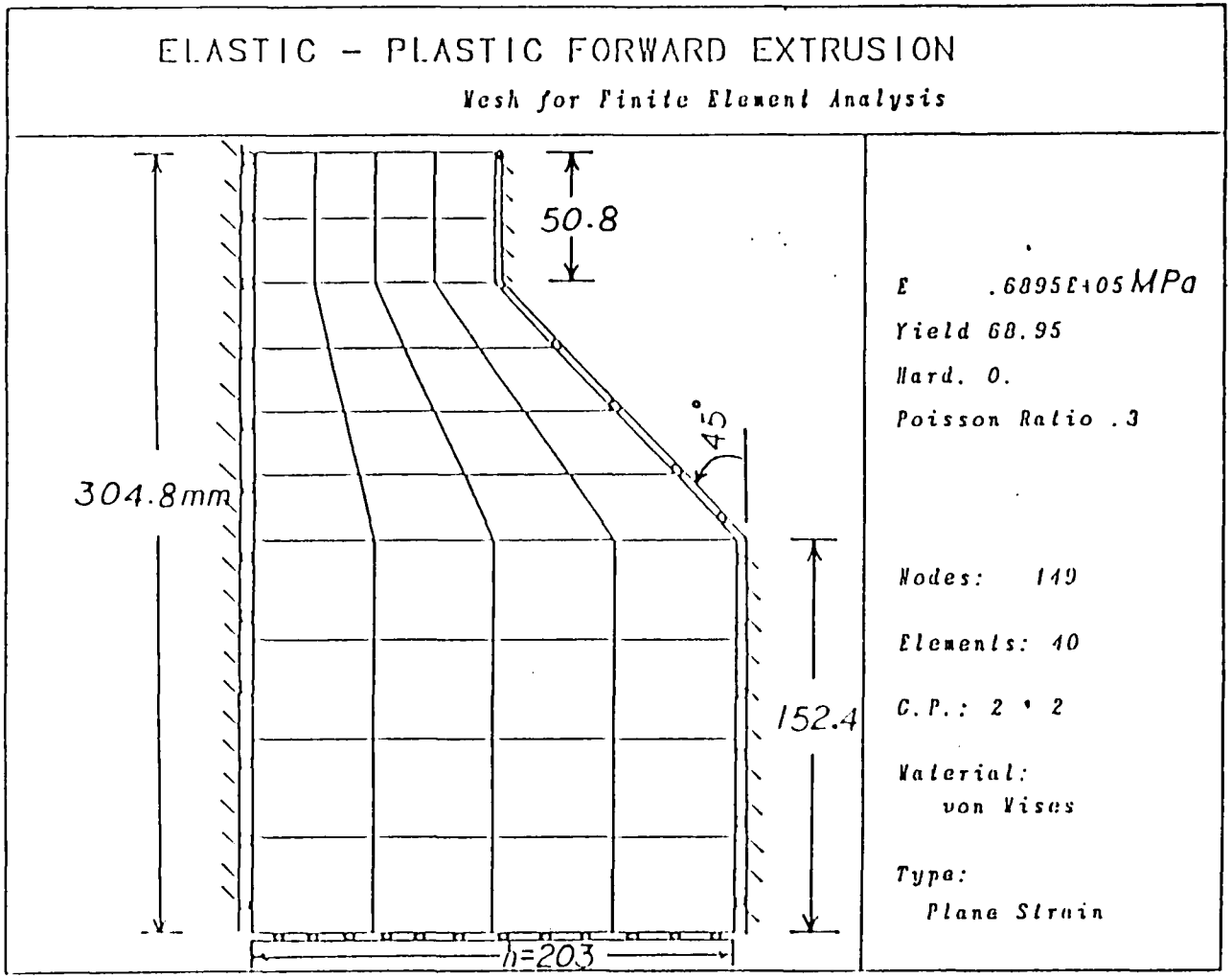

Figure 3.5 ELASTIC-PLASTIC FORWARD EXTRUSION:
Mesh for Finite Element Analysis

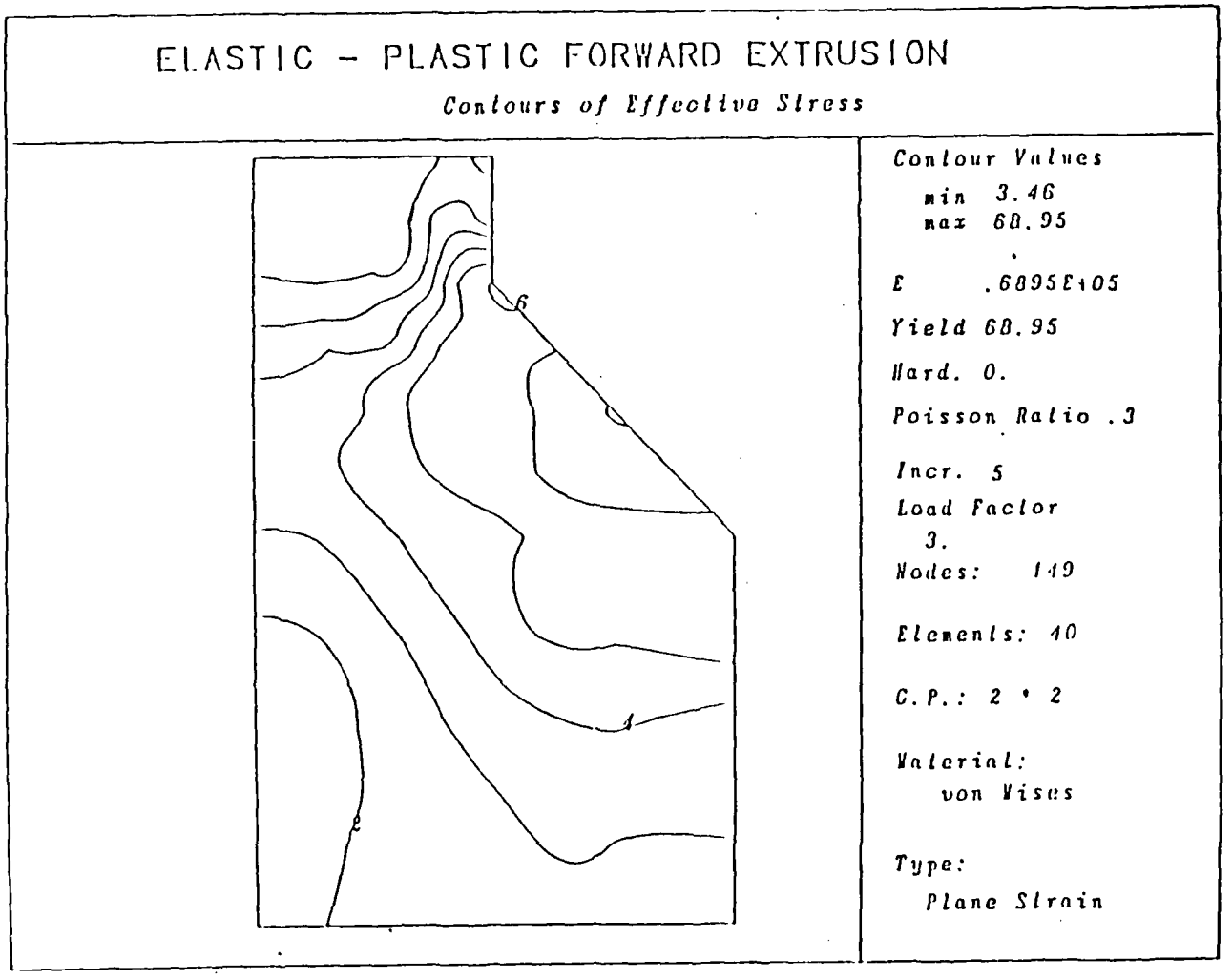

Figure 3.6 ELASTIC-PLASTIC FORWARD EXTRUSION:
Contours of Effective Stress

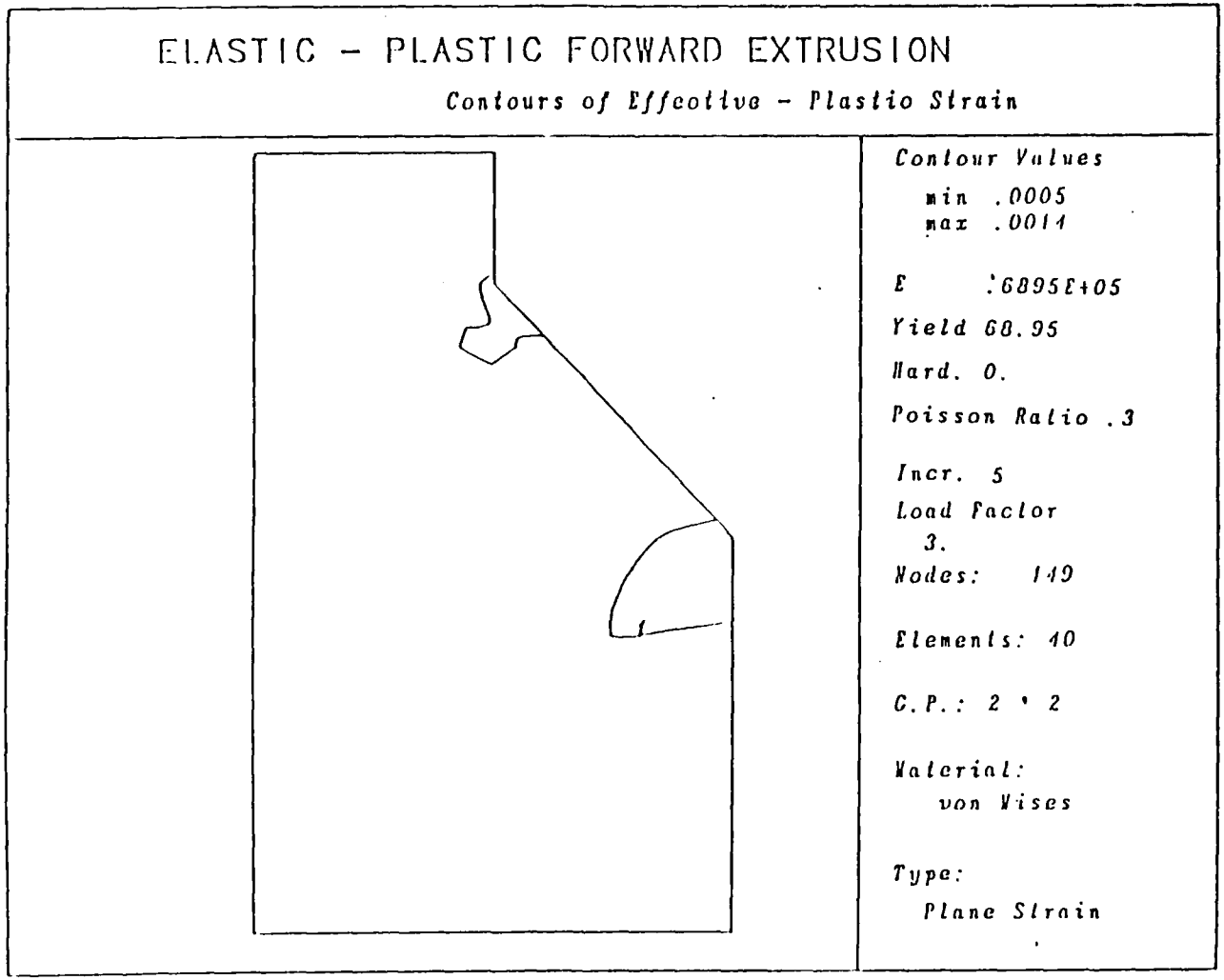

Figure 3.7 ELASTIC-PLASTIC FORWARD EXTRUSION:
Contours of Effective Plastic Strain

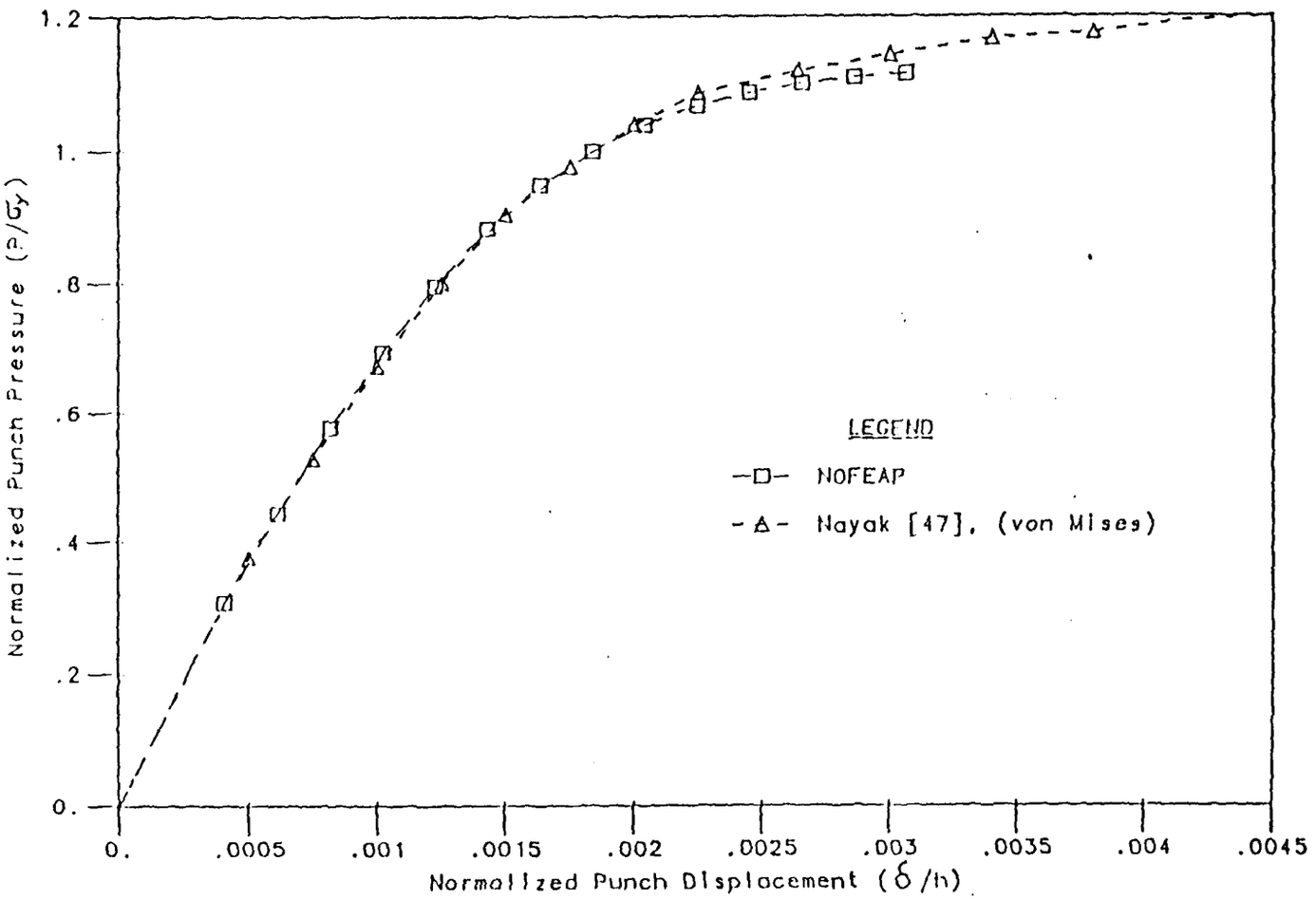

Figure 3.8 LOADING CURVE FOR FORWARD EXTRUSION PROBLEM

3.3 Large Displacement Analysis of a Cantilever

There is a dual purpose in selecting large displacement analysis of a cantilever to test the accuracy of the geometrically non-linear formulations. The problem has been solved both analytically (Holden [79]) and numerically (Bathe [59]). It not only provides a comparison between these results and those obtained by the total Lagrangian (TL) and the updated Lagrangian (ULJ) formulations, but also between the TL and ULJ methods themselves. The latter comparison is significant since with proper implementation of the two formulations with appropriate constitutive relations, identical numerical results should be obtained using either formulations.

The cantilever is modelled using eight-node isoparametric elements. The mesh and material properties are given in Fig 3.9. The beam is 254 mm long, and 25.4 mm in width and depth. The elastic modulus of the material is 82.74 MPa and the Poisson's ratio is 0.2. The yield stress is set to a sufficiently high value to maintain elastic response in the material.

The beam is subjected to uniformly distributed loads along the top and the bottom surfaces. The pressure is increased in steps of 689.5 Pa for 100 increments. The displacement of the beam at 13,790 Pa is shown in Fig 3.10. A comparison of the various loading curves is given in Fig 3.11, which shows the variation in the vertical displacement at the tip with increasing pressure.

A linear (small displacement) solution is superimposed on other curves in Fig 3.11 to emphasize the difference in geometrically non-linear analysis from a linear analysis. It should be noted that the results of NOFEAP for TL and ULJ formulations, with the load applied in 100 steps, match exactly with each other, indicating a consistent implementation of these formulations in the program.

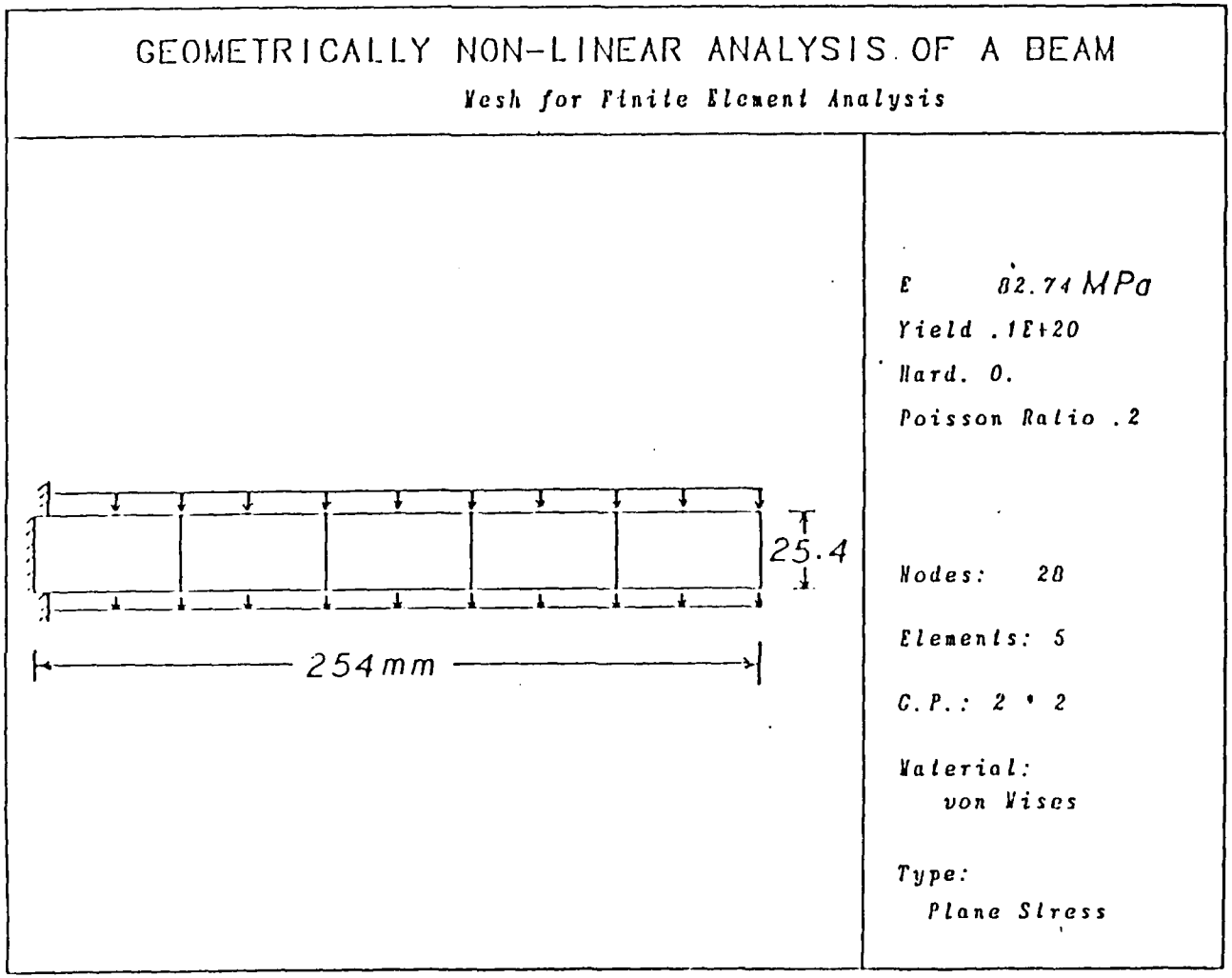

Figure 3.9 GEOMETRICALLY NON-LINEAR ANALYSIS OF A BEAM:
Mesh for Finite Element Analysis

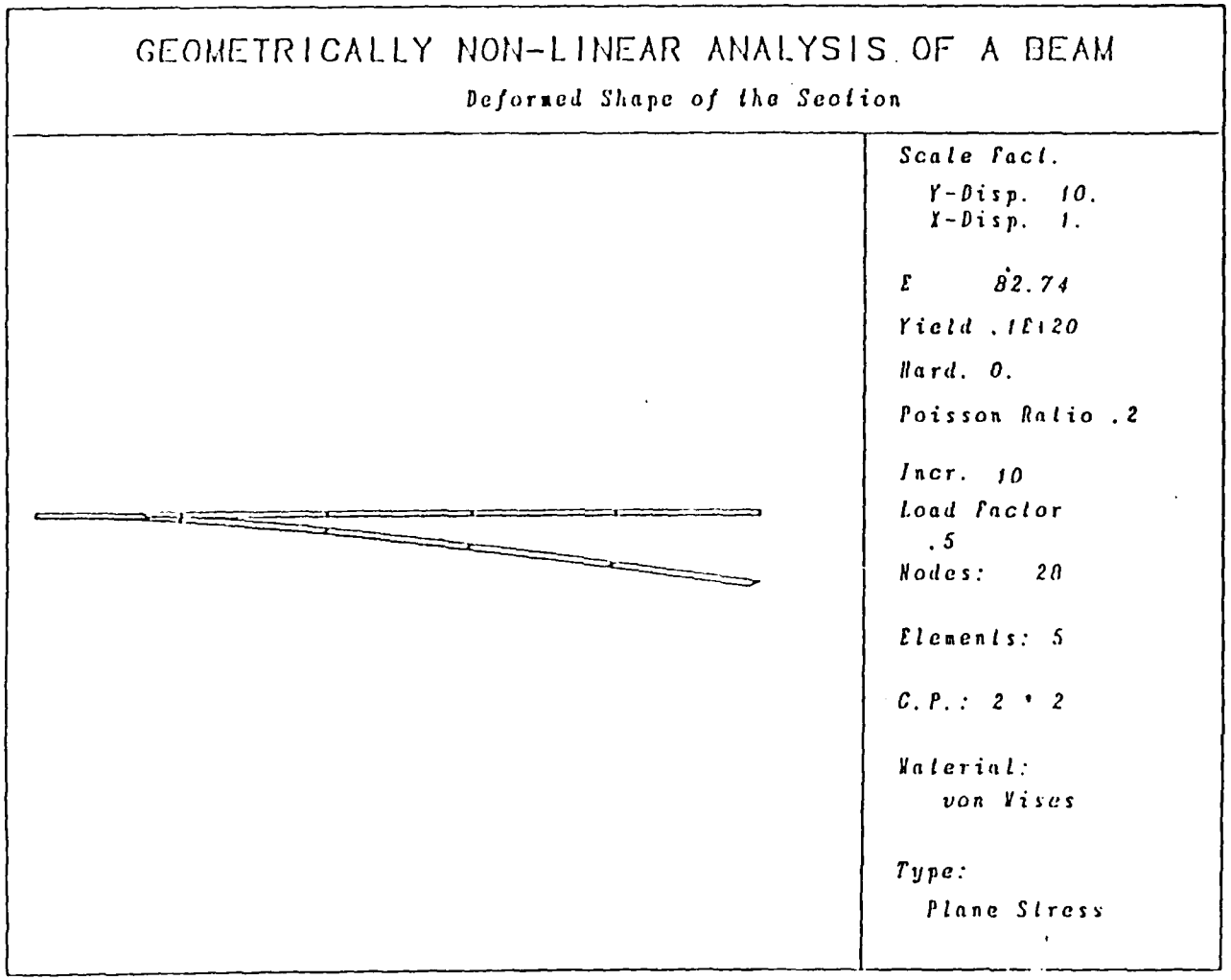

Figure 3.10 GEOMETRICALLY NON-LINEAR ANALYSIS OF A BEAM:
Deformed Shape of the Section

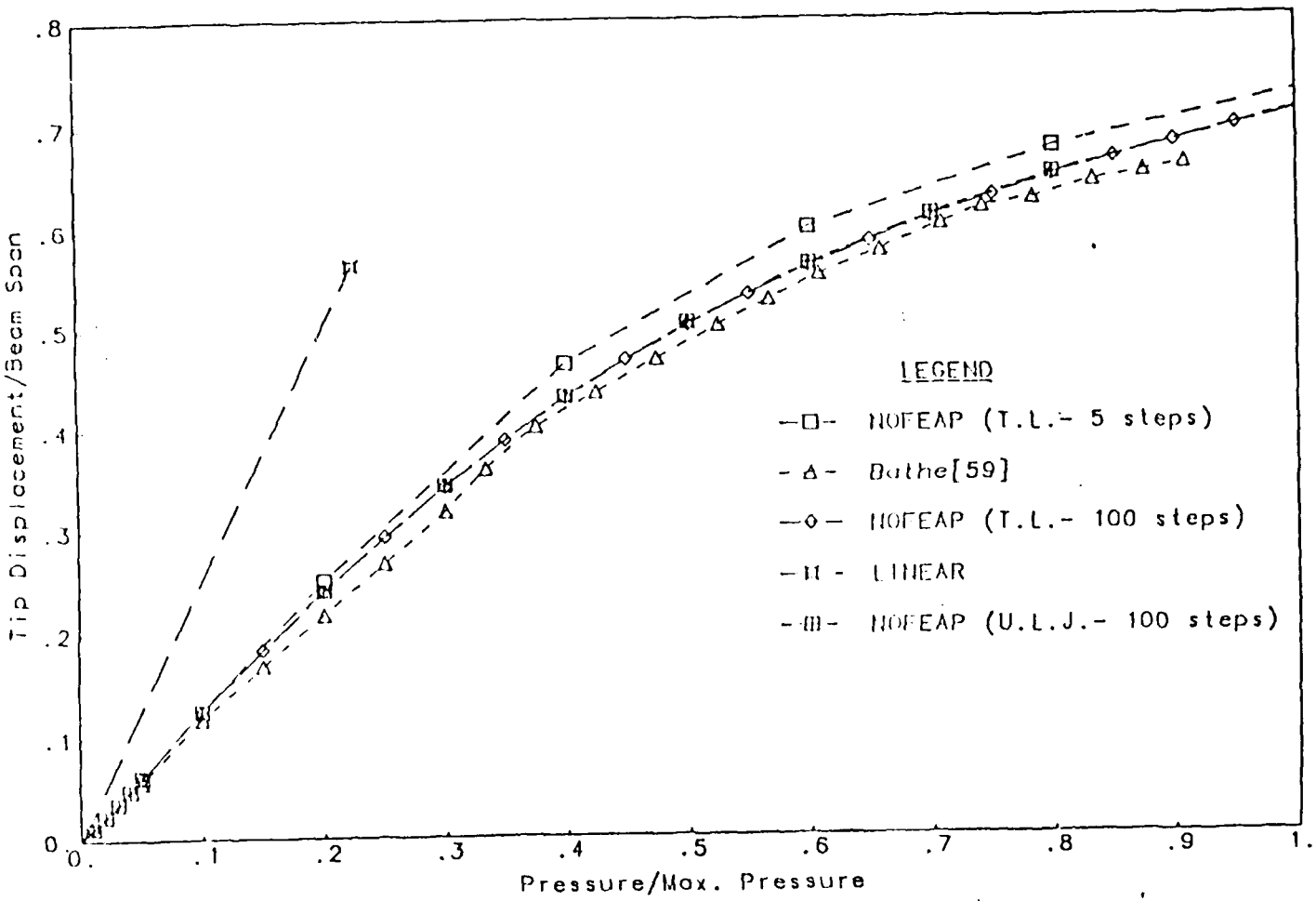

Figure 3.11 LOADING CURVE FOR LARGE DEFLECTION ANALYSIS OF A CANTILEVER

These results compare extremely well with those of Bathe [59]. The irregularity in the reproduced curve of Bathe's is ascribed to human error in reading the curve from the published article. The analytical results of Holden [79] are not reproduced here, since these have been shown [59] to match Bathe's solutions.

The agreement of the non-linear formulations of NOFEAP and the existing analytical as well as numerical solutions is found to be satisfactory. As a further test, the load was applied in only five steps and convergence iterations were performed for TL formulation. The load-deflection curve obtained for this case (Fig 3.11) still compares fairly well with other results, indicating further the accuracy and reliability of the formulation. In the next example, both the material and geometric non-linearities are combined in one problem.

3.4 The Upsetting Process

The upsetting of a circular cylinder is characterized by large plastic deformations. As a benchmark problem for testing the validity of numerical methods for analysis of metal forming process, it has been solved by researchers both numerically [22,31] and experimentally [24].

The cylinder is initially 20 mm in radius and 30 mm in height. The mechanical properties of the material are as follows: elastic modulus = 200 GPa, Poisson's ratio = 0.3, yield stress = 700 MPa, and slope of hardening curve = 300 MPa. Only a quarter of the cylinder is analyzed using "4-CST" elements (Fig 3.12) due to symmetry. Fully sticking conditions are assumed from the top of the block. The block is deformed by compressing at the top in steps of 0.25% of initial height to reach a final reduction of 30% in height. A second study using 0.50% reduction in height as step size has also been conducted to observe the effect of load step on the stresses and loads.

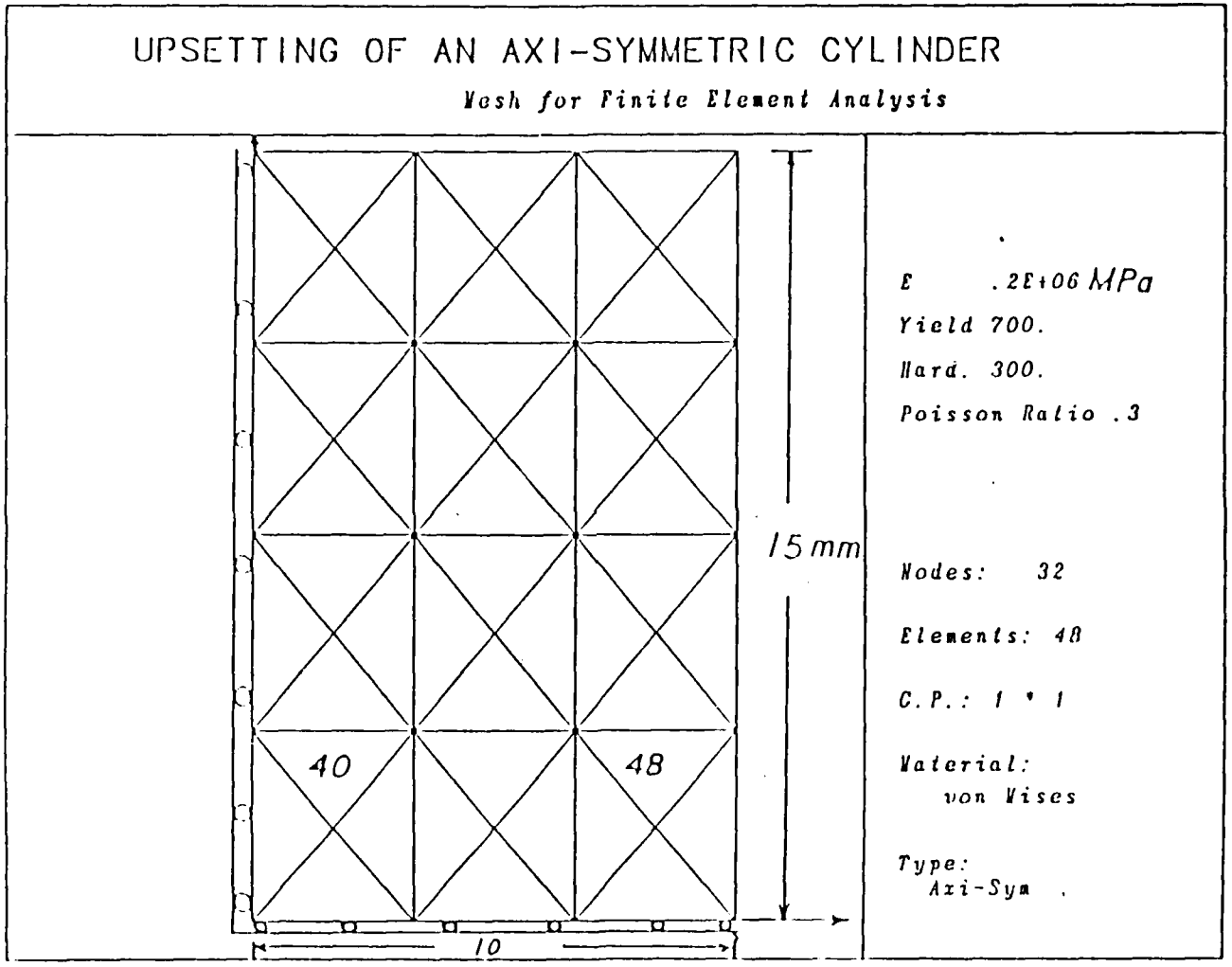

Figure 3.12 UPSETTING OF AN AXISYMMETRIC CYLINDER:
Mesh for Finite Element Analysis

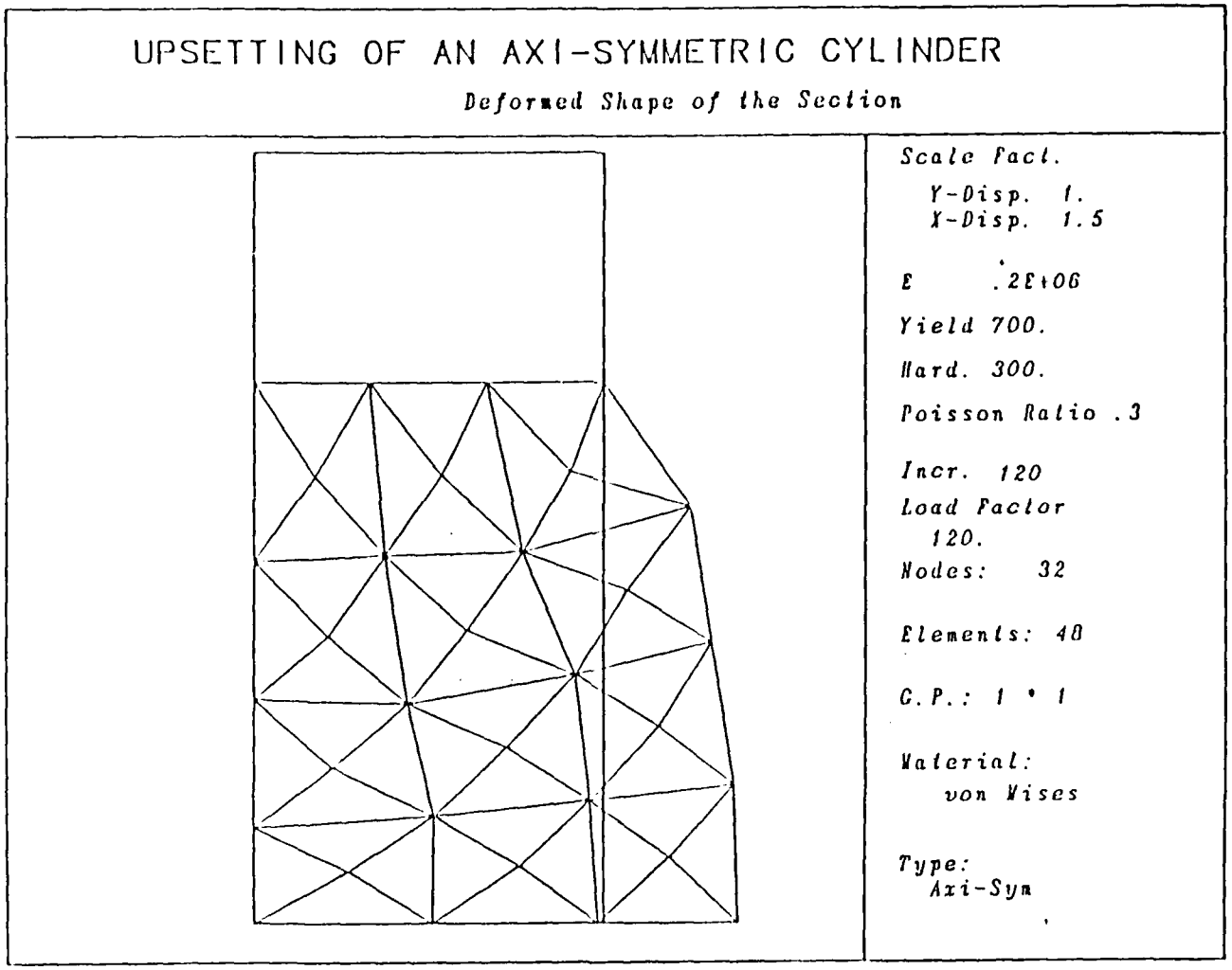

Figure 3.13 UPSETTING OF AN AXISYMMETRIC CYLINDER:
Deformed Shape of the Section

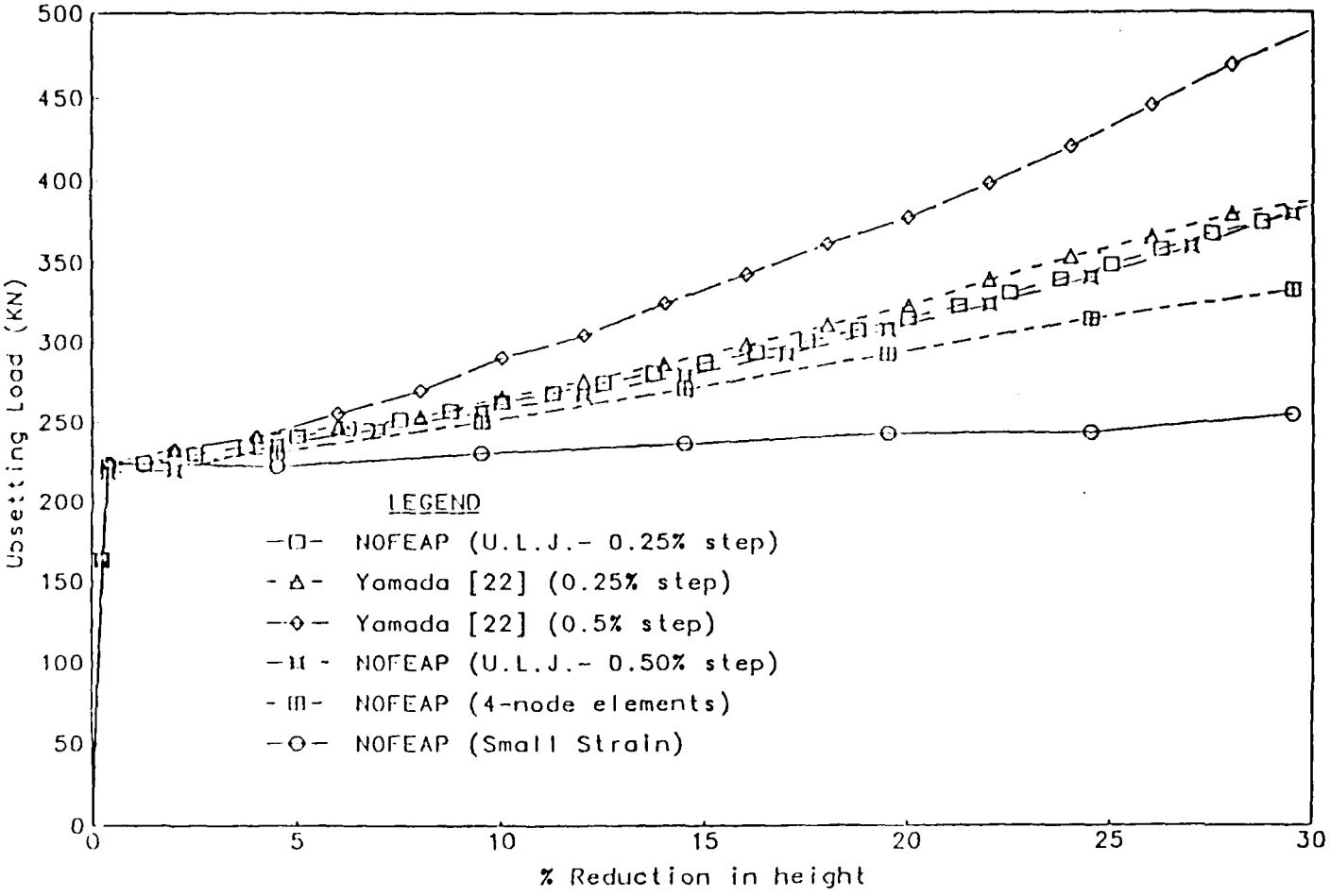

Figure 3.14 UPSETTING LOAD VERSUS PERCENT REDUCTION IN HEIGHT

The deformed cylinder, Fig 3.13, shows the bulging at the centerline, as has been reported in the experiments of Böer [24]. The loading curves for the upsetting process for various cases are shown in Fig 3.14, along with curves for two different load steps computed by Yamada [22]. The maximum error between Yamada's solution and NOFEAP solution for a step size of 0.25% has been found to be 1.2% – an acceptable value considering the non-linearities involved in the problem. Although Yamada [22] (and Cheng [31]) has reported a large variation in the solution with step-size, as can be seen in Fig 3.14, the deviation has not been significant in the results obtained using NOFEAP. Fig 3.14 also demonstrates the underestimation of the upsetting load using small strain formulation or by using four-node elements in ULJ formulation. An explanation for the latter phenomenon can be obtained by referring to the studies of Nagtegaal [80] and Kikuchi [26], which recommend the use of "4CST-elements" in large strain applications. Fig 3.15 shows the plastic hardening curve for two elements in the mesh. These curves are found to exactly follow the specified material properties, indicating the accuracy of the stress reduction scheme in NOFEAP. The bulging behavior of the cylinder has been compared to Yamada's solution in Fig 3.16, and the agreement is found to be excellent.

The sample examples given so far have verified the elastic-plastic and geometrically non-linear formulations in NOFEAP. The next two examples compare the contact problem formulation with the Hertzian theory.

3.5 Hertz Contact Problem

The classical Hertzian contact problem is selected to verify the accuracy of the contact problem formulation. The problem involves contact between two cylinders, whose longitudinal axes are parallel. The two cylinders are assumed to be identical in geometry and material properties in the following examples. This assumption

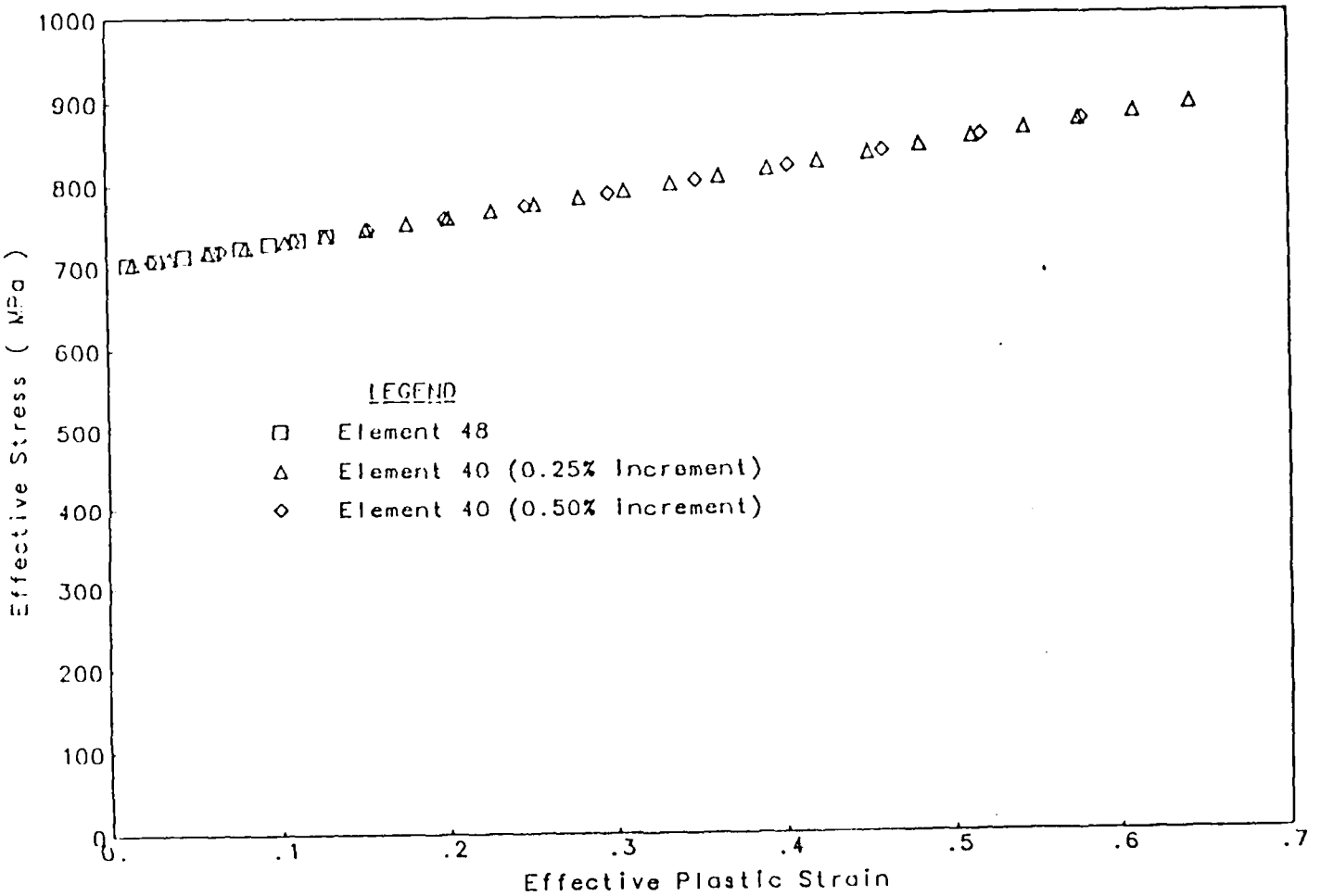

Figure 3.15 EFFECTIVE STRESS VERSUS PLASTIC STRAIN

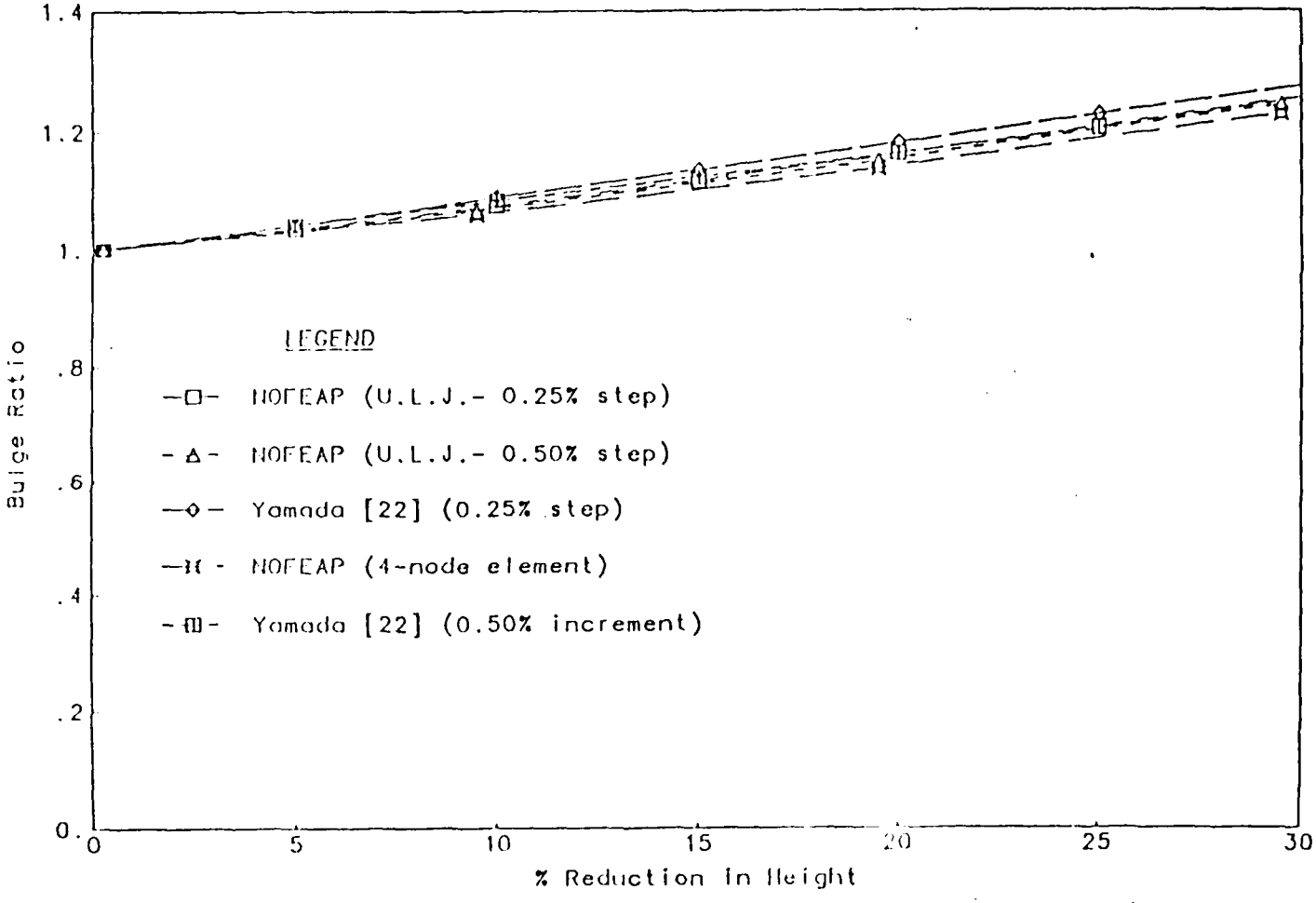

Figure 3.16 BULGE RATIO FOR UPSETTING PROCESS

computationally simplifies the problem by symmetry considerations to that of one cylinder pressed on a rigid half-space.

The finite element mesh, shown in Fig 3.17, consists of 117 elements, each with four or five nodes. The details of region ABCD, near the contact surface, are given in Fig 3.18. Only a portion of the cylinder has been modelled. The rigid half-plane is modelled by 18 fixed nodes. Candidate contact nodes are distributed along the contact surface of the cylinder. The cylindrical surface has a radius of curvature of 254 mm. A single concentrated load, P, is applied at the node at left top corner, as shown in Fig 3.17. The load is increased from an initial value of 1779.2 N to a maximum of 8896 N in four equal increments.

The theoretical solution relating the load to contact length and stress distribution is obtained from the reference [81]. The numerical resuls are compared with the Hertzian solutions in Fig 3.19 through 3.22. The effect on contact length and maximum nodal stress (traction) at various loads is shown in Fig 3.19 and 3.20 respectively. The numerical results differ slightly from the analytical ones. The distribution of stress, however, is found to match the Hertzian stress distribution, as seen in Fig 3.20.

The tangential and normal stress along the load axis are plotted in Fig 3.21 and 3.22 respectively. The stresses drop from a maximum at the contact surface to a negligible value at a depth of the magnitude of the contact length. These stresses also follow the Hertzian distribution but differ in magnitude by a small factor. The error in the contact length and stresses is found to be less than 5% and is considered to be satisfactory.

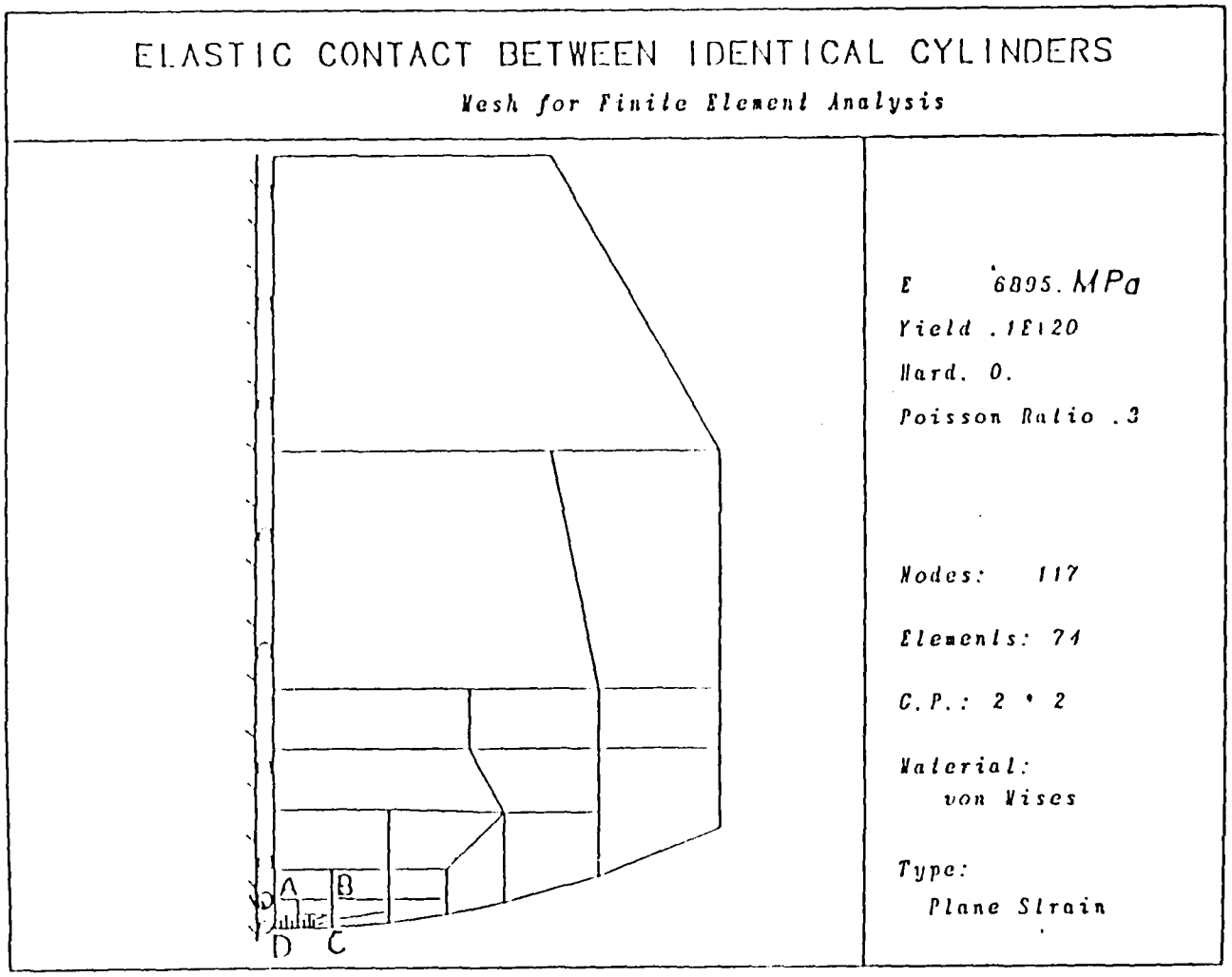

Figure 3.17 ELASTIC CONTACT BETWEEN IDENTICAL CYLINDERS: Mesh for Finite Element Analysis

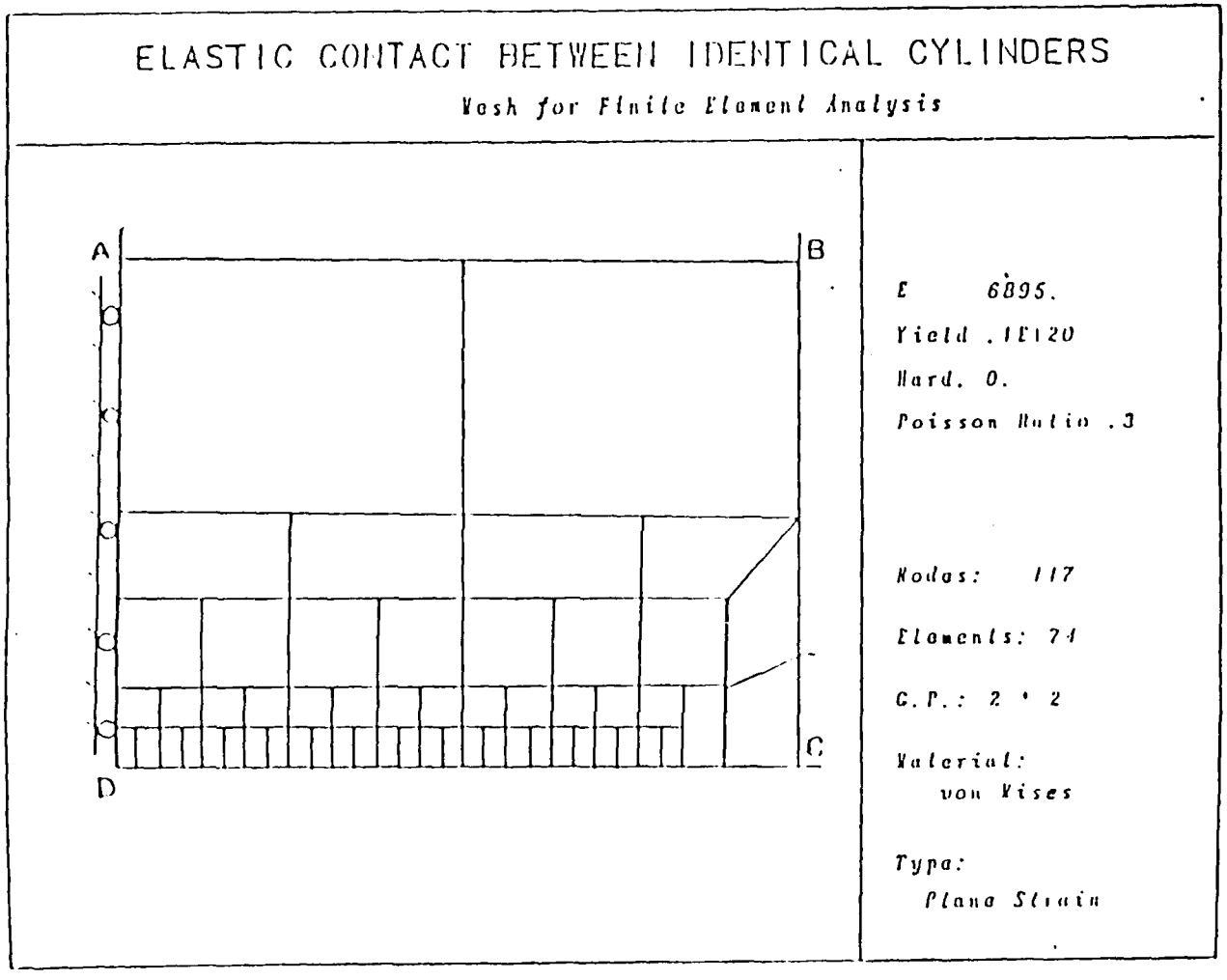

Figure 3.18 ELASTIC CONTACT BETWEEN IDENTICAL CYLINDERS: Mesh for Finite Element Analysis (Section ABCD)

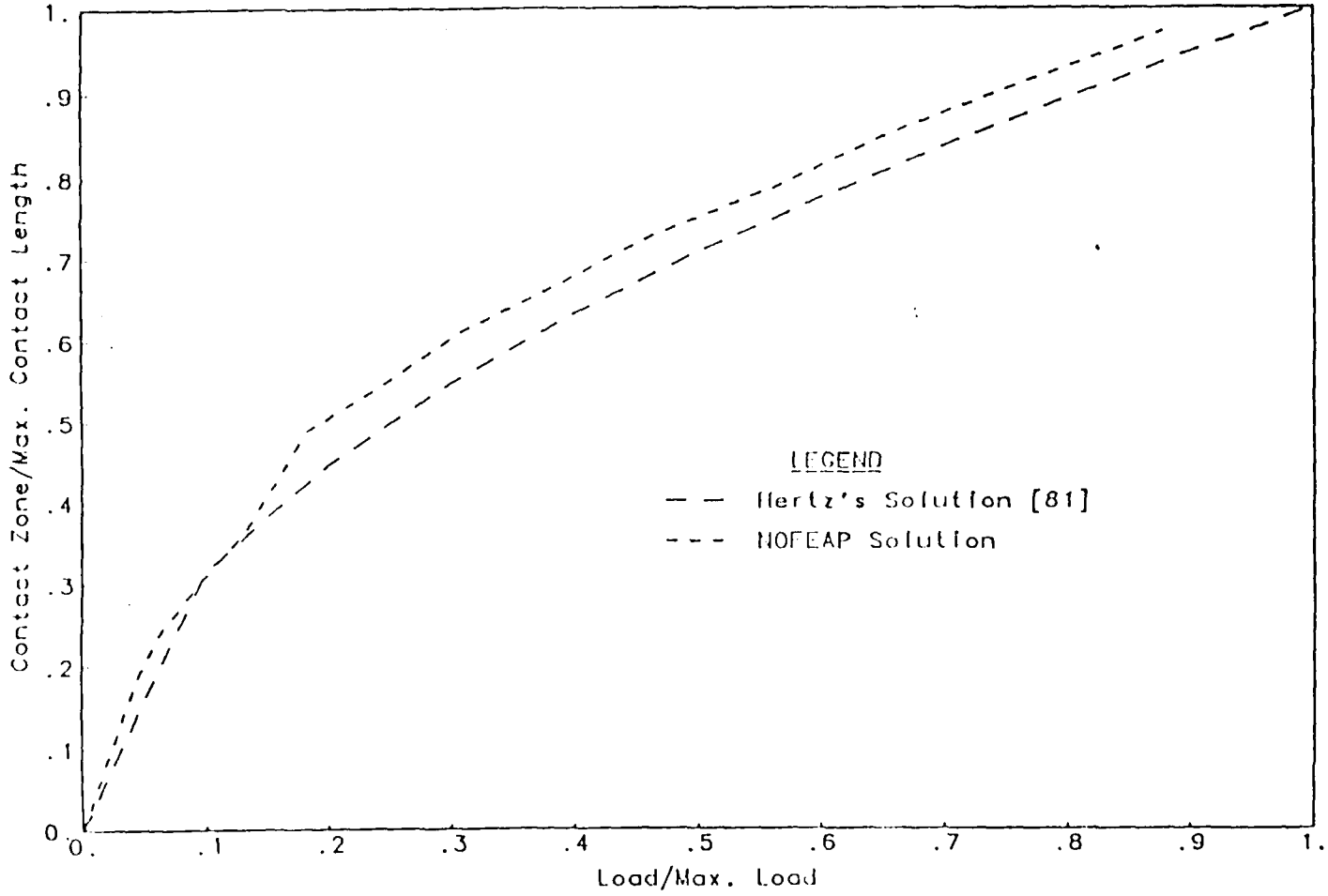

Figure 3.19 LOAD VERSUS CONTACT LENGTH FOR HERTZ CONTACT PROBLEM

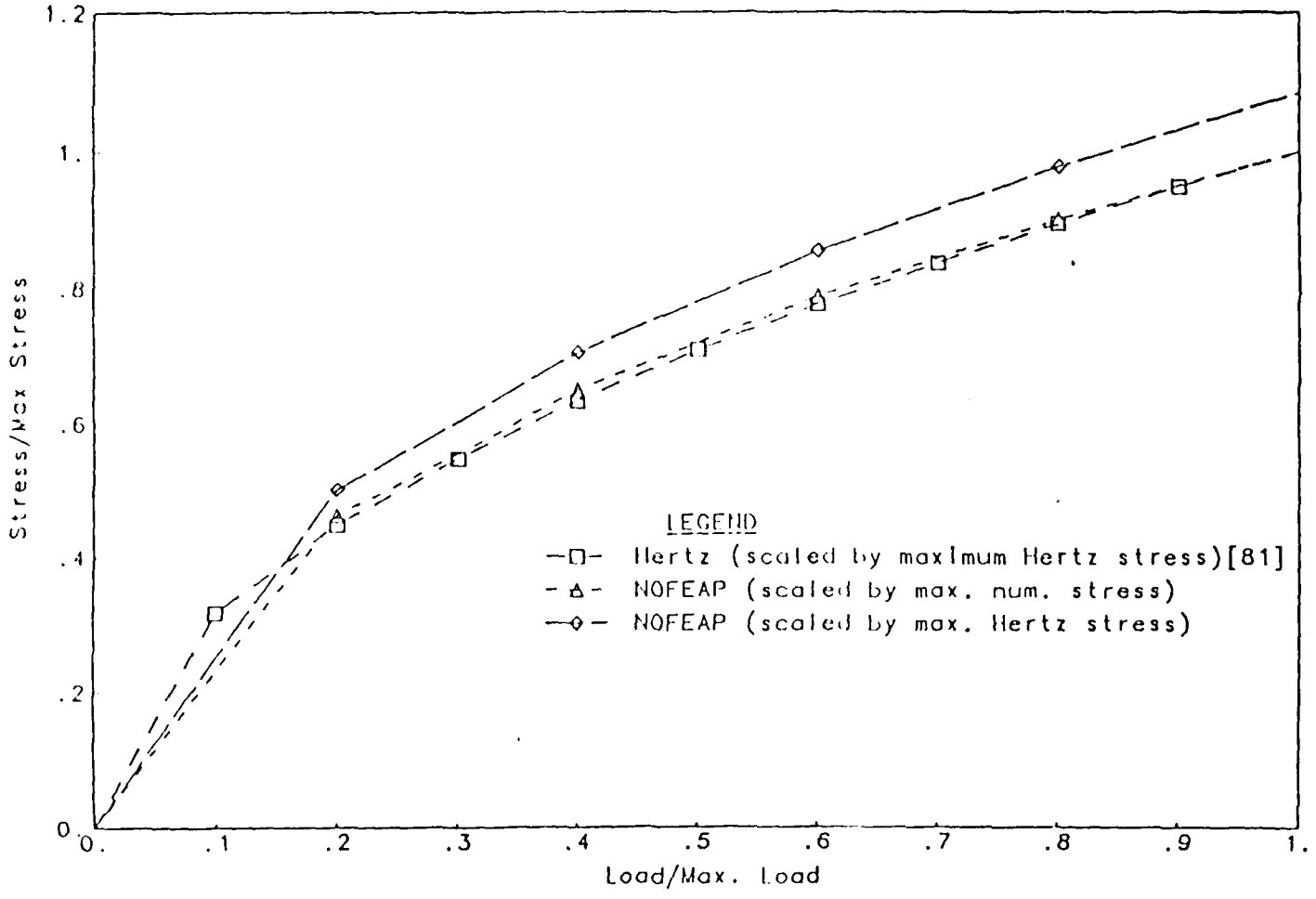

Figure 3.20 LOAD VERSUS CONTACT STRESS FOR HERTZ CONTACT PROBLEM

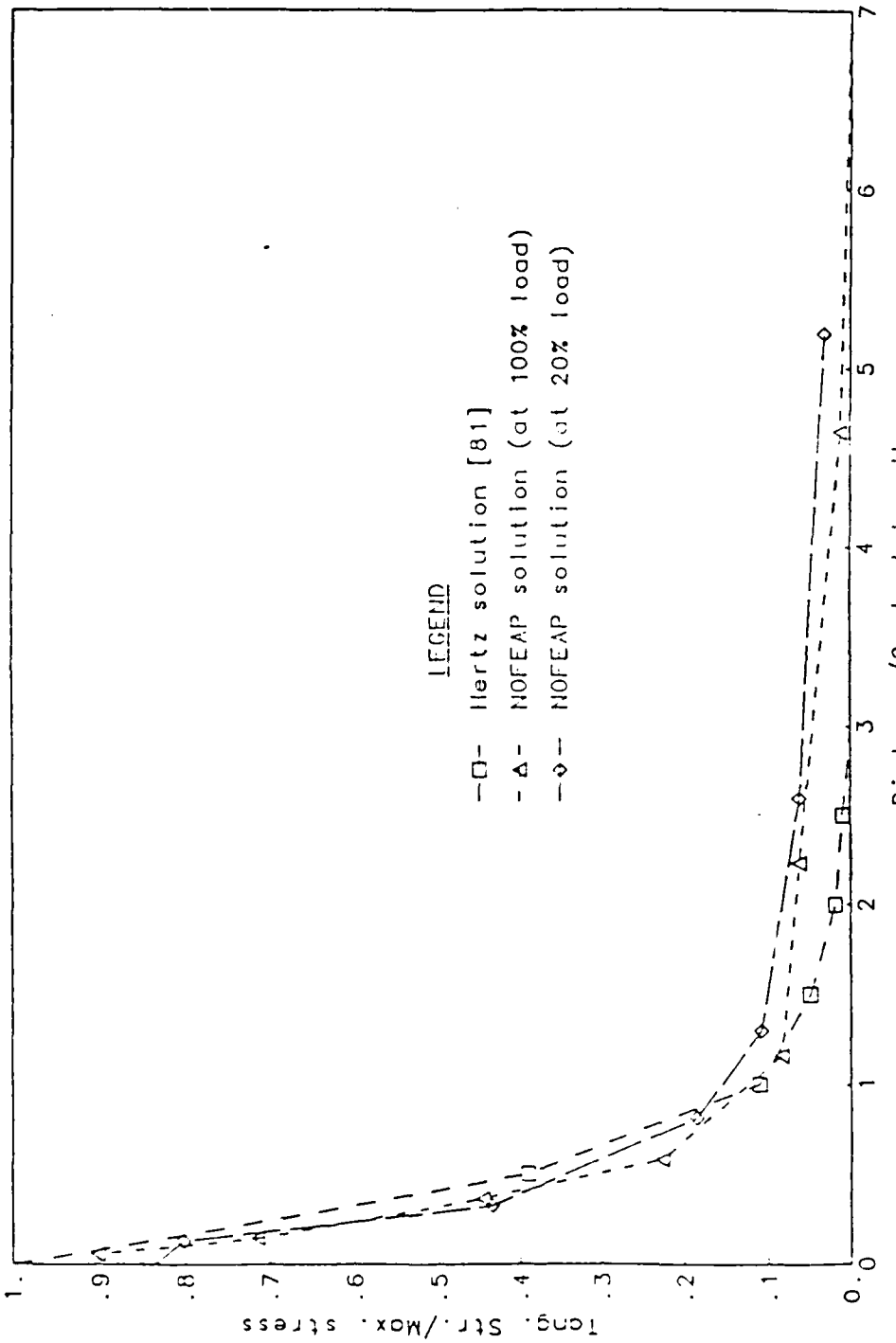

Figure 3.21 VARIATION IN TANGENTIAL STRESS WITH DEPTH FROM CONTACT SURFACE

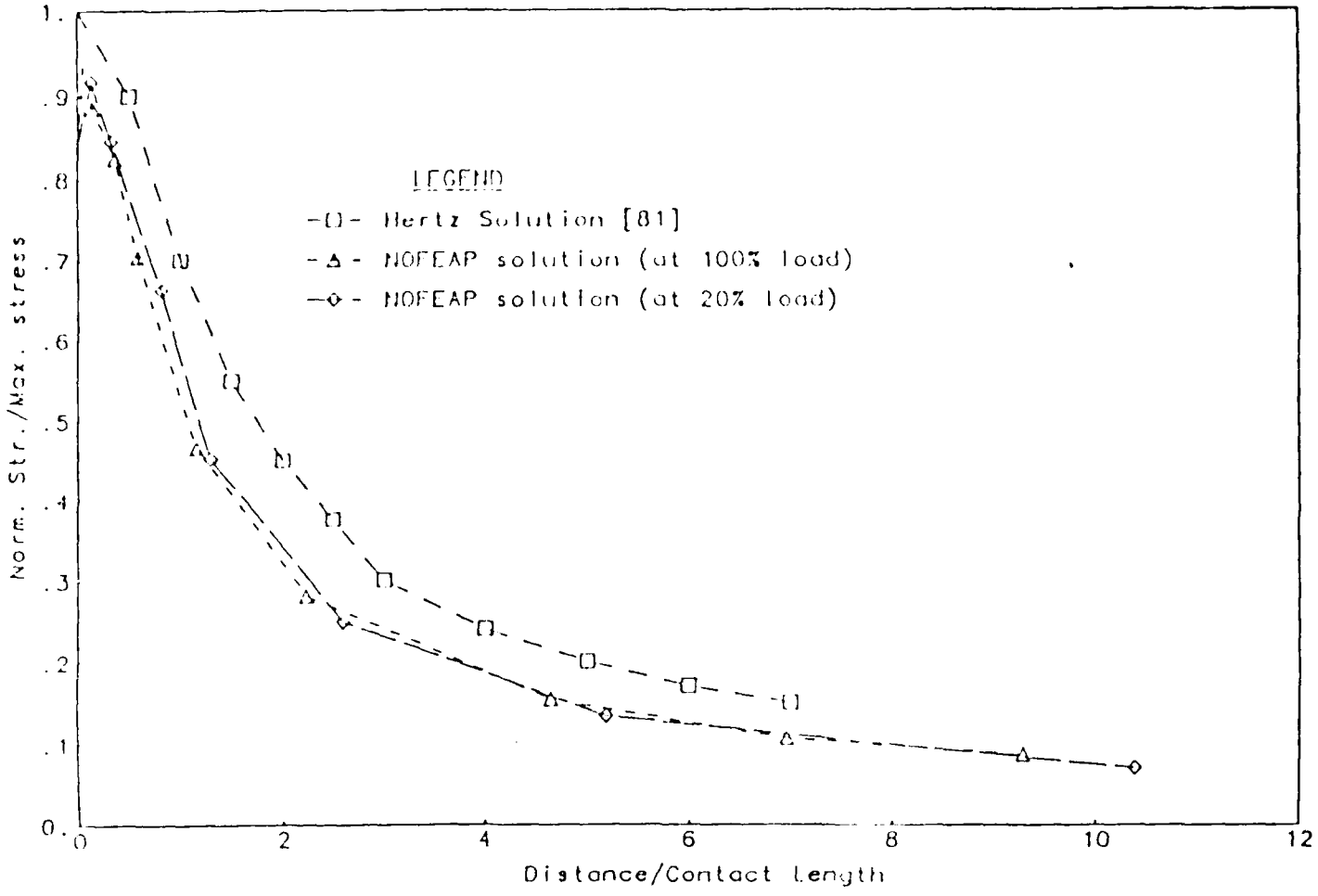

Figure 3.22 VARIATION IN NORMAL STRESS WITH DEPTH FROM CONTACT SURFACE

3.6 An Indentation Problem

The indentation of a cylindrical punch into a flat semi-infinite slab provides a variety of examples. For a frictionless interface between the punch and an elastic slab, the problem can be solved using Hertz's contact theory. The effect of friction along the interface can be studied for indentation into an elastic or elastic-plastic slab. The problem has also been analyzed in detail by Cheng [31]. Various combinations of material and interface properties have been used to provide a number of solutions to the indentation problem. Some of these solutions are presented next.

The same finite element mesh (with 4-node isoparametric elements), Fig 3.23, has been used to solve the different cases of the problem. For an elastic analysis, the yield stress is set to an appropriately high value. The slab is deformed by pushing the cylindrical punch into the slab in steps of 0.025 cm until a maximum indentation equal to half the thickness of the slab is reached.

The elastic deformations and the distribution of effective stresses in the slab are plotted in Fig 3.24 and 3.25 respectively. Similar plots for an elastic-plastic analysis with a non-zero friction coefficient (0.3) are given in Fig 3.26 through 3.28. The main difference in the deformation patterns can be seen along the far edge of the slab. While the elastic slab produces more lifting behavior and less expansion of the edge, the elastic-plastic slab produces more lateral plastic flow than the vertical movement along the edges. That there is significant plastic deformation in the latter case can be confirmed by observing Fig 3.27, which suggests that better than 75% of the slab has permanently deformed. The difference in the effective stress contours (Fig 3.25, 3.28) in the two cases can also be attributed to redistribution of stresses due to plastic flow in the elastic-plastic slab.

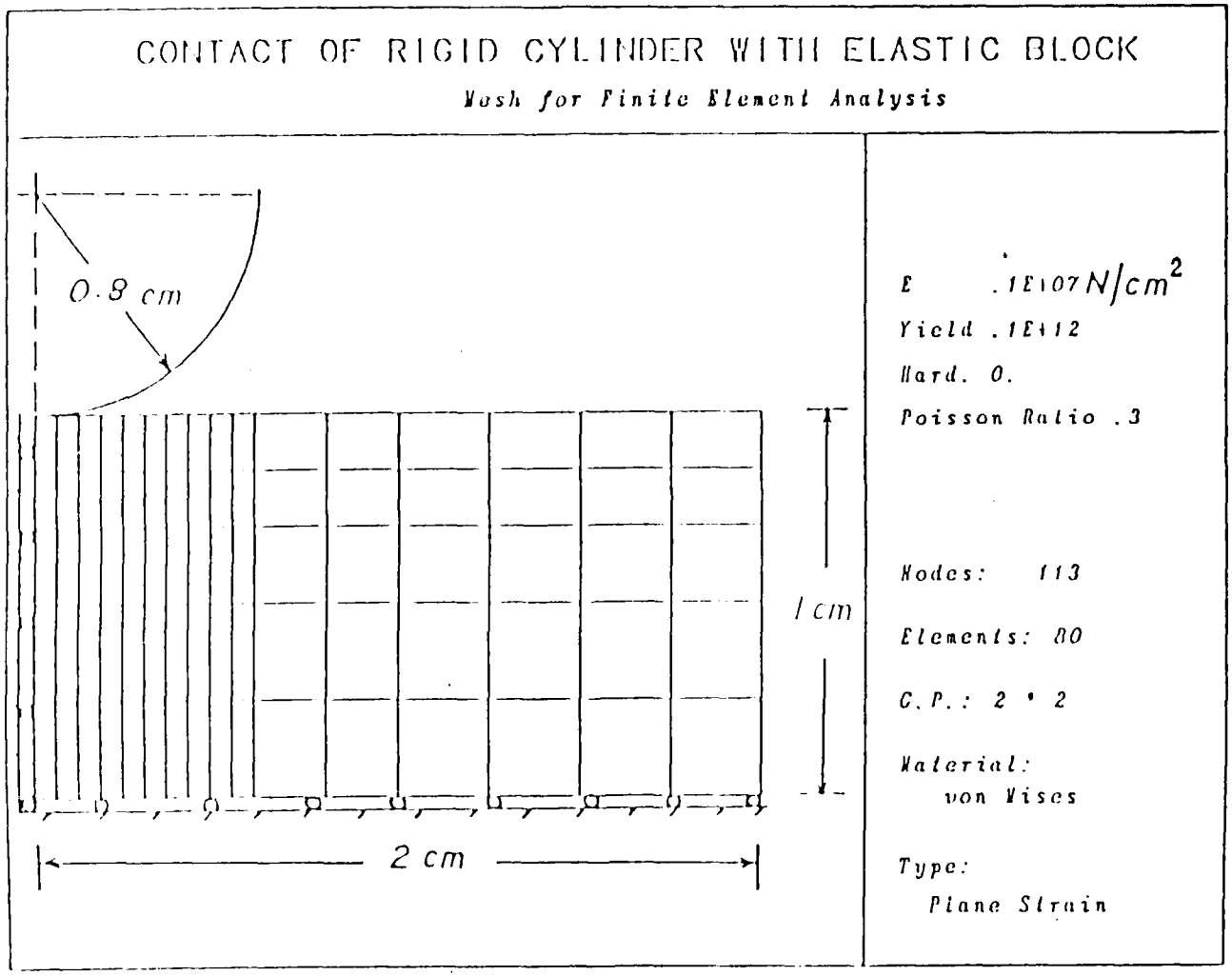

Figure 3.23 CONTACT OF RIGID CYLINDER WITH ELASTIC BLOCK: Mesh for Finite Element Analysis

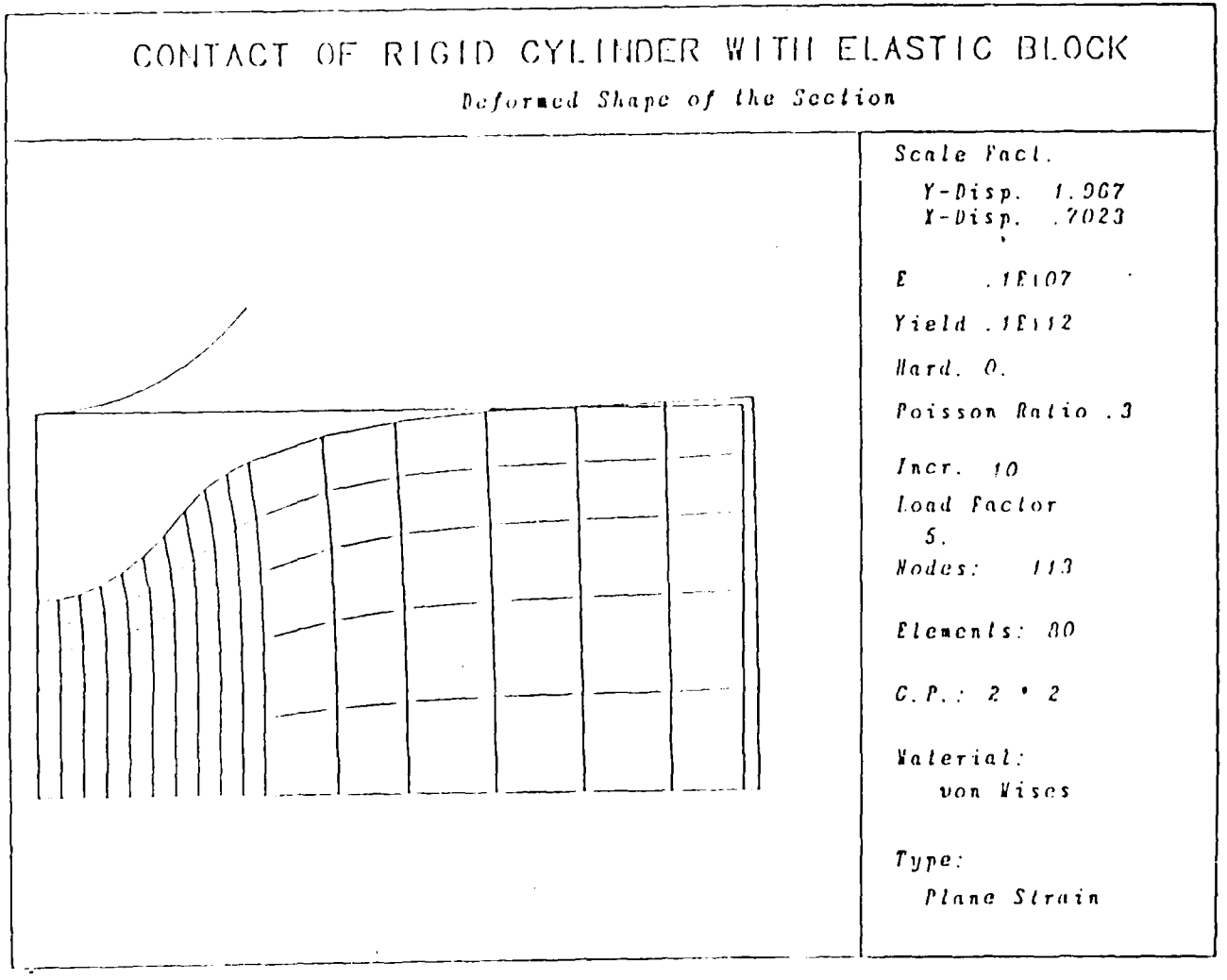

Figure 5.24 CONTACT OF RIGID CYLINDER WITH ELASTIC BLOCK:
Deformed Shape of the Section

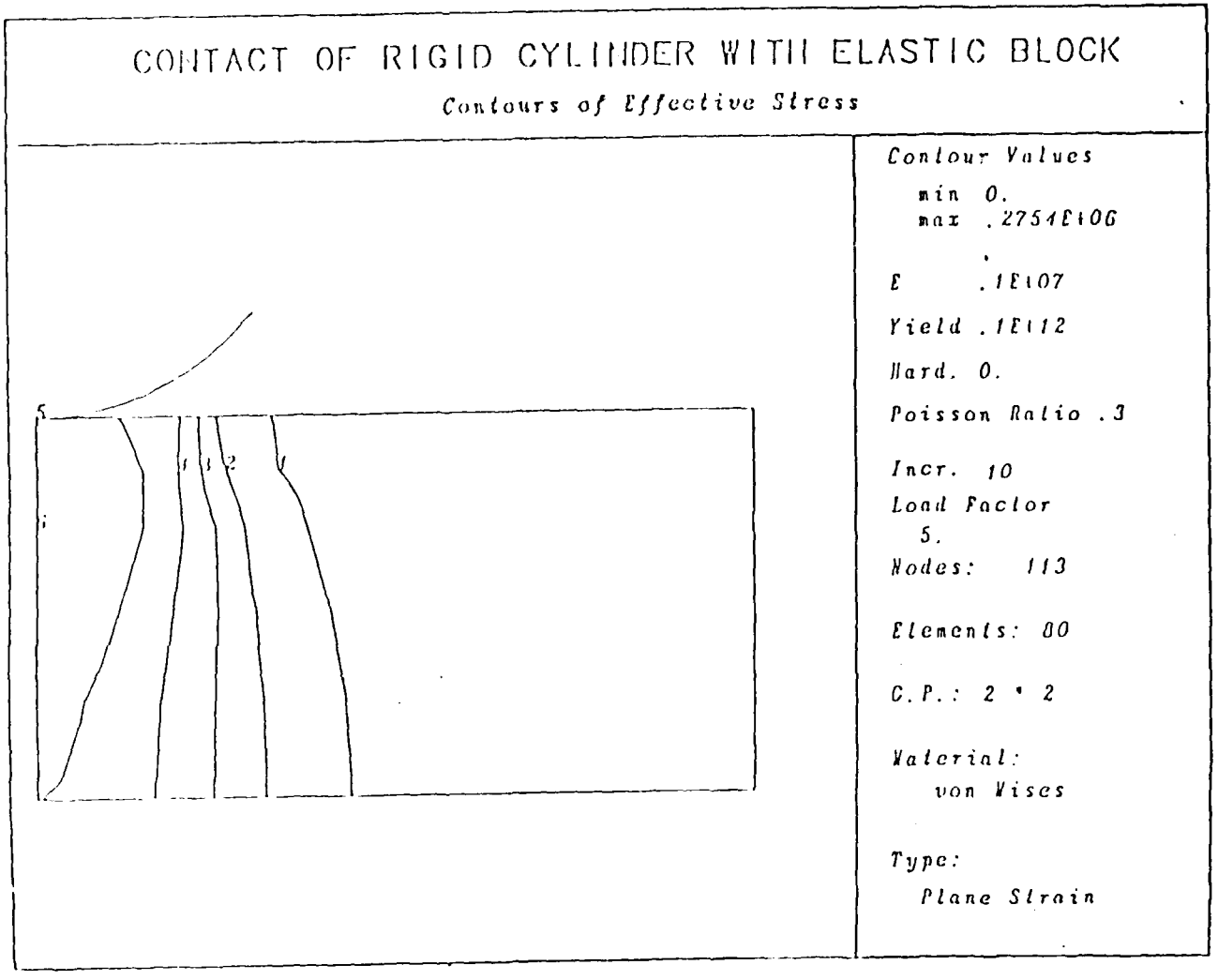

Figure 3.25 CONTACT OF RIGID CYLINDER WITH ELASTIC BLOCK:
Contours of Effective Stress

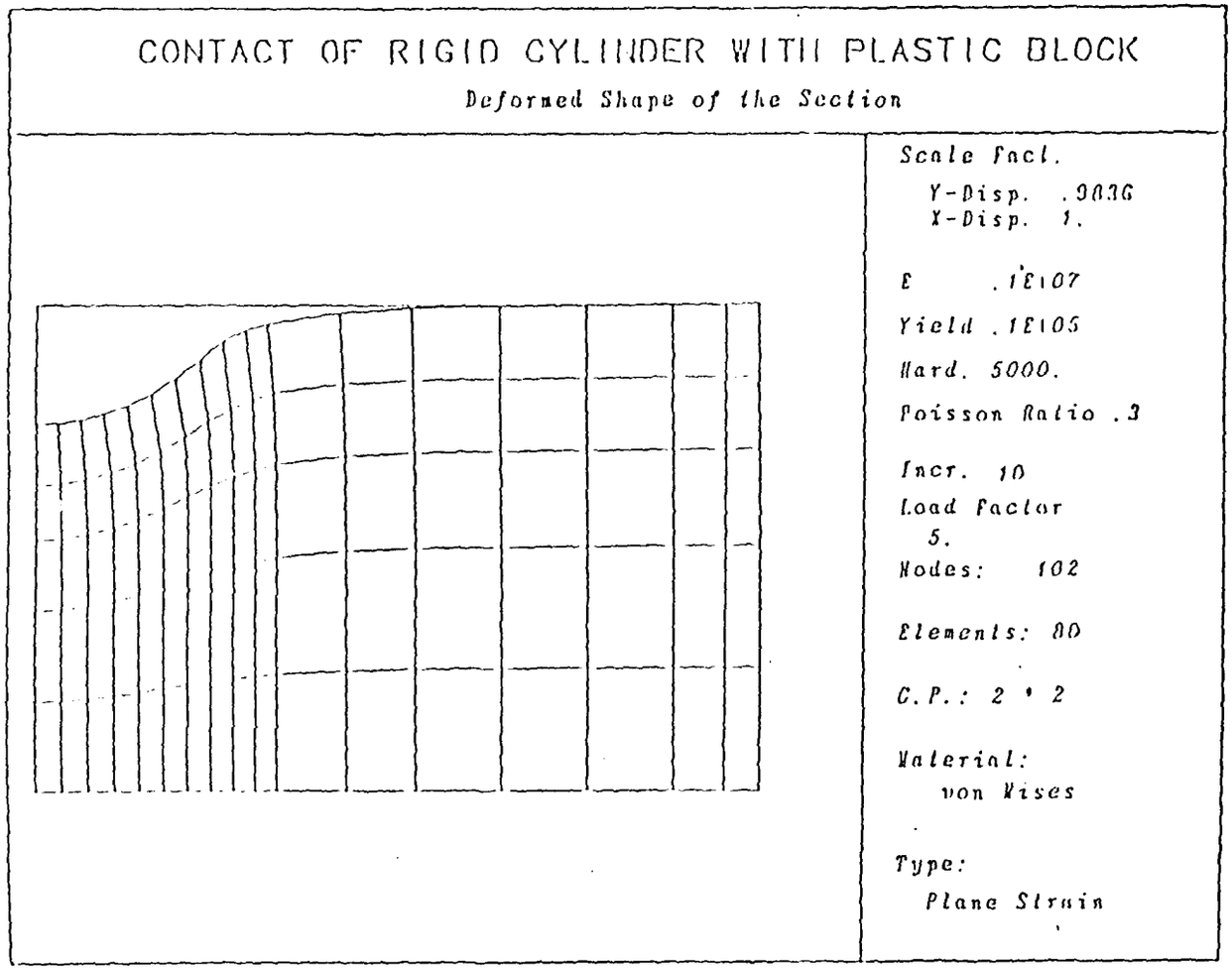

Figure 3.26 CONTACT OF RIGID CYLINDER WITH ELASTIC-PLASTIC BLOCK: Deformed Shape of the Section

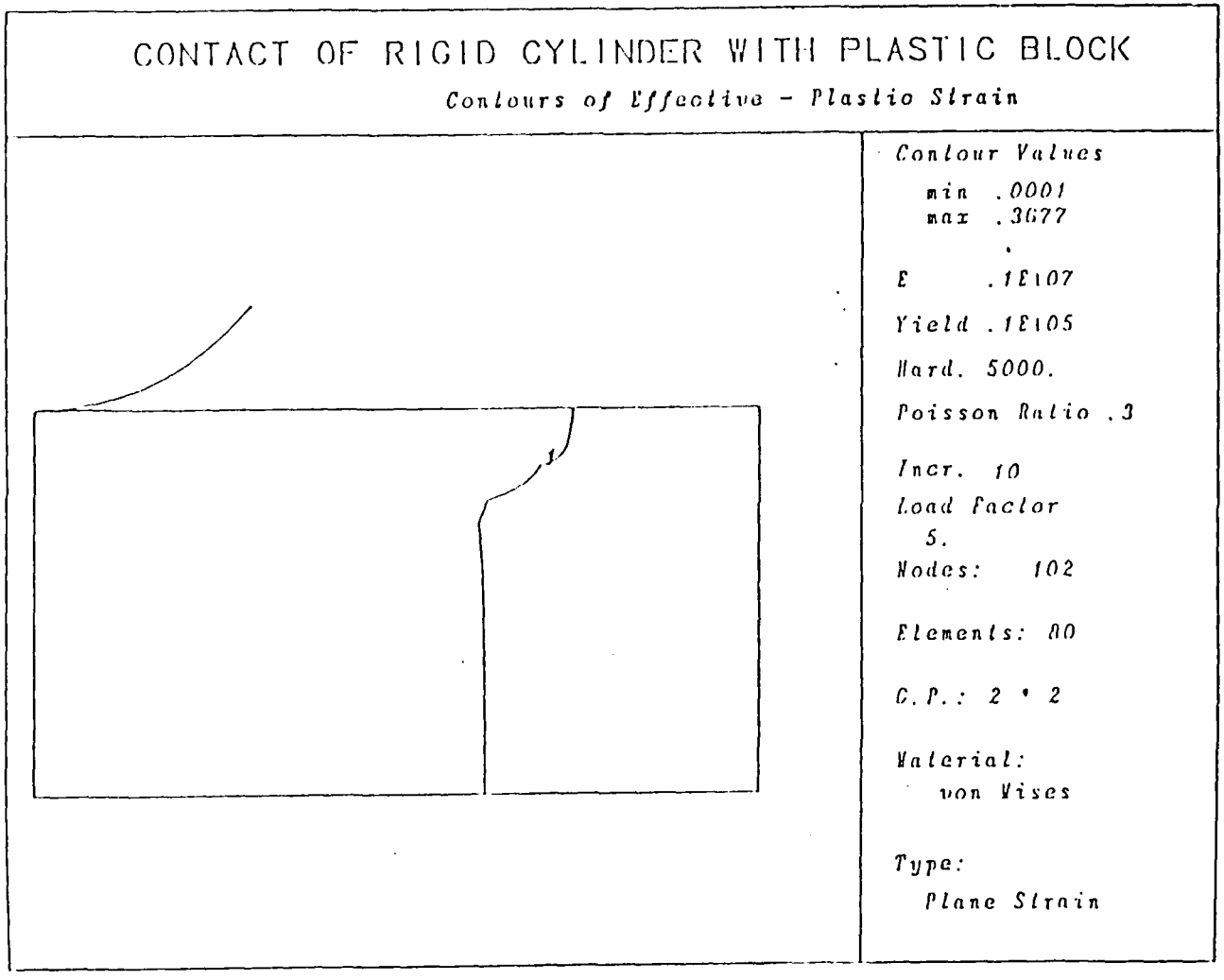

Figure 3.27 CONTACT OF RIGID CYLINDER WITH ELASTIC-PLASTIC BLOCK: Contours of Effective Plastic Strain

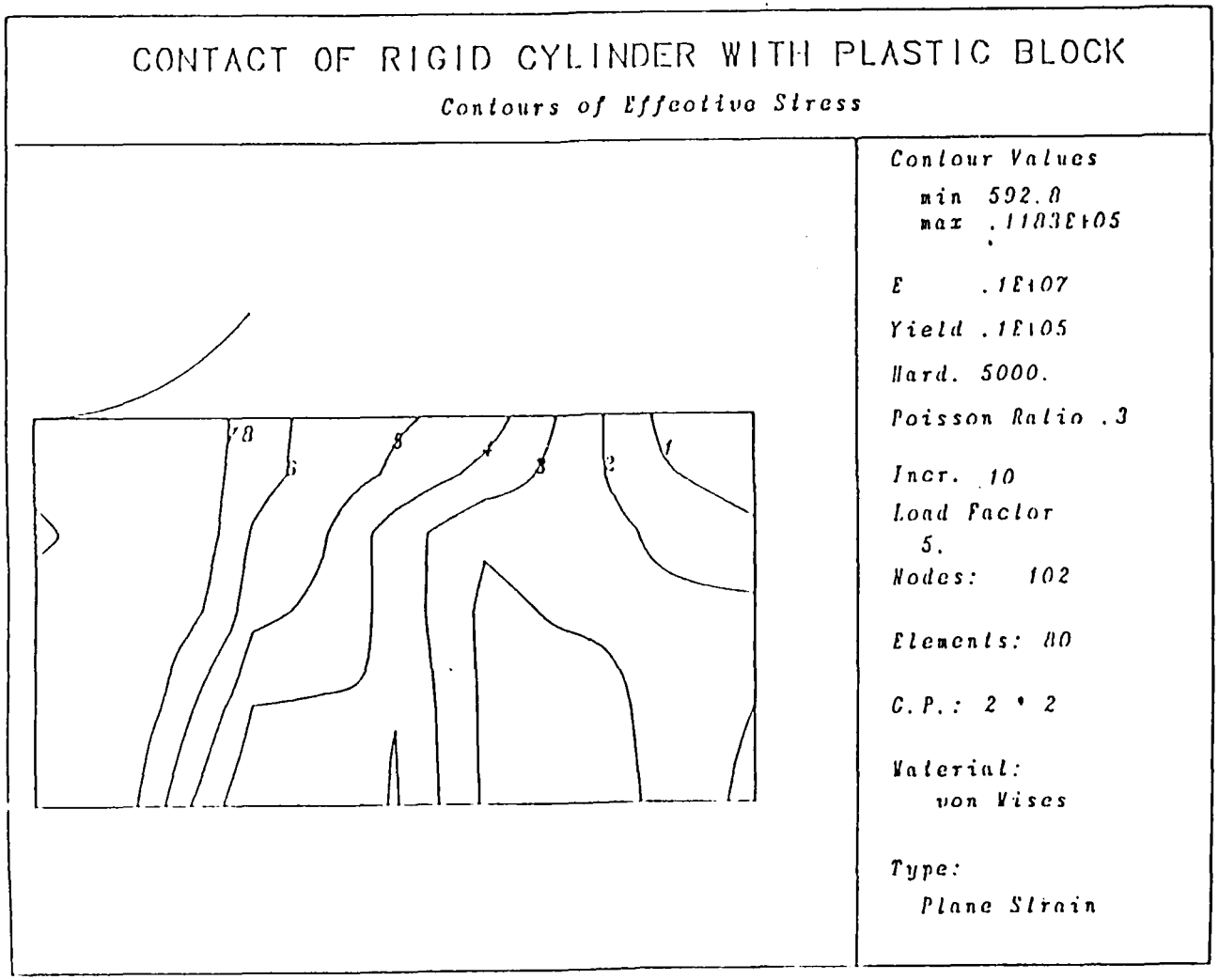

Figure 3.28 CONTACT OF RIGID CYLINDER WITH ELASTIC-PLASTIC BLOCK: Contours of Effective Stress

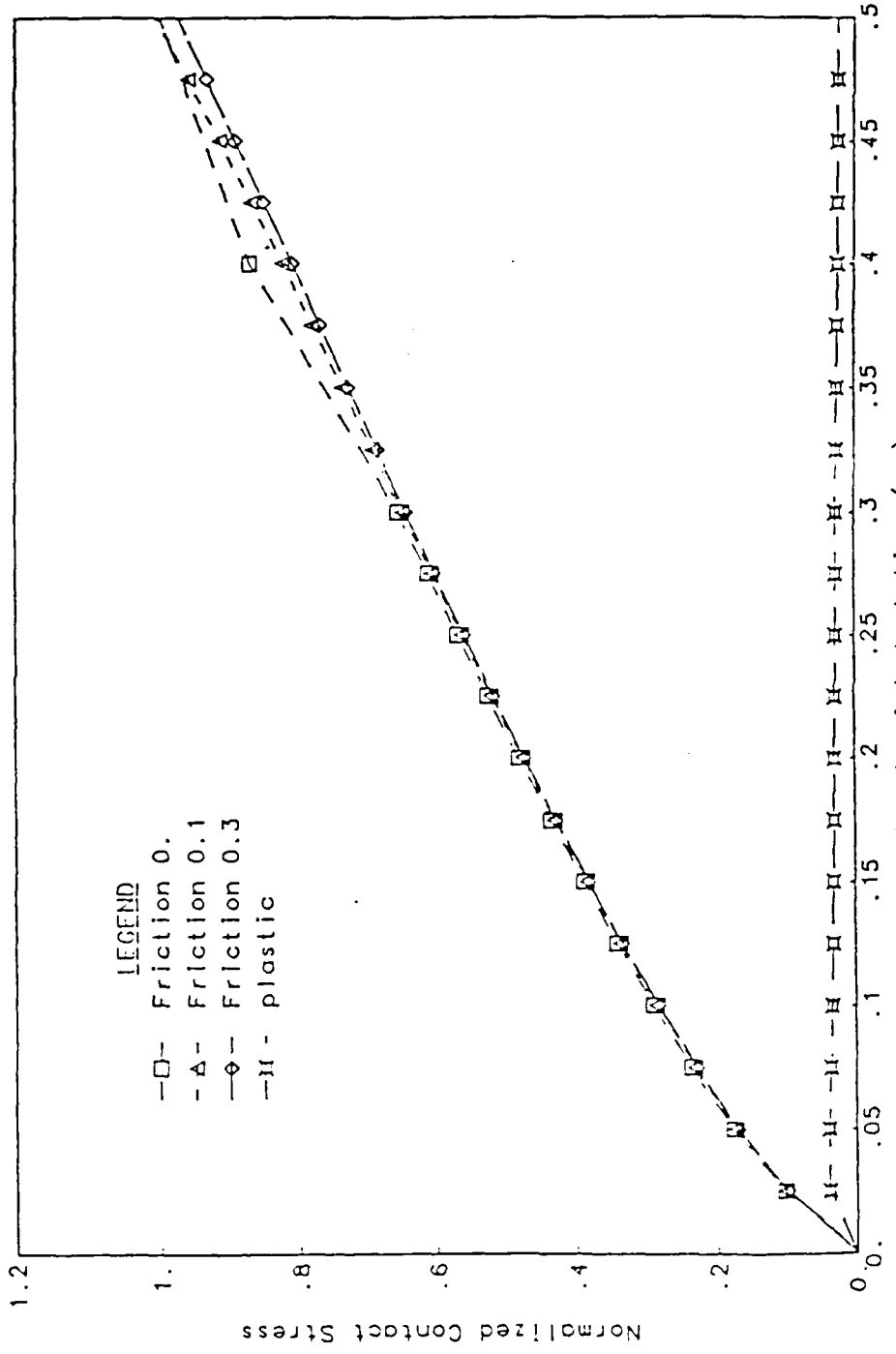

Figure 3.29 MAXIMUM CONTACT STRESS WITH INCREASING INDENTATION

The variation in maximum contact stress (traction) at nodes with increasing depth of indentation is plotted in Fig 3.29. The stresses have been normalized with the maximum normal stress for the frictionless case. Although the difference in frictional and frictionless elastic cases is not significant, all of these produce considerably higher stresses compared to the elastic-plastic slab. The change in contact zone with depth of indentation is shown in Fig 3.30. The effects of friction values, indentation depths and work-hardening properties of the material on contact conditions have been plotted in Fig 3.31. The contact stresses have been normalized with the maximum stress for the first curve in the plots. A high slope of hardening curve produces a significant increase in both contact stresses and contact length. Increasing the friction coefficient along the interface produces higher stressess without affecting the contact zone.

The contact zone for plastic contact is, expectedly, higher than that for elastic contact. The frictionless, elastic solutions are plotted with the Hertzian solutions [82] in Fig 3.32. The agreement between the numerical and analytical contact lengths and stresses is fairly good. The solutions of Cheng [31] have not been reproduced here for a number of reasons. Cheng's solutions have been found to differ from the computed NOFEAP (and Hertzian) solutions by a significant factor. However, Cheng has produced plots of contact stresses versus contact length which shows an exact match with Hertzian solution, even for contact lengths of the order of 65% of the punch radius. According to the hypothesis of Hertz's theory [82], the theoretical derivation may be used provided that the surface of contact is very small compared to the radii of curvature of the contacting bodies and as long as the surface of contact is along a plane tangent to the two contacting bodies. Clearly, both these constraints are no longer satisfied for large contact zones in the indentation problem. With these observations in mind, Cheng's solution is

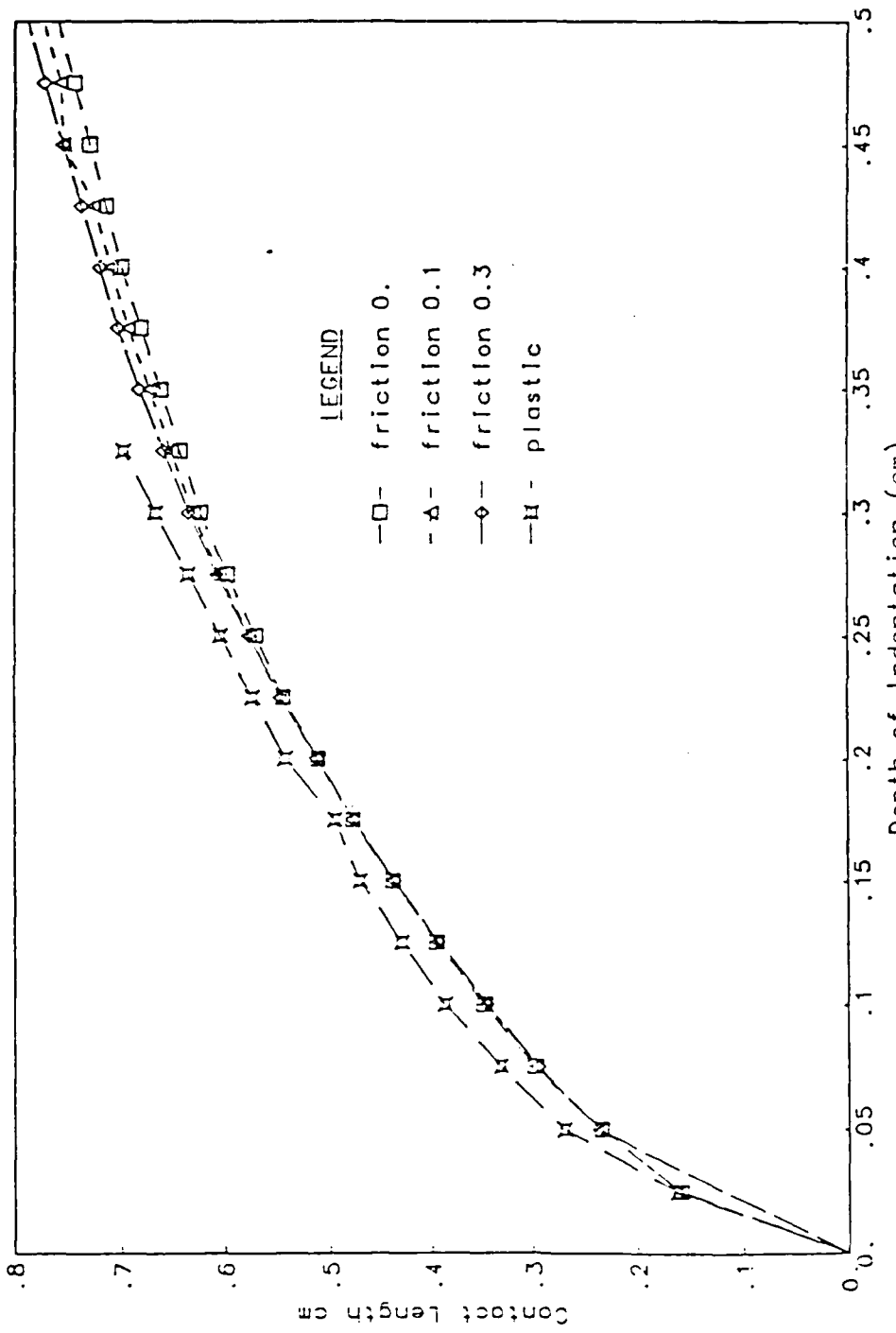

Figure 3.30 CONTACT LENGTH WITH INCREASING INDENTATION

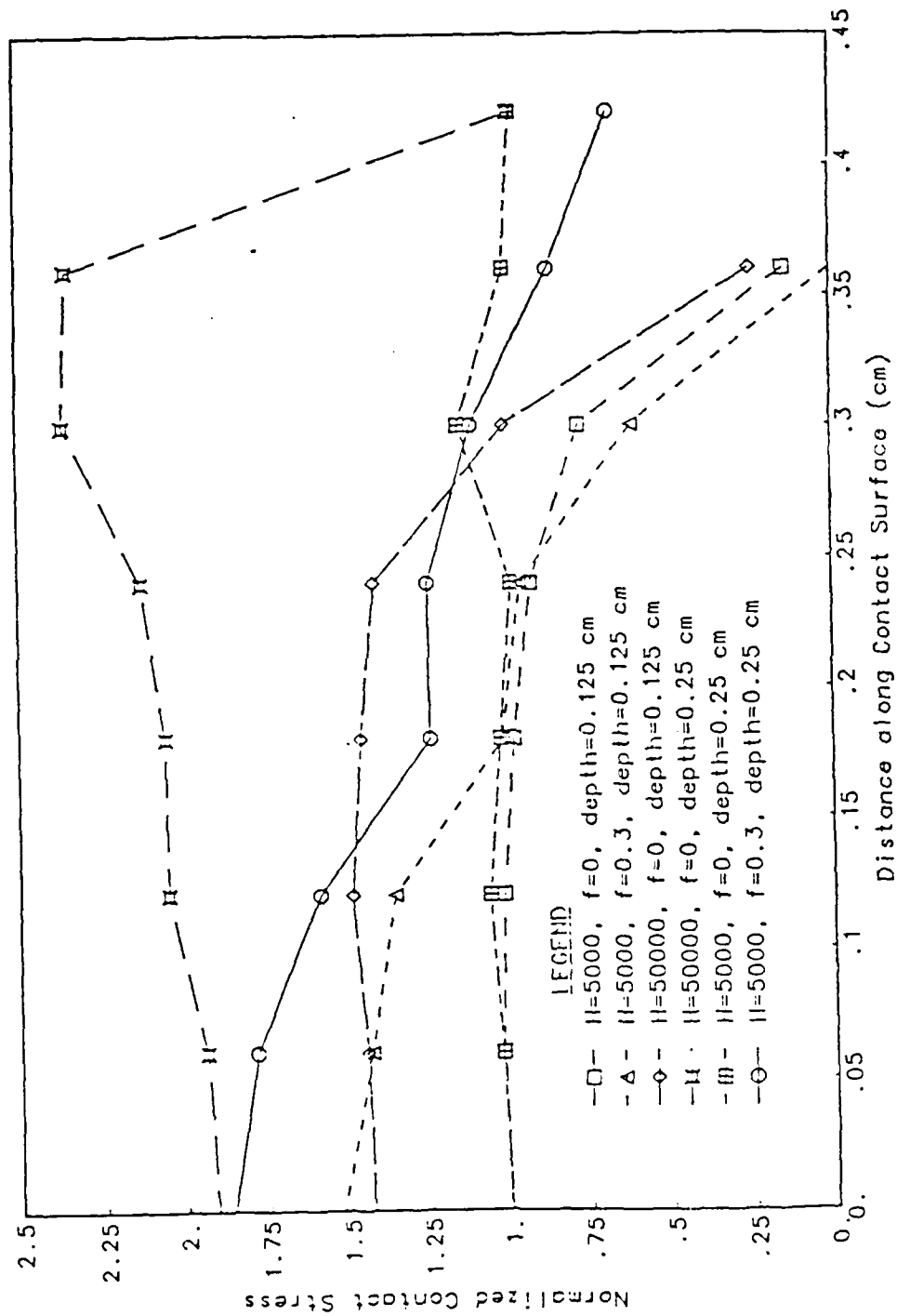

Figure 3.31 CONTACT STRESS ALONG CONTACT SURFACE FOR PLASTIC INDENTATION

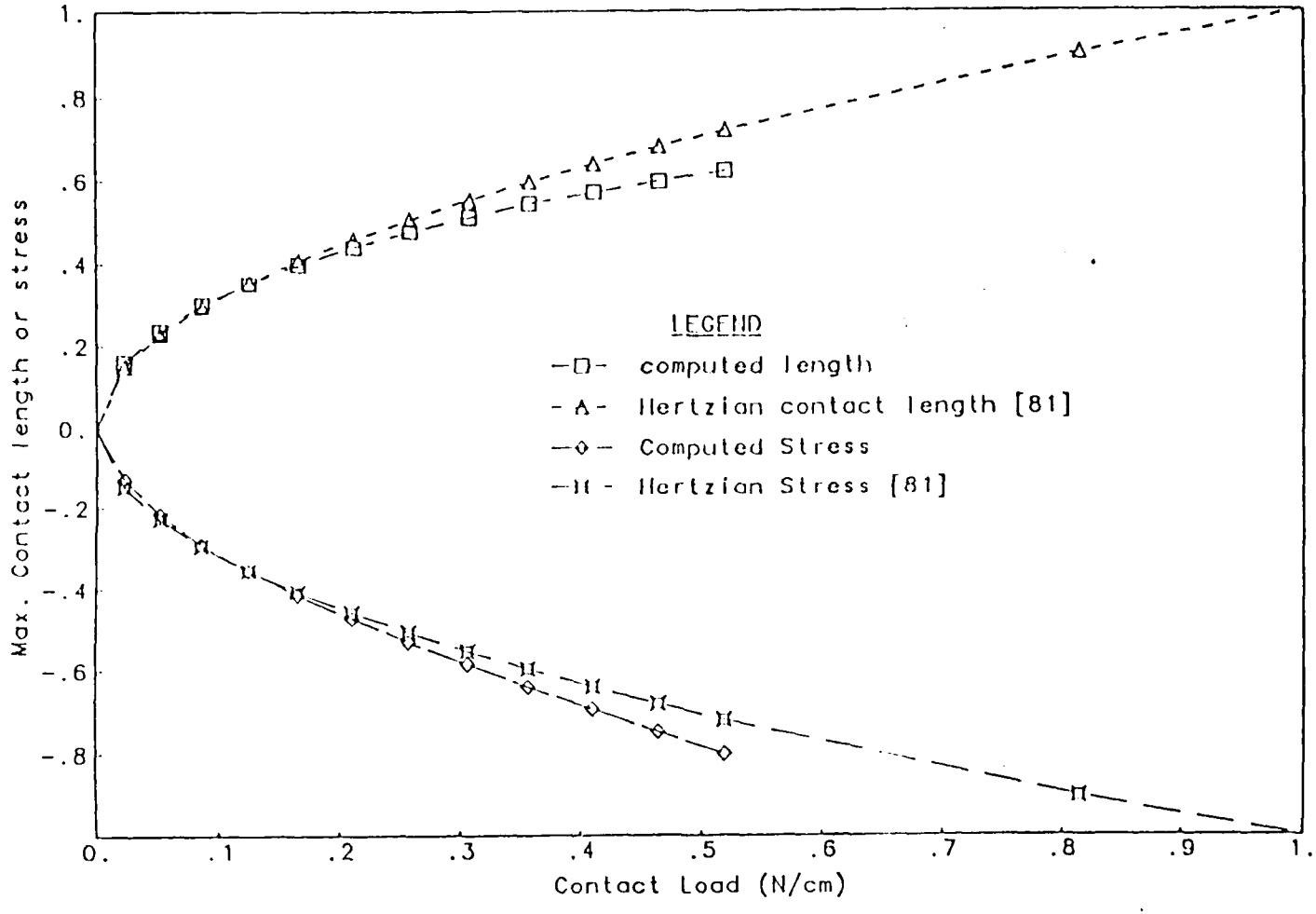

Figure 3.32 VARIATION IN CONTACT LENGTH AND STRESSES FOR ELASTIC CONTACT

not consistent with the Hertzian theory, and therefore, those results have not been included for comparison in this thesis.

The examples given in the previous sections compare the non-linear formulations, individually and in combinations, with available numerical, analytical and experimental calculations. Several other problems, such as stretching of a necked or perforated specimen, large deflection of a spherical shell, elastic contact between a crankshaft and a pin, etc., have been solved using NOFEAP and the results have been found to be satisfactory. The next example combines all three non-linearities into one problem to demonstrate the application of NOFEAP to a metal forming process.

3.7 Head Forming Process

The head forming process is characterized by large plastic deformations coupled with contact conditions at the die-workpiece interface. The finite element mesh, shown in Fig 3.33, is used for two separate cases with both frictionless and perfectly sticking friction conditions at the top surface. The frictionless case also assumed a frictionless die, while non-zero friction coefficient has been used at the horizontal die with no-slip conditions at the top of cylinder. The head is formed by reducing the height of the cylinder in steps of 0.25% of the initial height for 160 steps. The material properties of the cylinder are assumed to be the following: modulus of elasticity = 200 GPa, yield stress = 700 MPa, secondary modulus = 300 MPa, and Poisson's ratio = 0.3.

The deformed shape of the cylinder for no-stick and no-slip conditions at the top interface are shown in Fig 3.34 and 3.35 respectively. In the frictionless case, the top surface expands laterally indicating that the punch radius is assumed to be much larger than the radius of the cylinder. For the no-slip case, however,

the punch and the cylinder are assumed to be of the same radius, permitting the bulging of the cylinder, as shown in Fig 3.35.

The load-deflection curve for the two cases are shown in Fig 3.36. The load is computed from the reactions at the top of the cylinder. The two curves separate when the cylinder first makes contact with the horizontal part of the die. The frictionless cylinder, as expected, requires less force to reach a deformation state than the rough cylinder. Finally, the contact forces, for the two cases at the horizontal part of the die, are plotted in Fig 3.37. The friction force, at the horizontal die, for the no-slip case causes excess force to be required as shown in Fig 3.36.

The examples given in the previous sections verify various non-linear formulations in NOFEAP and also demonstrate the applicability of the program to metal forming processes. The next chapter presents a model of the rolling process and presents the analyses of deformations in rolling cylinders and gear teeth.

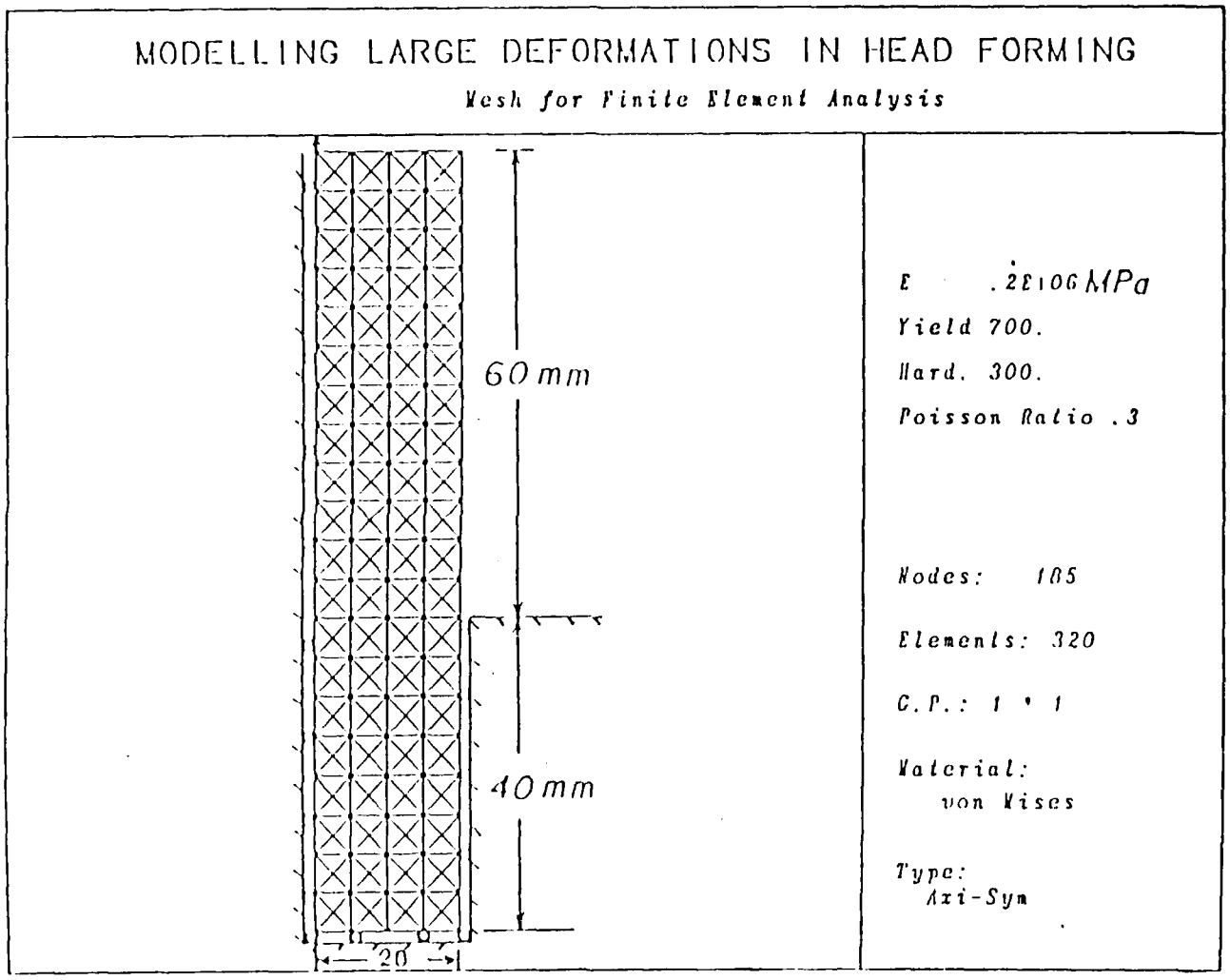

Figure 3.33 MODELLING LARGE DEFORMATIONS IN HEAD FORMING:
Mesh for Finite Element Analysis

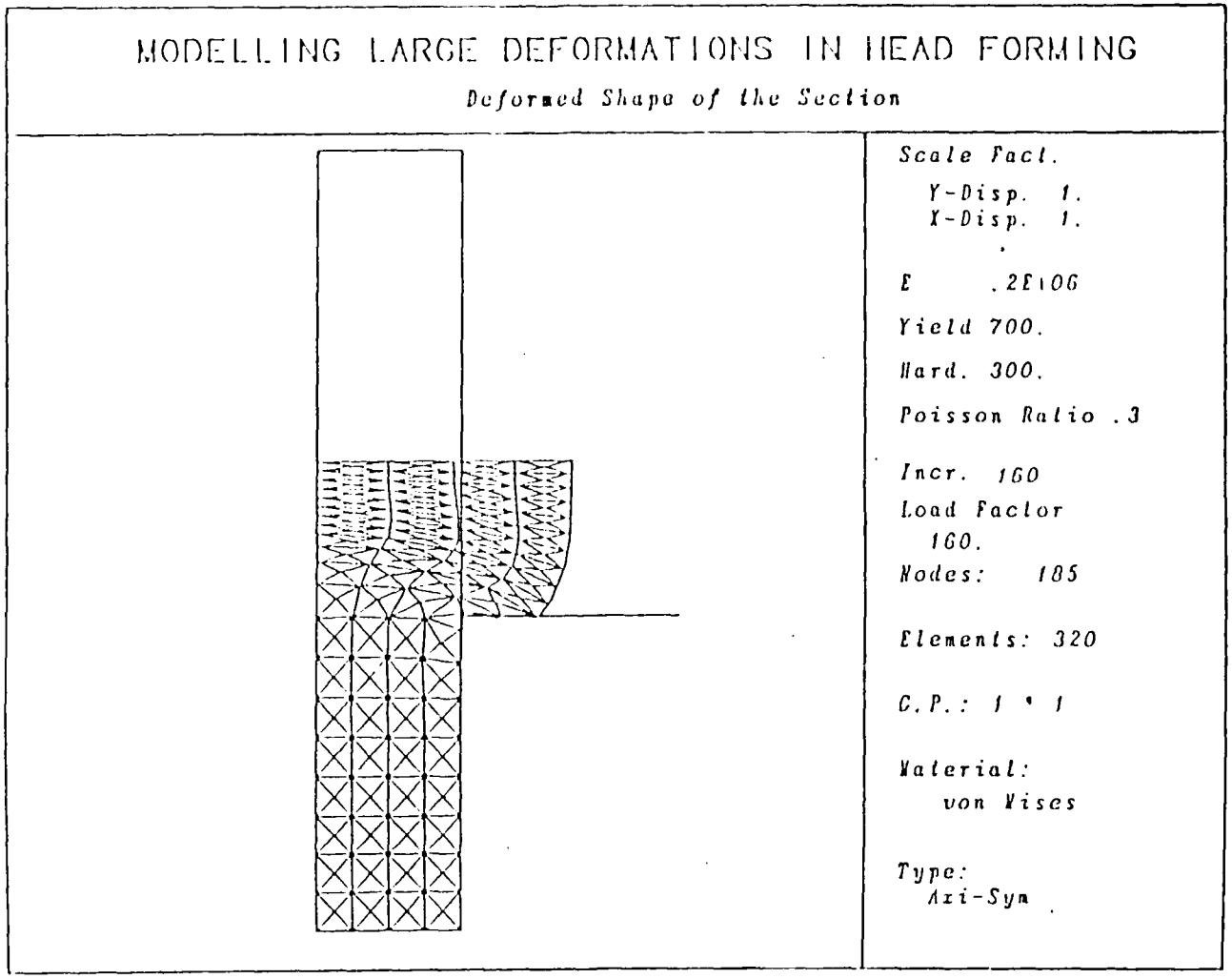

Figure 3.34 MODELLING LARGE DEFORMATIONS IN HEAD FORMING:
Deformed Shape of the Section for Frictionless Surface

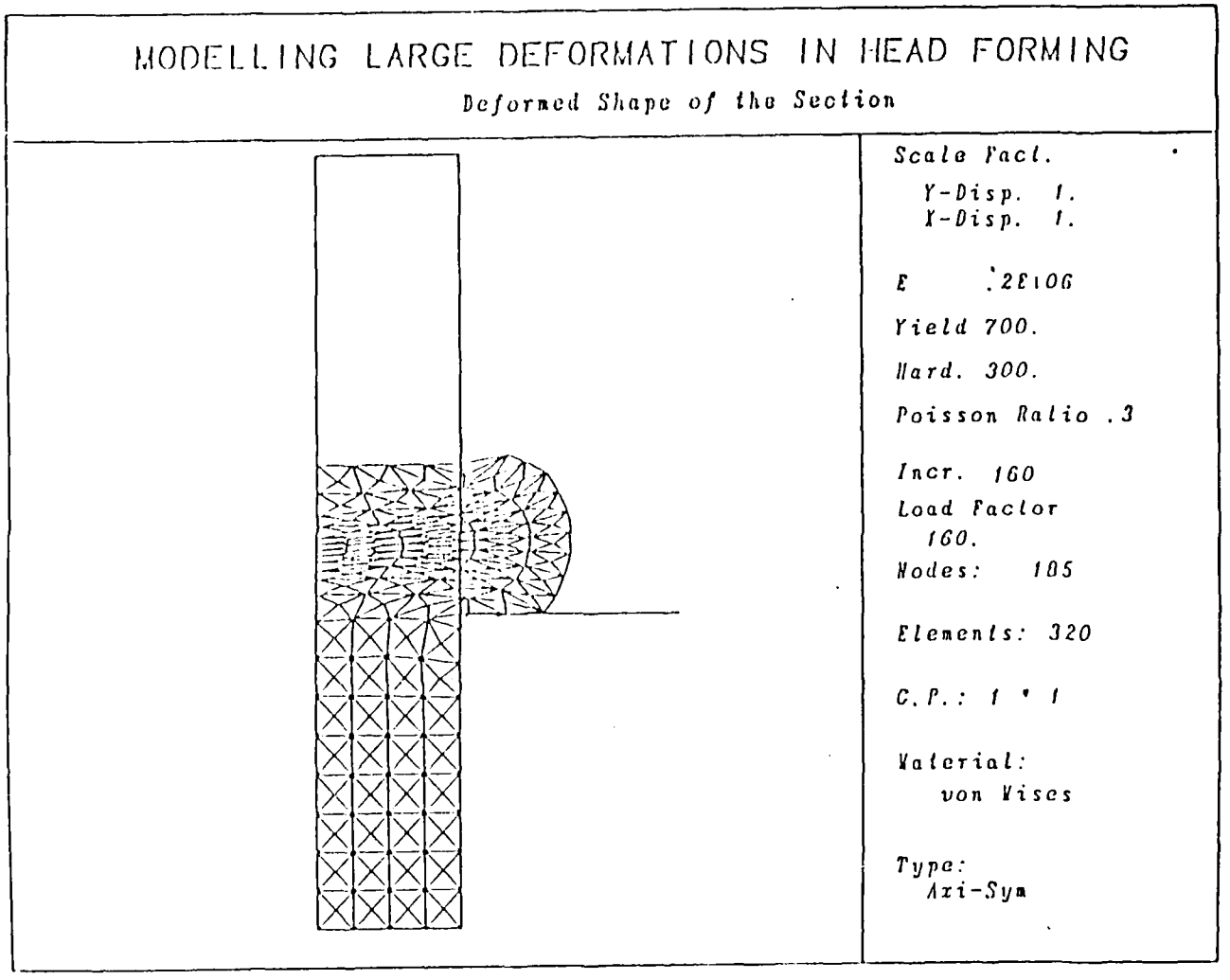

Figure 3.35 MODELLING LARGE DEFORMATIONS IN HEAD FORMING:
Deformed Shape of the Section for Sticking Contact

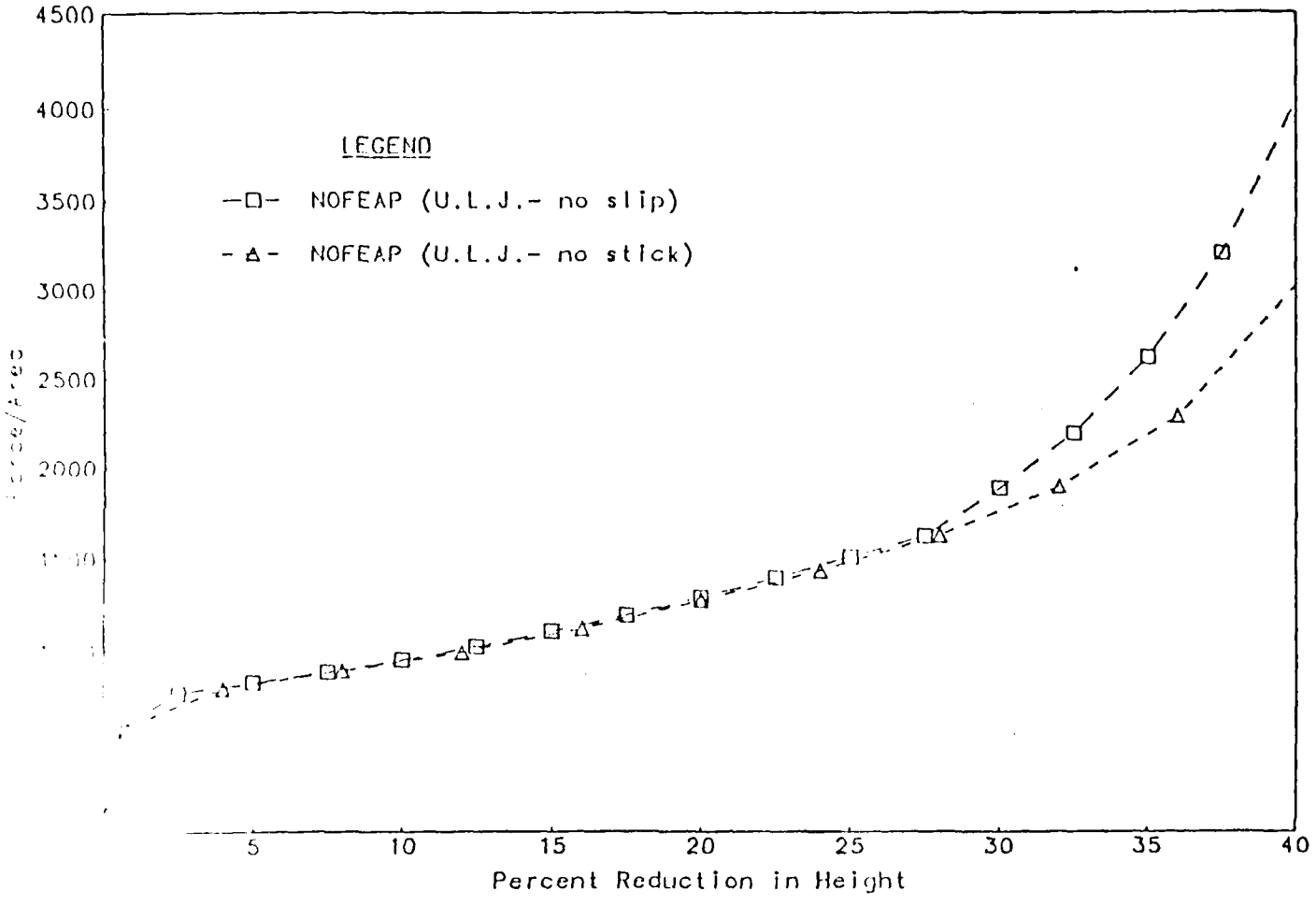

LOAD VERSUS REDUCTION CURVE FOR HEAD FORMING PROCESS

AD-A187 576 FINITE ELEMENT MODELLING OF LARGE PLASTIC STRAINS IN A ROLLING CONTACT ME..(U) PENNSYLVANIA STATE UNIV STATE COLLEGE APPLIED RESEARCH LAB S N KHER ET AL. AUG 87 2/2

UNCLASSIFIED TR-87-004 F/G 20/11 NL

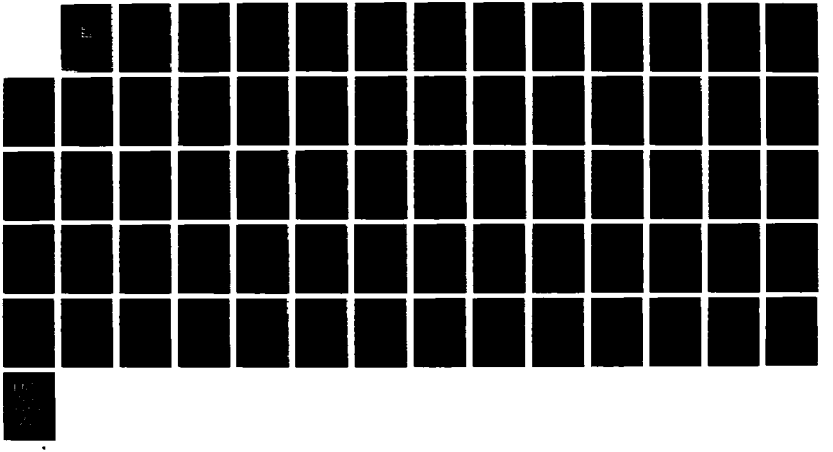

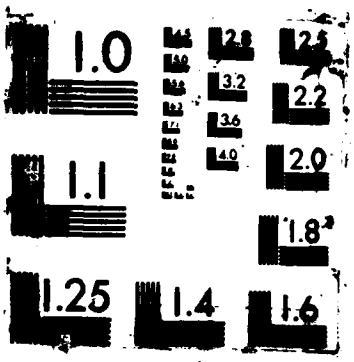
1.0
1.1
1.25
1.4
1.6
1.8
2.0
2.2
2.5
2.8
3.2
3.6
4.0

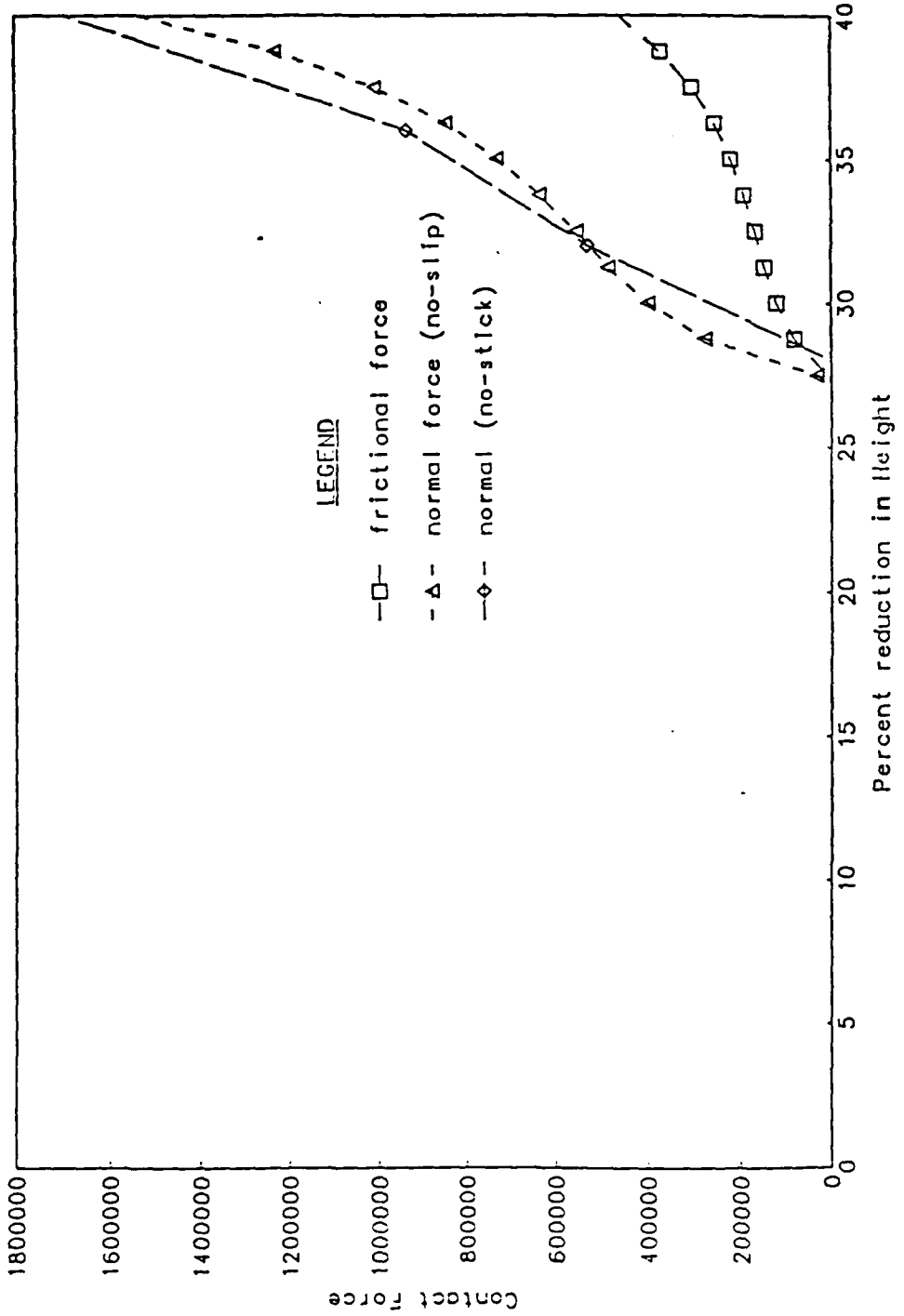

Figure 3.37 CONTACT FORCES IN HEAD FORMING PROCESS

Chapter 4

MODELLING THE AUSROLLING PROCESS

Previous chapters have discussed the characteristics of ausrolling and the mathematics of the non-linear formulations necessary to represent the plastic flow in ausrolling. This chapter addresses the remaining critical feature, from a numerical point of view, of ausrolling which is the rolling process. A model of the rolling process, included in the NOFEAP program, is explained in the next sections. The effectiveness of the solution algorithm for modelling deformations in a disk subjected to rolling loads is compared to some experimental observations in the subsequent sections. The deformations in a gear tooth, when the gear is rolled against a hard die, are modelled using NOFEAP. These results are presented in the last section of this chapter.

4.1 A Model of the Rolling Process

A numerical model of the sheet metal rolling processes has been attempted by several authors. A method of using estimated pressure values at the roll-sheet interface [9] has been popular due to its simplicity. Another approach by Bhargava [10,11] simulates rolling by translating a semi-elliptic pressure distribution along the surface of a flat workpiece. The advantage offered by the simplicity of the method is lost when an attempt is made to apply the method to modelling plastic deformations of a curved, possibly complex surface. Therefore, the rolling process is modelled in NOFEAP using some geometric and kinematic considerations.

Consider two cylinders, of radii R_D and R_G respectively, tangent to a common plane as shown in Figure 4.1. The subscripts D and G refer to the die and the deformable body, i.e., the workpiece gear respectively. The two circles of Figure 4.1 may be taken to represent the pitch circles of two mating gears, and the cylinders

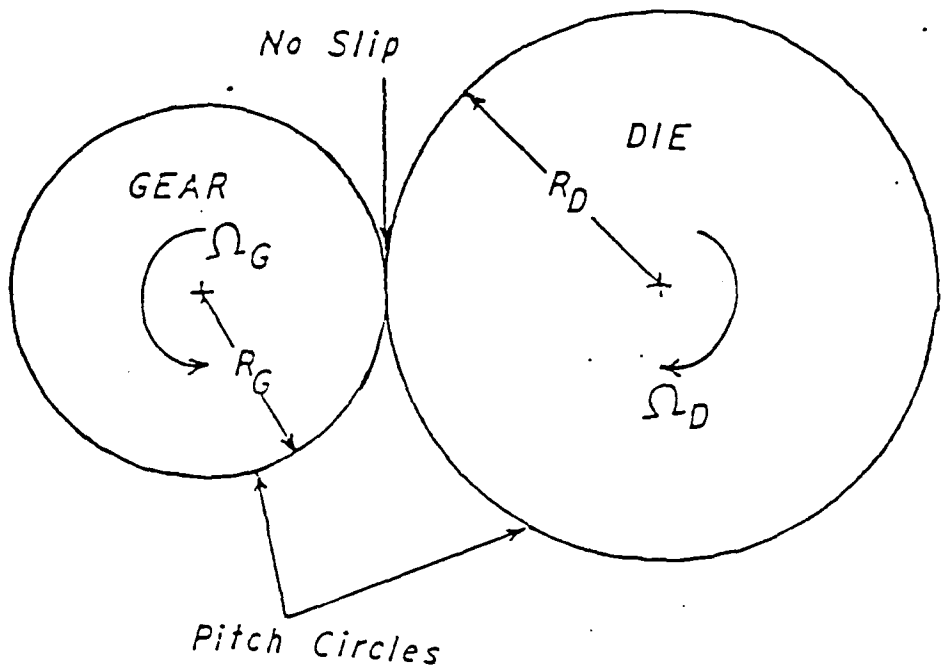

Figure 4.1 ILLUSTRATION OF ROLLING CYLINDERS

will henceforth be referred to as the gear and the die. Assuming no slipping along the surface, the speeds of rotation, Ω_D and Ω_G, of the die and the gear are related by the following constraint:

$$\Omega_D * R_D = \Omega_G * R_G. \tag{4.1}$$

so that the distance travelled along the circumference of the two cylinders is the same at any time. If the rotational degree of freedom (DOF) of the gear G is constrained while the translational as well as the rotational DOF of the die D is unconstrained, a rotation of the die with no associated slip will also result in a translation of D along the circumference of the gear resulting in a planetary gear motion (Figure 4.2). If the angle travelled along the circumference of the gear is taken to be θ_G, the die undergoes two mutually separable motions: (1) a rigid body translation of the gear as it is rotated about the center of the gear by an angle θ_G, and (2) a rigid body rotation of the die about its own center by an angle θ_D given by

$$\theta_D = \left(\frac{R_D + R_G}{R_D}\right) * \theta_G. \tag{4.2}$$

This concept is used in NOFEAP to model the rolling process. The gear is assumed to be non-rotating while the die revolves around its own axis as well as the axis of the gear. The model, although exceedingly simple in concept, has provided satisfactory results with the total angle of rotation θ_G applied in small enough increments as shown in the following sections.

Since the angle of secondary rotation, θ_D, is a function of the radii of the gear and the die, by changing the radii, rolling about varying surfaces can be simulated.

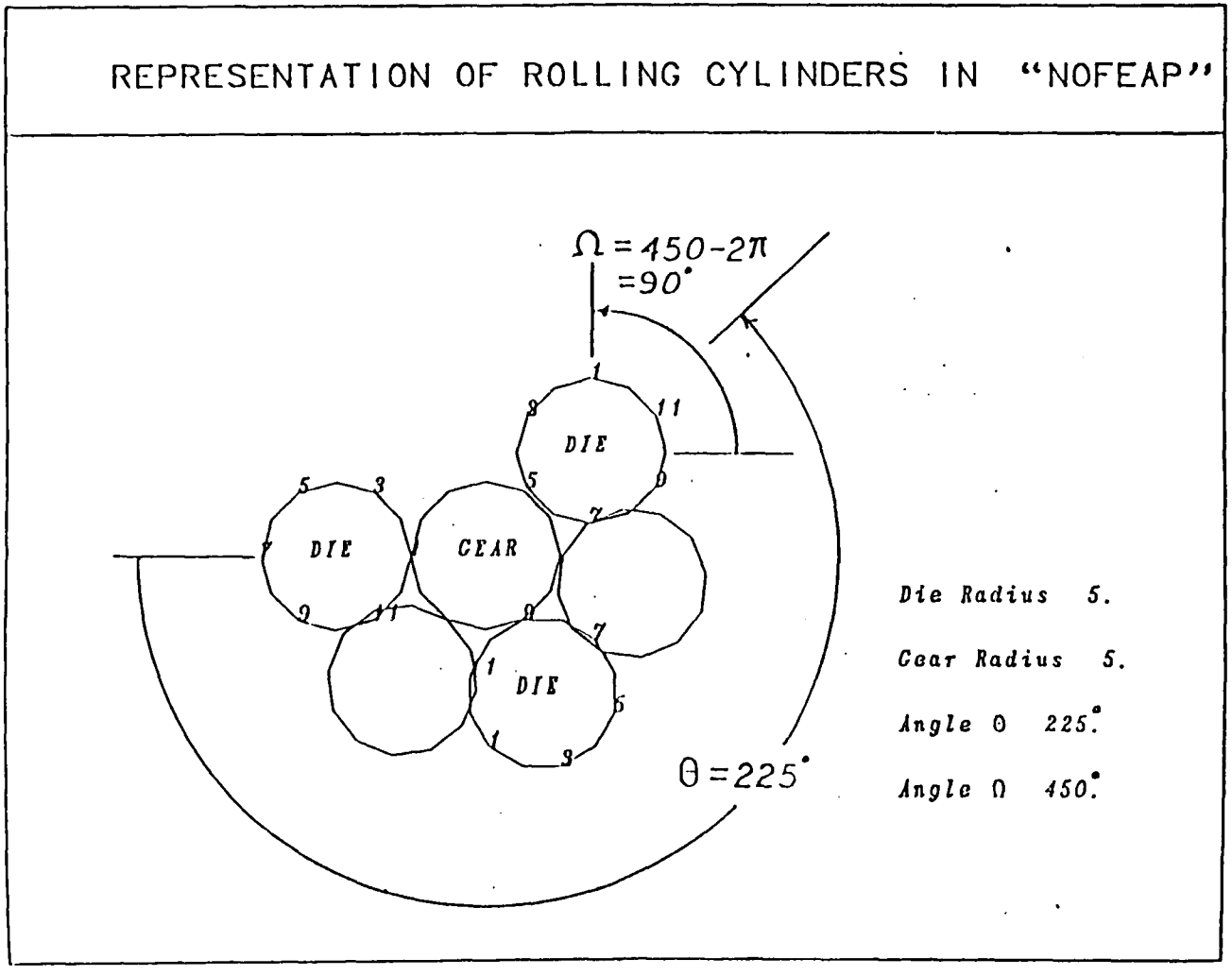

Figure 4.2 REPRESENTATION OF ROLLING CYLINDERS IN ''NOFEAP''

Another simple modification could be the introduction of slipping at the interface by defining the secondary angle by

$$\theta_D = \beta\Big(\frac{R_D + R_G}{R_D}\Big)\theta_G + (1-\beta)\theta_S. \tag{4.3}$$

where $0 \leq \beta \leq 1$ can be used to allow conditions ranging from pure rolling ($\beta = 1$) to pure slipping ($\beta = 0$), and θ_S, the angle of slipping, taken as an independent parameter. This correction has not been introduced in NOFEAP, since pure rolling condition at some radius is ensured in gear rolling.

This model of the rolling process, coupled with the non-linear formulations of Chapter 2, has been used to analyze deformations in a disk subjected to rolling loads. This cumulative model is compared to experimental observations as given in the next section.

4.2 Study of Disk-Rolling

In order to test the model of rolling process, the numerical results have been compared with experimental tests of rolled aluminum disks. The next section describes the experimental procedure which is followed by a description of the numerical simulation of disk-rolling.

4.2.1 Experimental Procedure and Results

A number of experimental rolling tests have been conducted on Aluminum 6061 disks using a round-faced carbon steel die and a flat-faced high speed tool steel die (Figure 4.3). The inner and outer radii of the workpieces were 0.701 and 1.7145 inches (17.80 and 43.55 mm) respectively, and their thickness was one inch (25.4 mm). The outer radius of the round-faced die was 4.5905 inch (116.60 mm) and that of the flat-faced die was 4.5885 inch (116.55 mm).

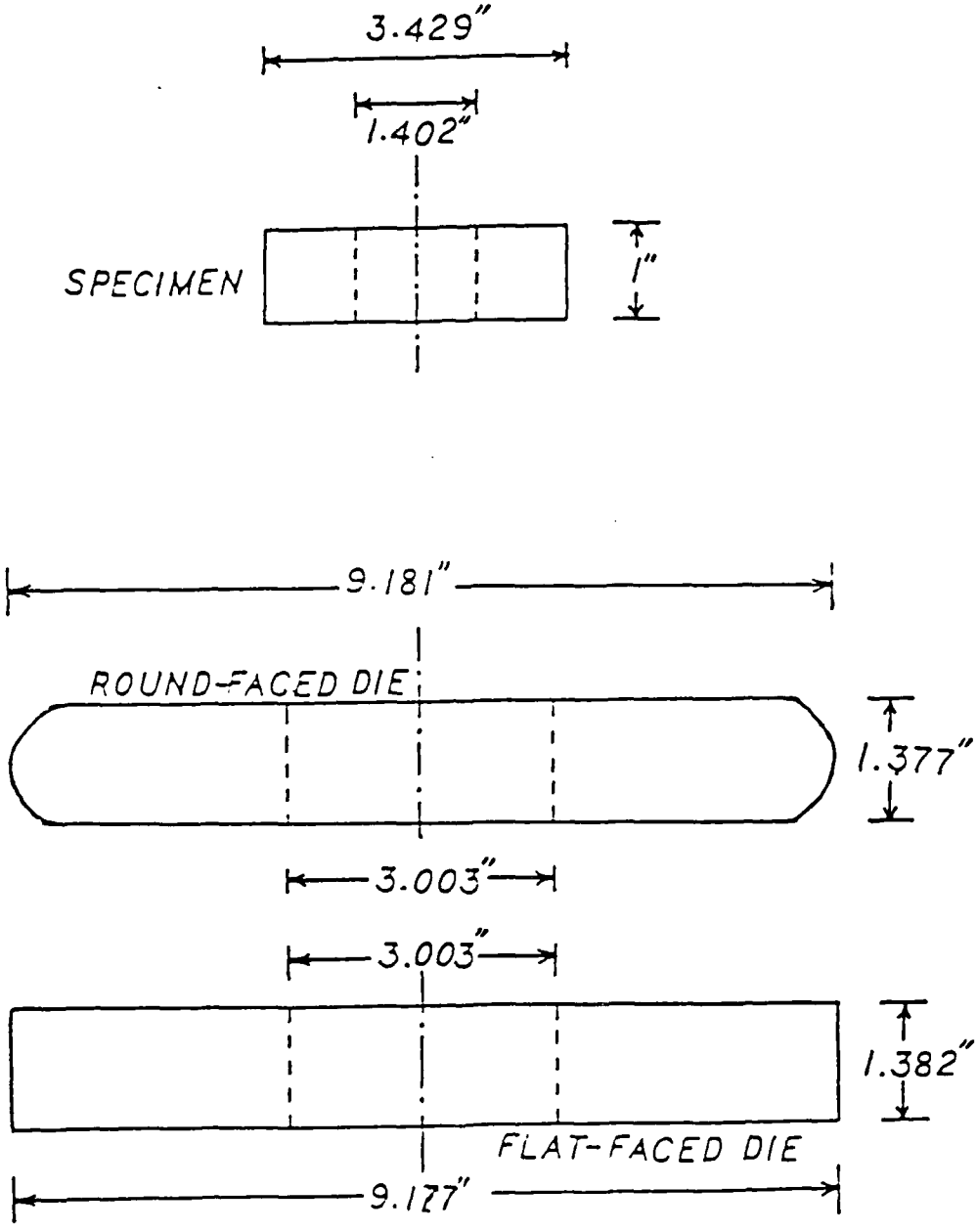

Figure 4.3 WORKPIECE AND DIES IN EXPERIMENTAL ANALYSIS

The ausrolling machine, whose schematic representation is shown in Figure 1.3, was used to conduct the tests. The specimen was mounted in place of the gear (B), and was only pushed horizontally into the die (A) by moving the rear ram downwards. The die (A) was rotated for a specified time as soon as the workpiece was indented, thus working a portion of the circumference of the latter. The parameters controlling the depth of indentation and the time of working, along with other essential parameters were set and controlled by an 8088 microprocessor based personal computer and interfaced with the servo-controlled forming equipment using a Daytronic System 10 data acquisition and process control system.

The primary aim of the experiments was to compare the experimentally and numerically obtained deformation patterns. The force values obtained from the experiments could not be used directly as the force was the resultant force required to move the workpiece and to keep it pressed against the rotating die. Various deformation patterns were obtained by indenting the workpiece using either the round or the flat die and by rotating the die through different angles. Three indentations were made on a workpiece using the round die while only one test could be performed on a piece using the flat die. Various indentation depths were explored to obtain sufficient or measurable residual deformation on the disks. The complete experiment included the following steps: (1) set the parameters for indentation depth and time of rolling; (2) feed the disk into the die; (3) start rotating the die; (4) retract the disk after the preset time; (5) repeat steps 1 through 4 for indenting another part of the disk (for round die only); and/or (6) extract the disk and measure the residual deformations.

The residual deformations were measured using a dial guage of least count 0.0005 inch (0.0127 mm). One undeformed aluminum disk was used as reference

to measure both the initial and the deformed shapes of the remaining disks in order to maintain consistency of the zero setting of the dial guage. The residual deformations (dotted lines) of the disks were plotted by superimposing the magnified deformations on the initial undeformed shapes (solid lines) of the disks. Some of these plots are shown in Figures 4.4 through 4.10. Also displayed on the plots is the information such as the die type, angle of rolling, maximum force required in the experiment, maximum residual deformation as indicated by the indentation value, etc. The induced deformations using the flat die are quite small as compared to those produced by the round die whereas the forces follow an opposite trend. Such differences in magnitudes is to be expected since the flat die works the total thickness of the disk while the round die only makes a thin indentation of the order of $\frac{1}{8}$ inch (3.17 mm).

Numerical simulation of rolling aluminum disks were performed using NOFEAP to reproduce some of the experimental results. A discussion of the development of the solution algorithm is given in the next section.

4.2.2 Numerical Simulation

Numerical simulation of disk-rolling consisted of one initial run of the program to roll the disk by one complete revolution. Due to the computation time required for each run, it was not possible to individually simulate each experiment. The force and the deformations were obtained at a number of intermediate rolling steps so that these values could be compared to some experimental results.

The input data file used in the analysis is given in the Appendix B. Salient features of the input file are discussed here. Details of the commands used can be obtained from the NOFEAP user's manual [8]. The program is activated by the "NOFE" macro command placed at the top of the file. The control parameters

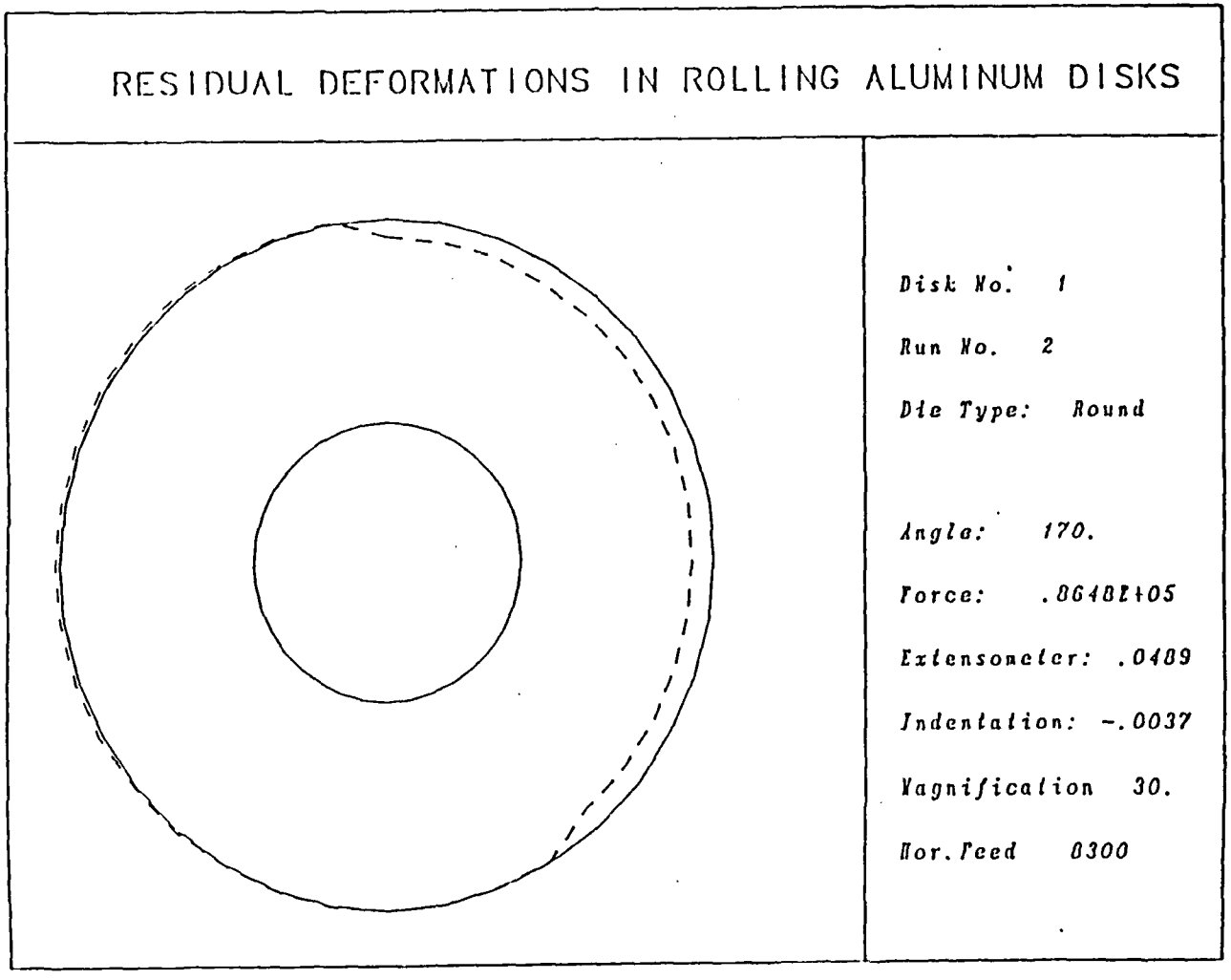

Figure 4.4 DEFORMATIONS IN ROLLING OF ALUMINUM DISKS:
Experiment Number 1-2

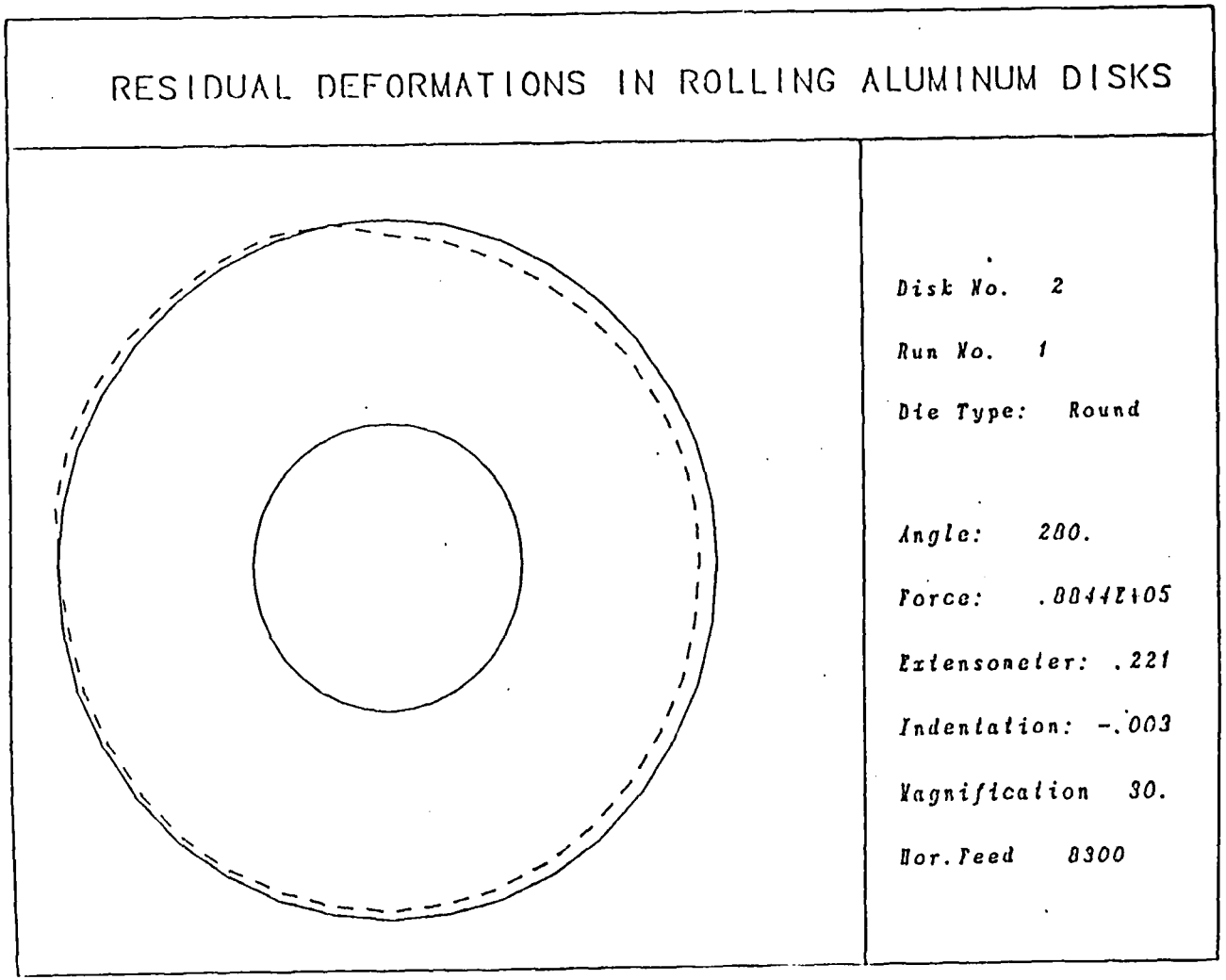

Figure 4.5 DEFORMATIONS IN ROLLING OF ALUMINUM DISKS:
Experiment Number 2-1

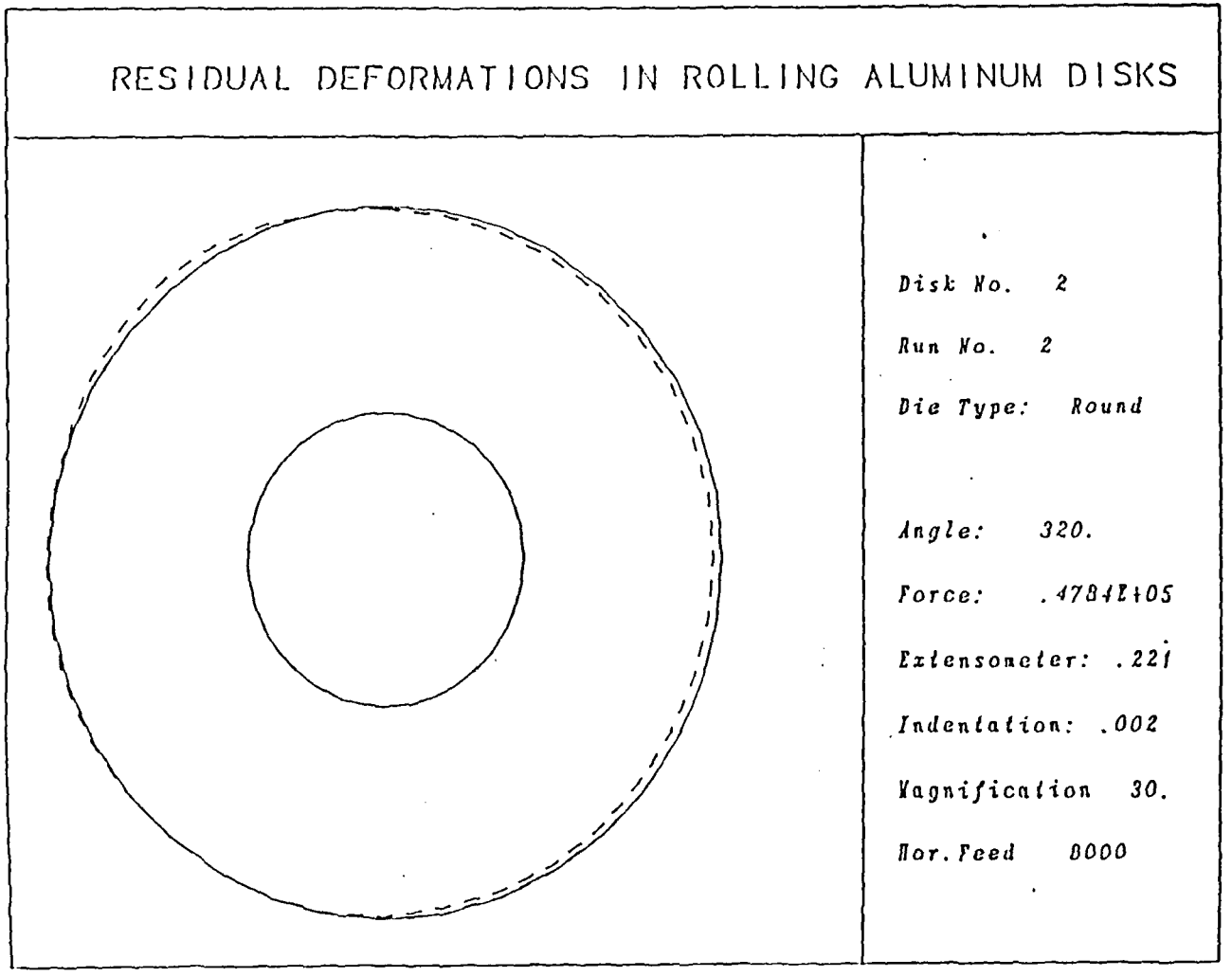

Figure 4.6 DEFORMATIONS IN ROLLING OF ALUMINUM DISKS:
Experiment Number 2-2

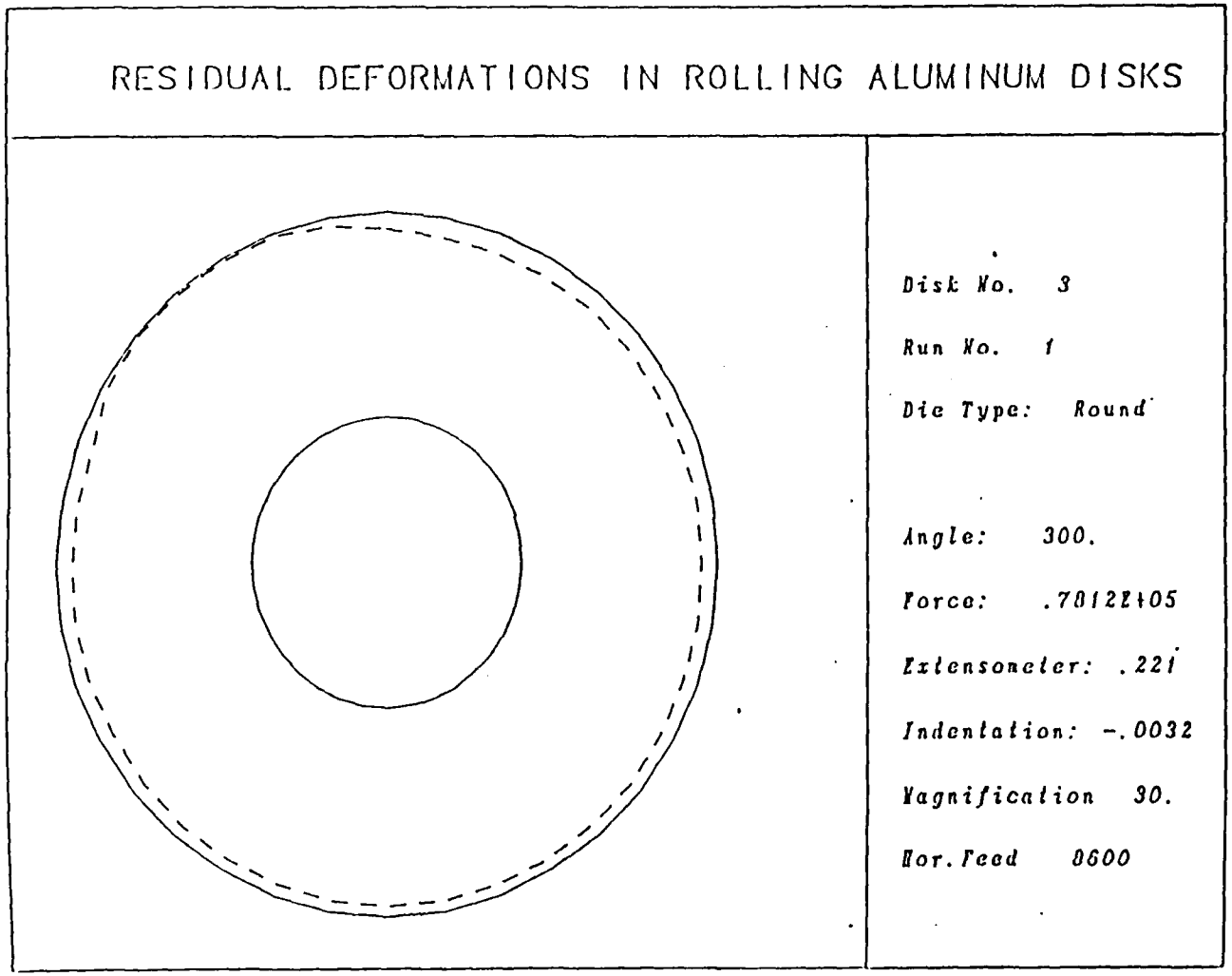

Figure 4.7 DEFORMATIONS IN ROLLING OF ALUMINUM DISKS:
Experiment Number 3-1

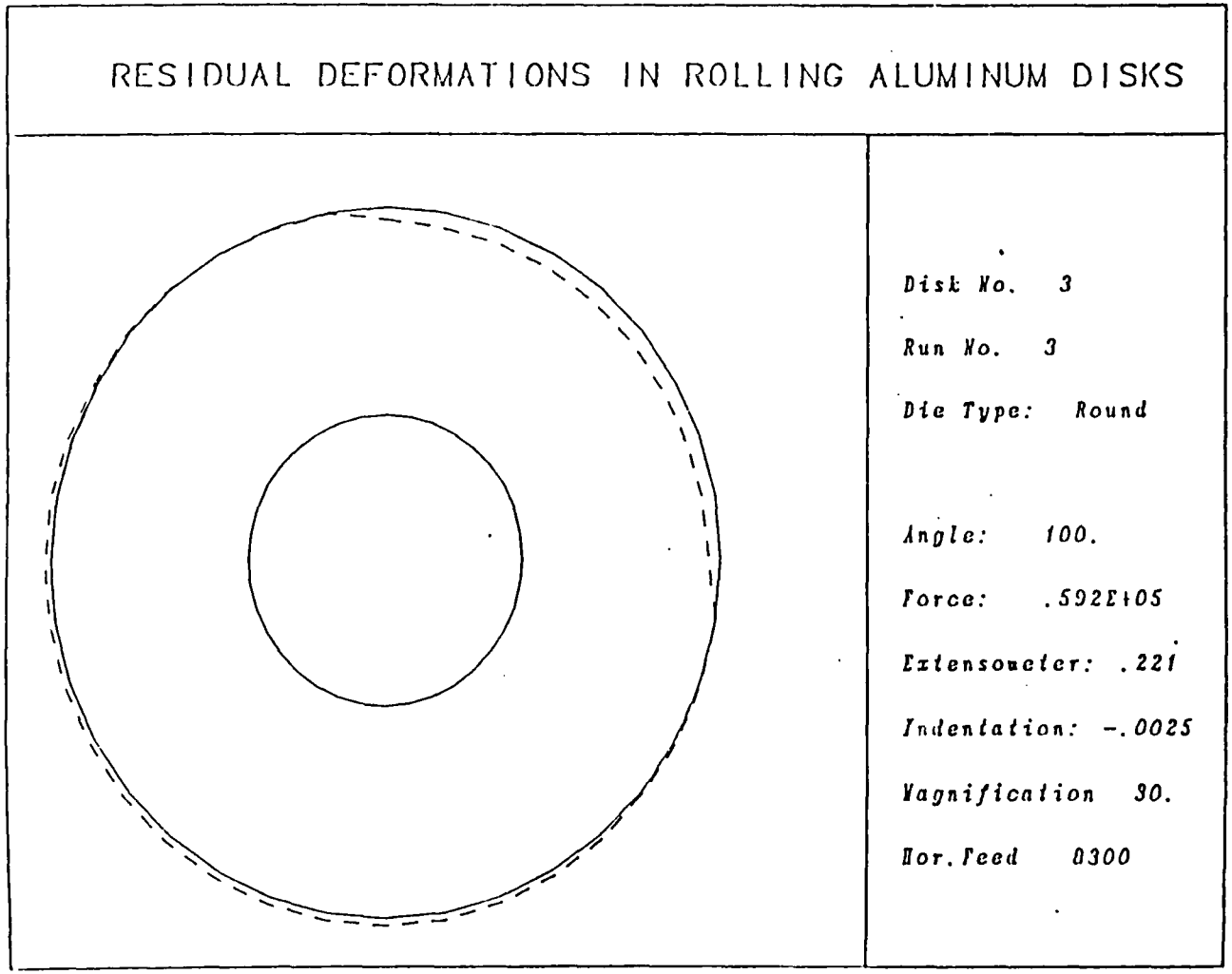

Figure 4.8 DEFORMATIONS IN ROLLING OF ALUMINUM DISKS:
Experiment Number 3-3

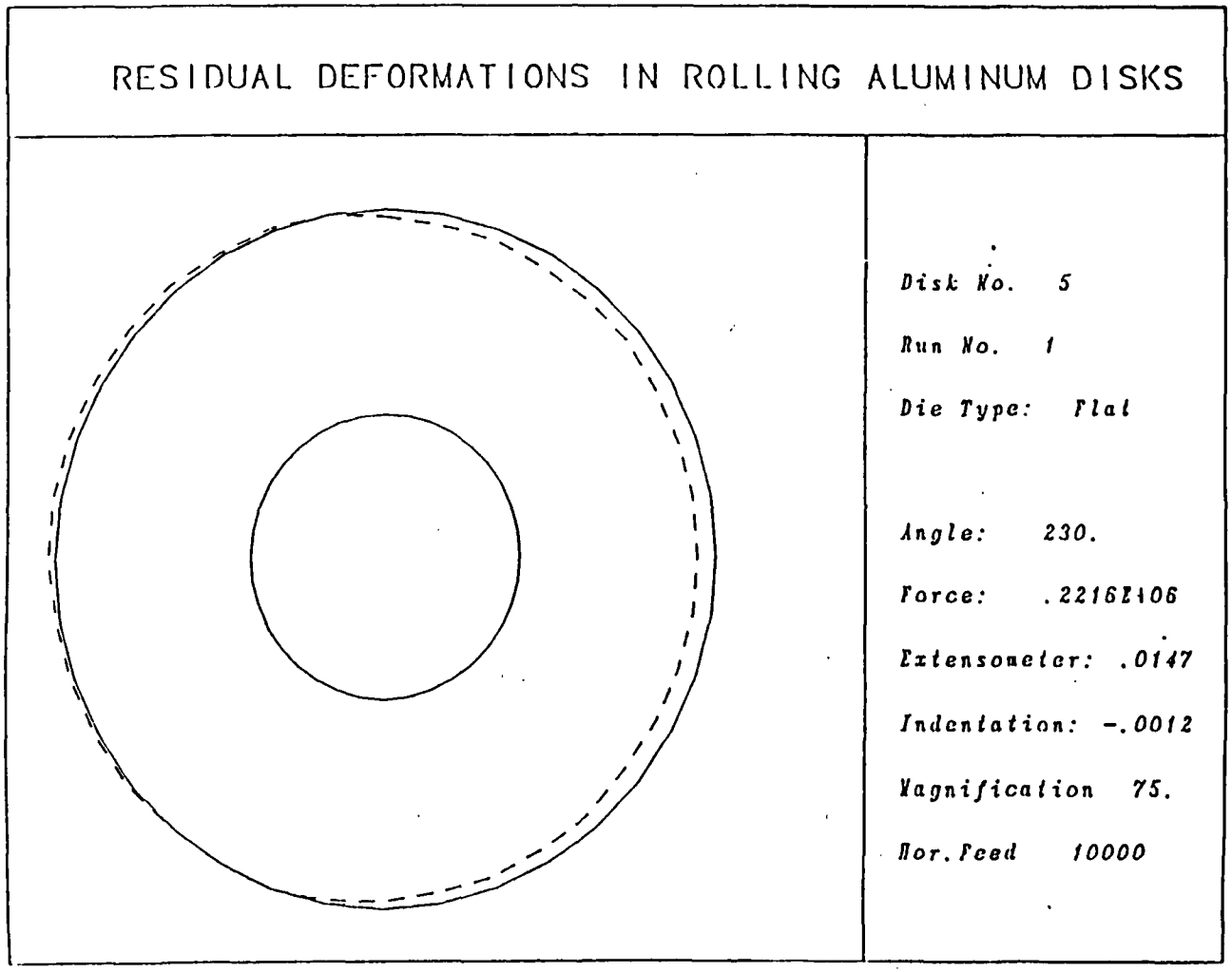

Figure 4.9 DEFORMATIONS IN ROLLING OF ALUMINUM DISKS:
Experiment Number 5-1

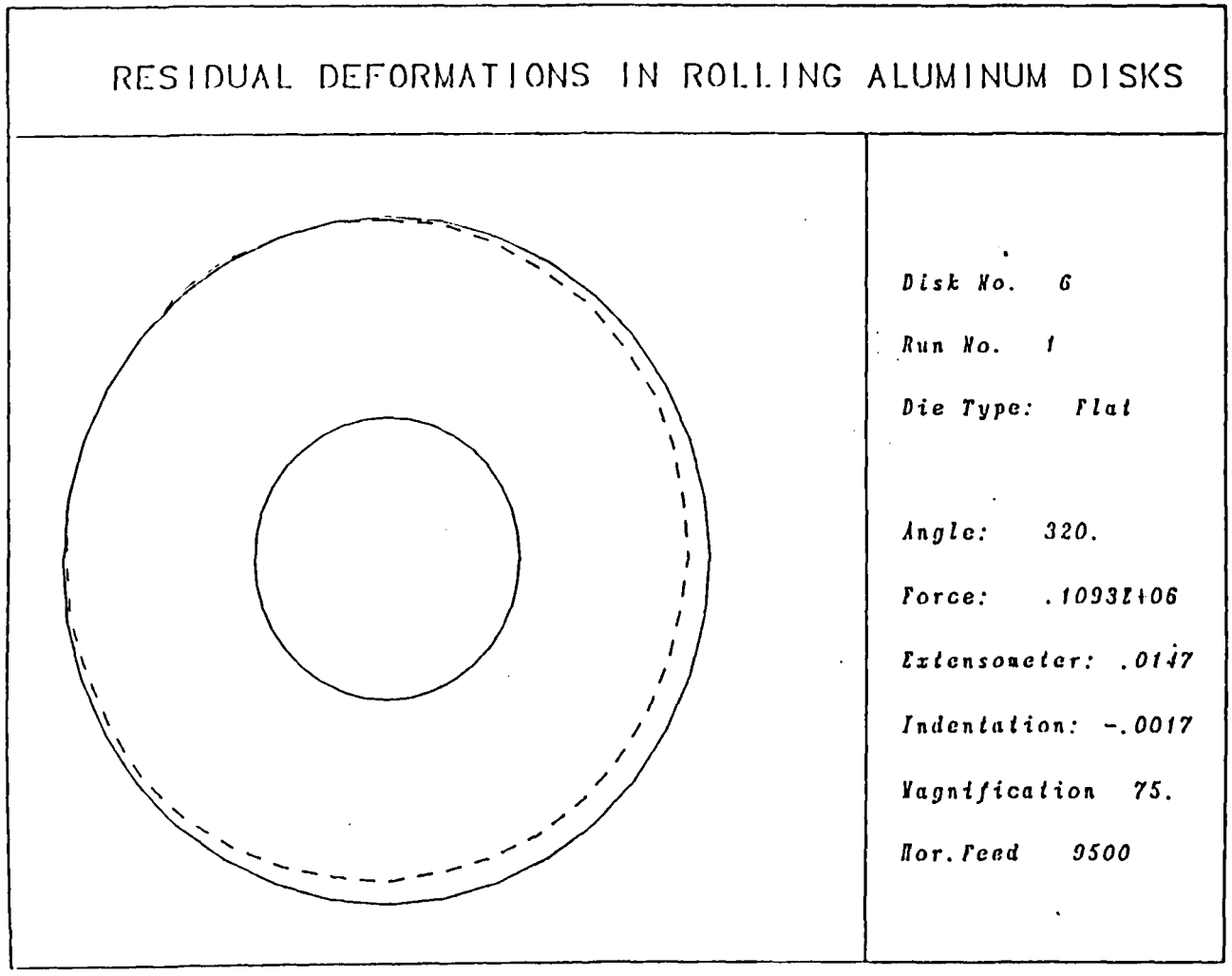

Figure 4.10 DEFORMATIONS IN ROLLING OF ALUMINUM DISKS:
Experiment Number 6-1

follow the NOFE command. The first line indicates the number of the bodies in the problem and is set to two in order to accomodate the workpiece (body #1) and the die (body #2). The workpiece is modelled by 144 nodes and 96 elements, each defined by five or less nodes. A plane strain type of analysis is performed and the material of the workpiece is assumed to follow the von Mises yield criterion. The geometric and material description follows the control data. The properties of Aluminum-6061 are used so that the elastic modulus is 10,000 Ksi (68.95 GPa), the Poisson's ratio is 0.33, the yield stress is 36 Ksi (248.22 MPa) and the slope of hardening curve is 35.3 Ksi (243,39 MPa). Four Gaussian points are used in each element for integrating the stiffness matrices and to compute the strains. Geometric non-linearities are not included in the analysis to keep the computation time within bounds. The workpiece is constrained using the "BOUN" command to enable it to translate as a rigid body. The die is only represented by its outer surface and is modelled by 129 nodes listed following the "BODY" command.

The contact surfaces of the workpiece and the die are defined following the "CONT" command in the mesh input phase. The contact surface of the former is modelled by 27 nodes, which represents slightly more than half its circumference, while all of 129 nodes are used to model the circumference of the die. Since the number of degrees of freedom in the contact problem solution phase is a function of the number of contact nodes on the workpiece, but not of those on a rigid die, including large number of nodes on the latter's contact surface does not always significantly increase the computation time. The nodes forming the contact surface of the workpiece are listed in counterclockwise direction. The coefficient of static friction is set to 0.3. The solution algorithm follows the "MACR" macro command. The comments following each command describe the function of the command. Further details are available in the user's manual [8].

The results in this section have been obtained from three runs of NOFEAP using three meshes of the workpiece and the die. The first run rolled the workpiece by 360° using a coarse mesh where the nodes were placed at an angular increment of 15°. In order to test the effect of the mesh size on the solution, a finer mesh was placed on the outer surface of the workpiece with an angular increment of $7\frac{1}{2}^\circ$ and the piece rolled by 180°. Finally, one-half of the first quadrant of the workpiece was again subdivided in $3\frac{3}{4}^\circ$ increment and a 45° rolling simulation was performed. The results of these numerical simulations are given in Figures 4.11 through 4.18. Some observations on the similarities and the differences between the numerical and experimental results are included next.

4.3 Comparison of Numerical and Experimental Results

The deformation plots at intermediate steps and the final deformed shapes of the disks for the experimental observations and the numerical simulations are compared here. It should be noted that the intermediate numerical plots are of deformations while the die is still in the process of rolling the workpiece and hence do not account for the elastic recovery of the material. On the other hand, all of the experimental results are the final shapes of the disks after the load has been removed. This causes certain differences in the magnitudes of deformations. However, the general shapes of the deformed disks compare well for the experimental and the simulated disks as given next.

The deformation plots are grouped according to their angles of rolling and a comparison is attempted as follows:

(1) The experimental disk 3-3 (Figure 4.8) with rolling angle of 100° can be matched against the numerical plots of $82\frac{1}{2}^\circ$ and $127\frac{1}{2}^\circ$ (Figures 4.12,4.13). The fineness of the mesh has caused the sharp change in the deformation at the end of rolled

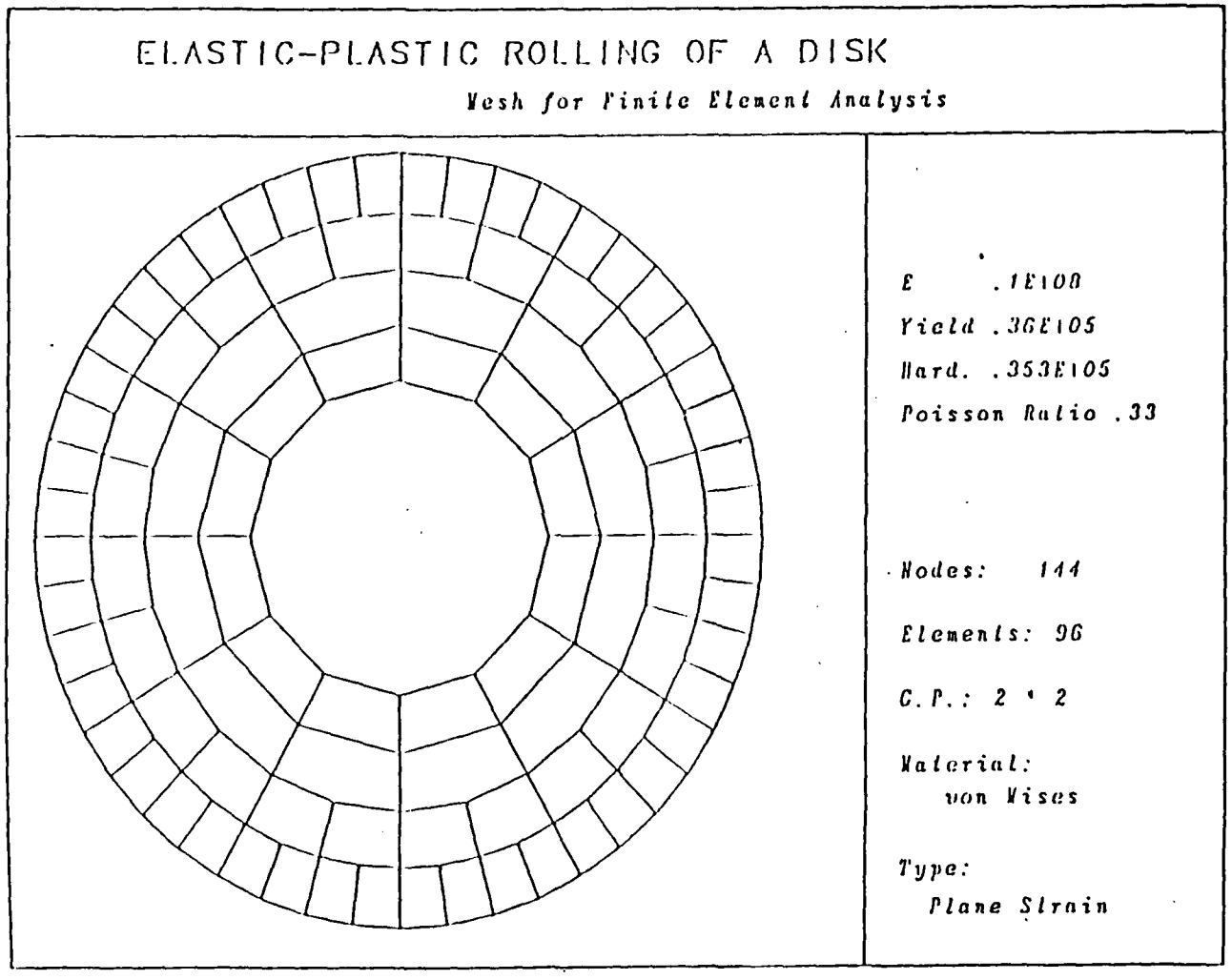

Figure 4.11 ELASTIC-PLASTIC ROLLING OF A DISK:
Mesh for Finite Element Analysis

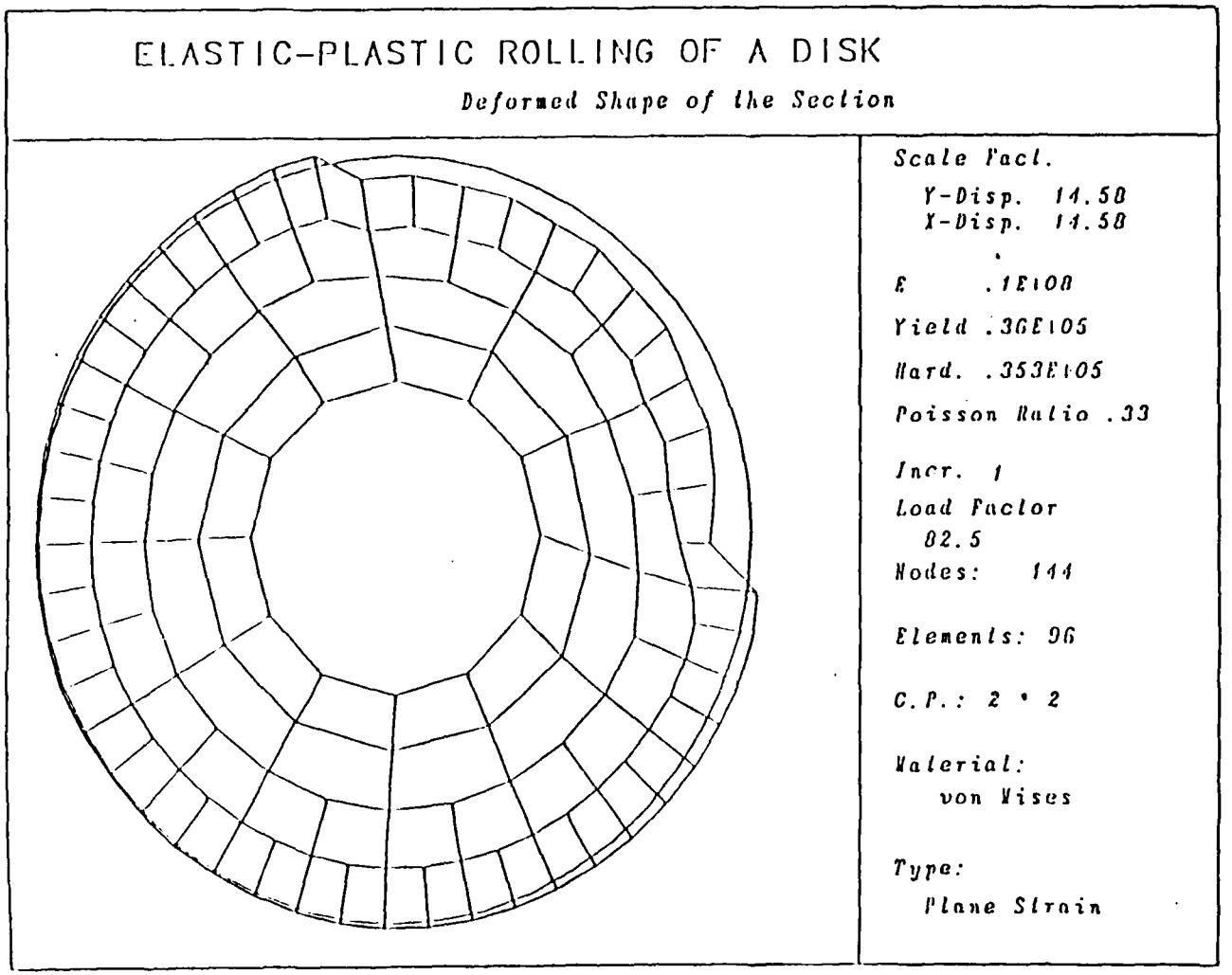

Figure 4.12 ELASTIC-PLASTIC ROLLING OF A DISK:
Deformed Shape of the Section at 82.5°

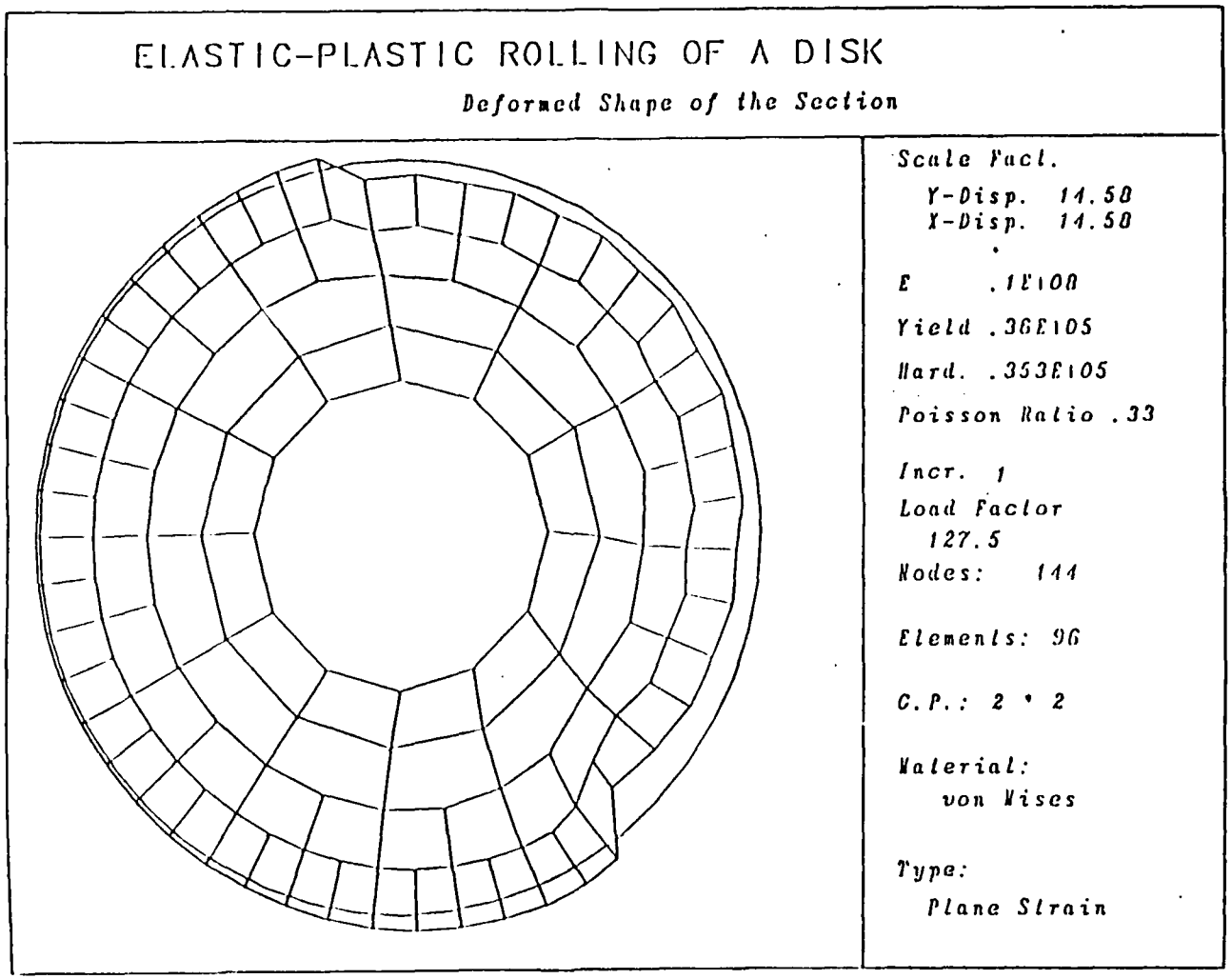

Figure 4.13 ELASTIC-PLASTIC ROLLING OF A DISK:
Deformed Shape of the Section at 127.5°

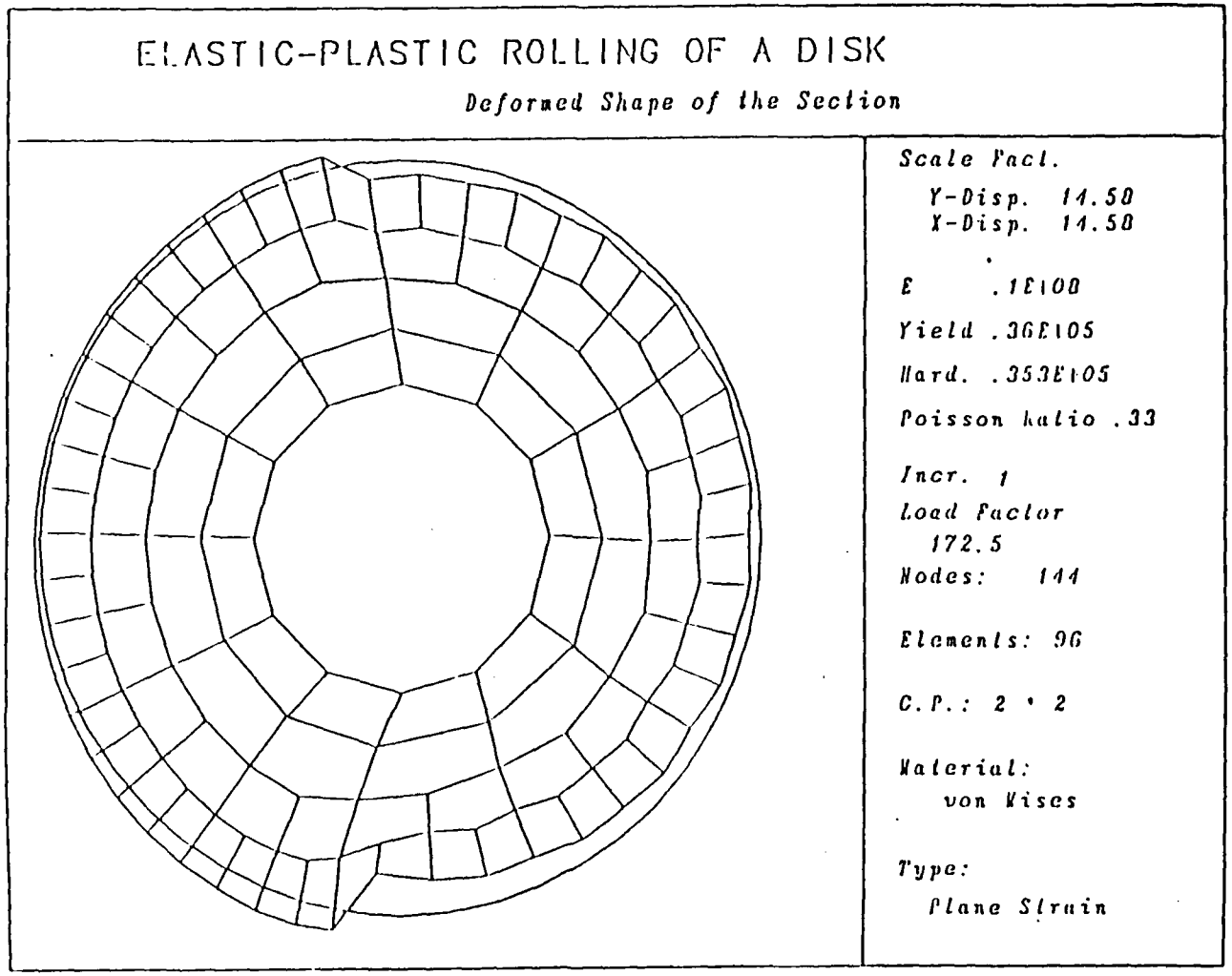

Figure 4.14 ELASTIC-PLASTIC ROLLING OF A DISK:
Deformed Shape of the Section at 172.5°

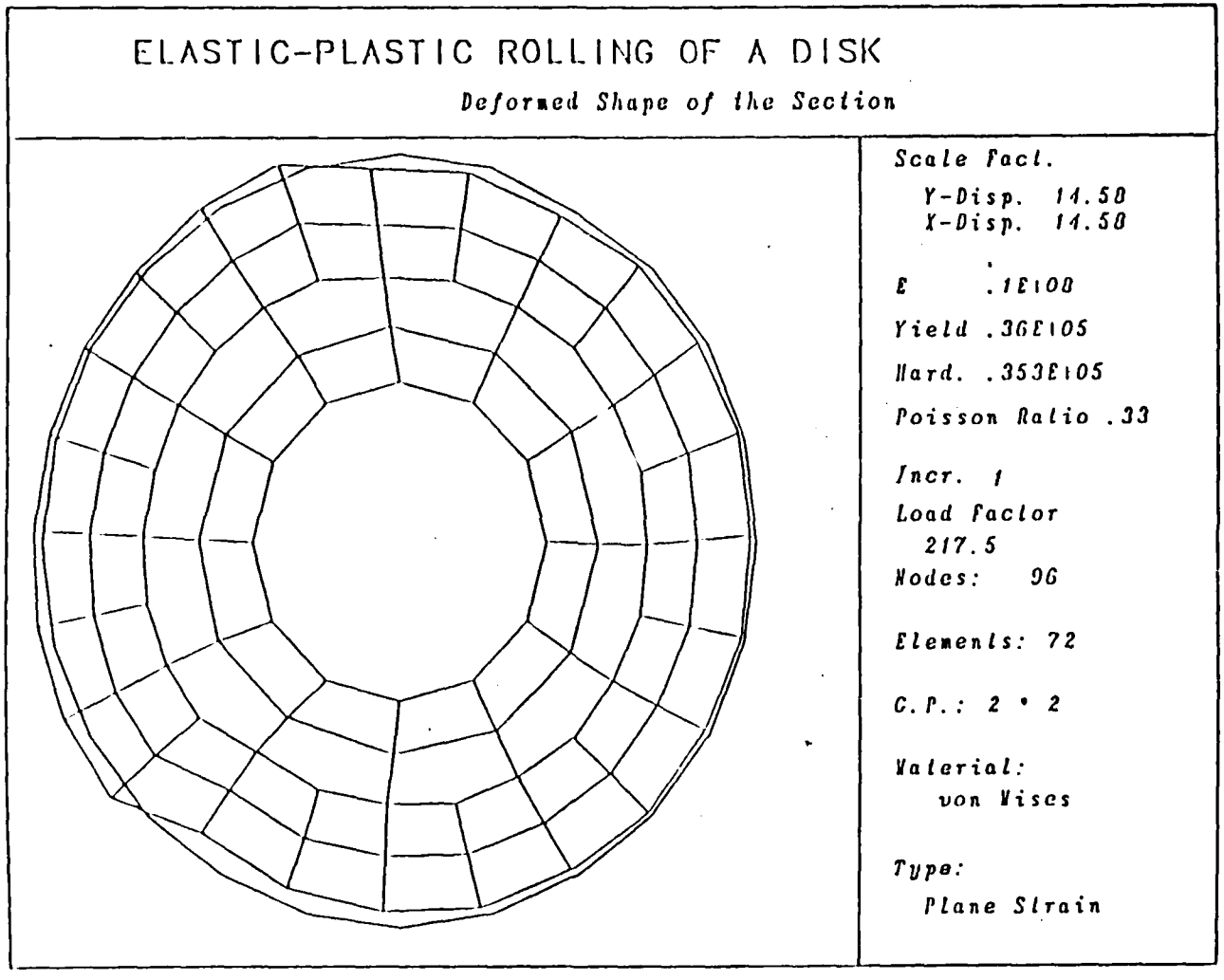

Figure 4.15 ELASTIC-PLASTIC ROLLING OF A DISK:
Deformed Shape of the Section at 217.5°

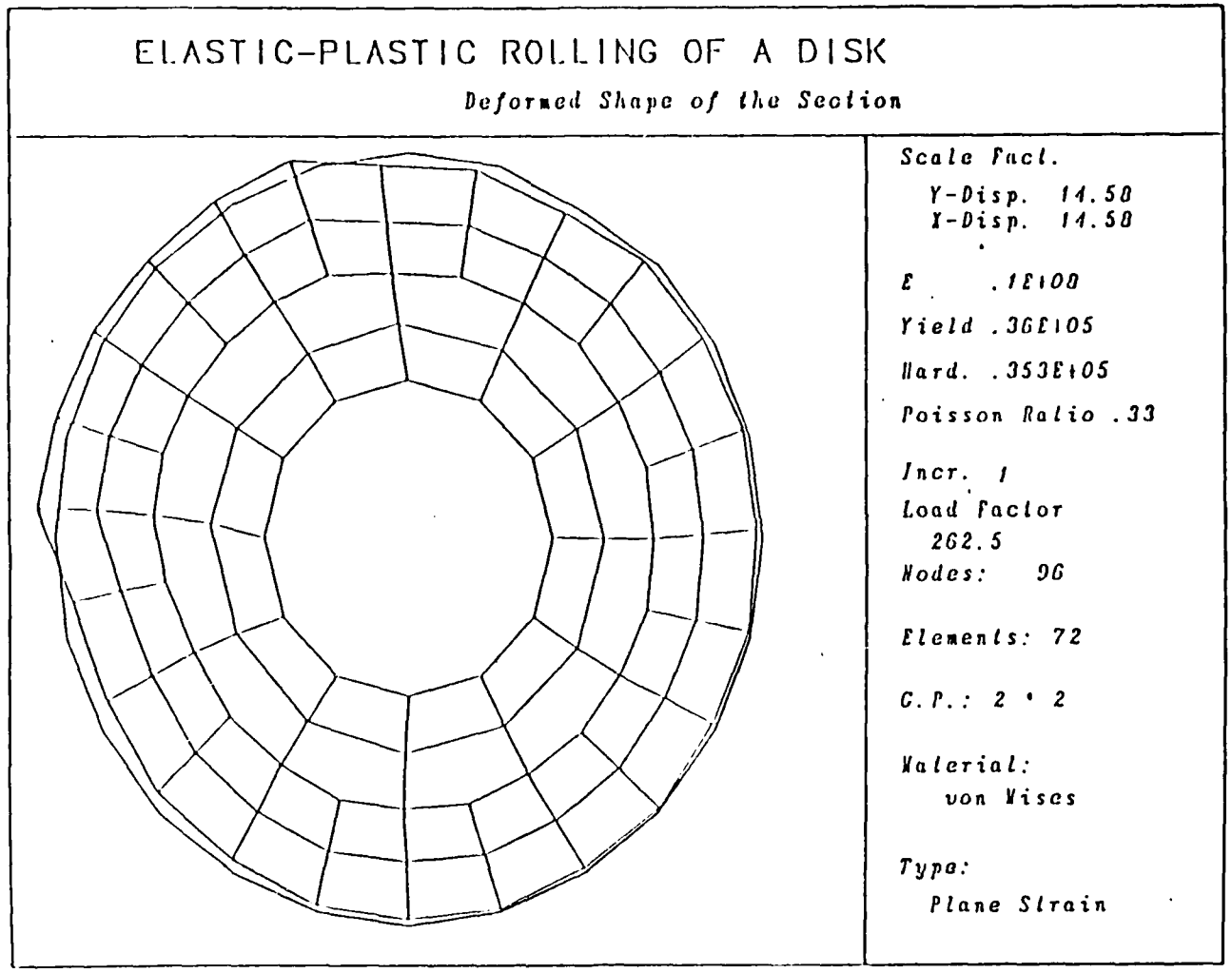

Figure 4.16 ELASTIC-PLASTIC ROLLING OF A DISK:
Deformed Shape of the Section at 262.5°

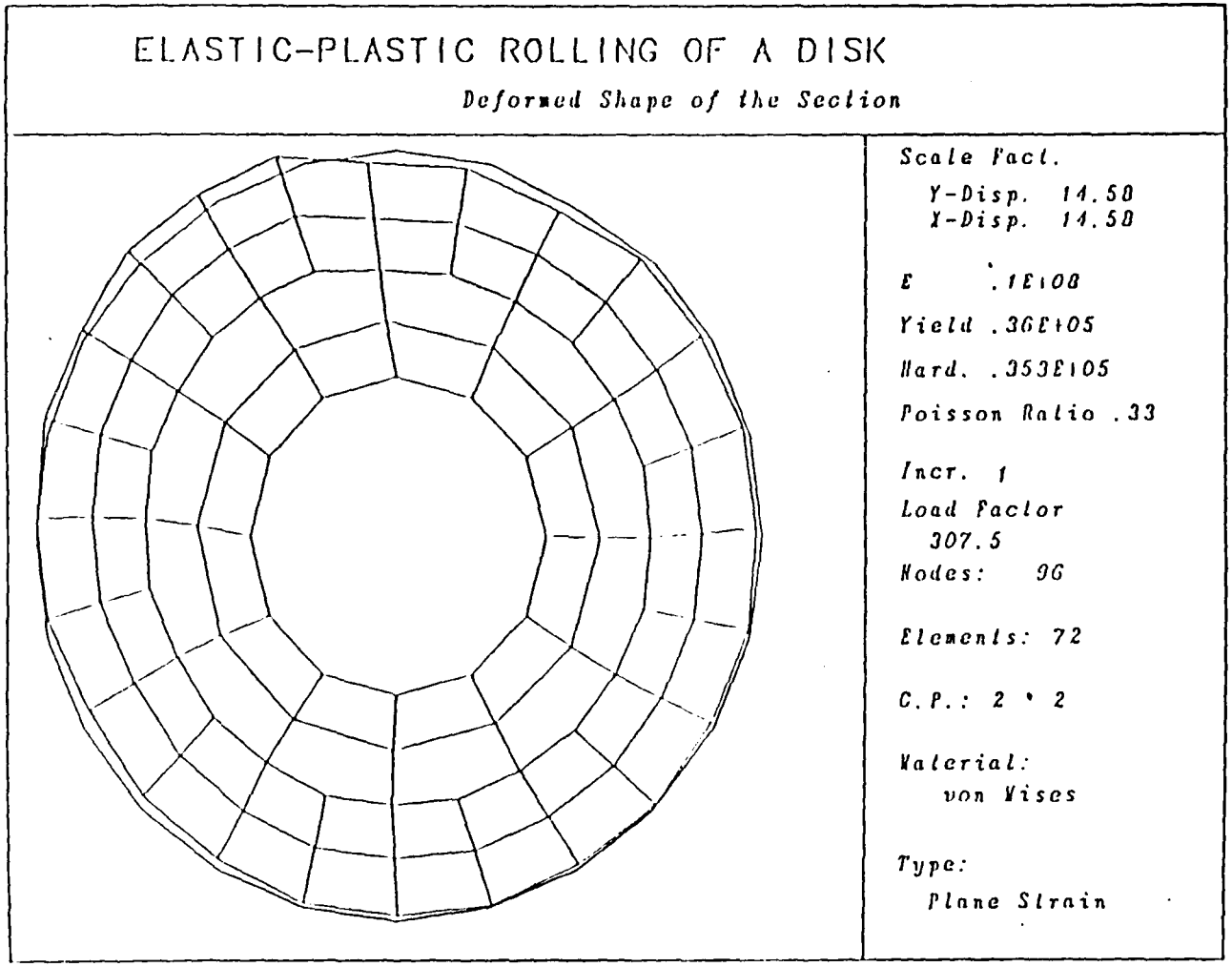

Figure 4.17 ELASTIC-PLASTIC ROLLING OF A DISK:
Deformed Shape of the Section at 307.5°

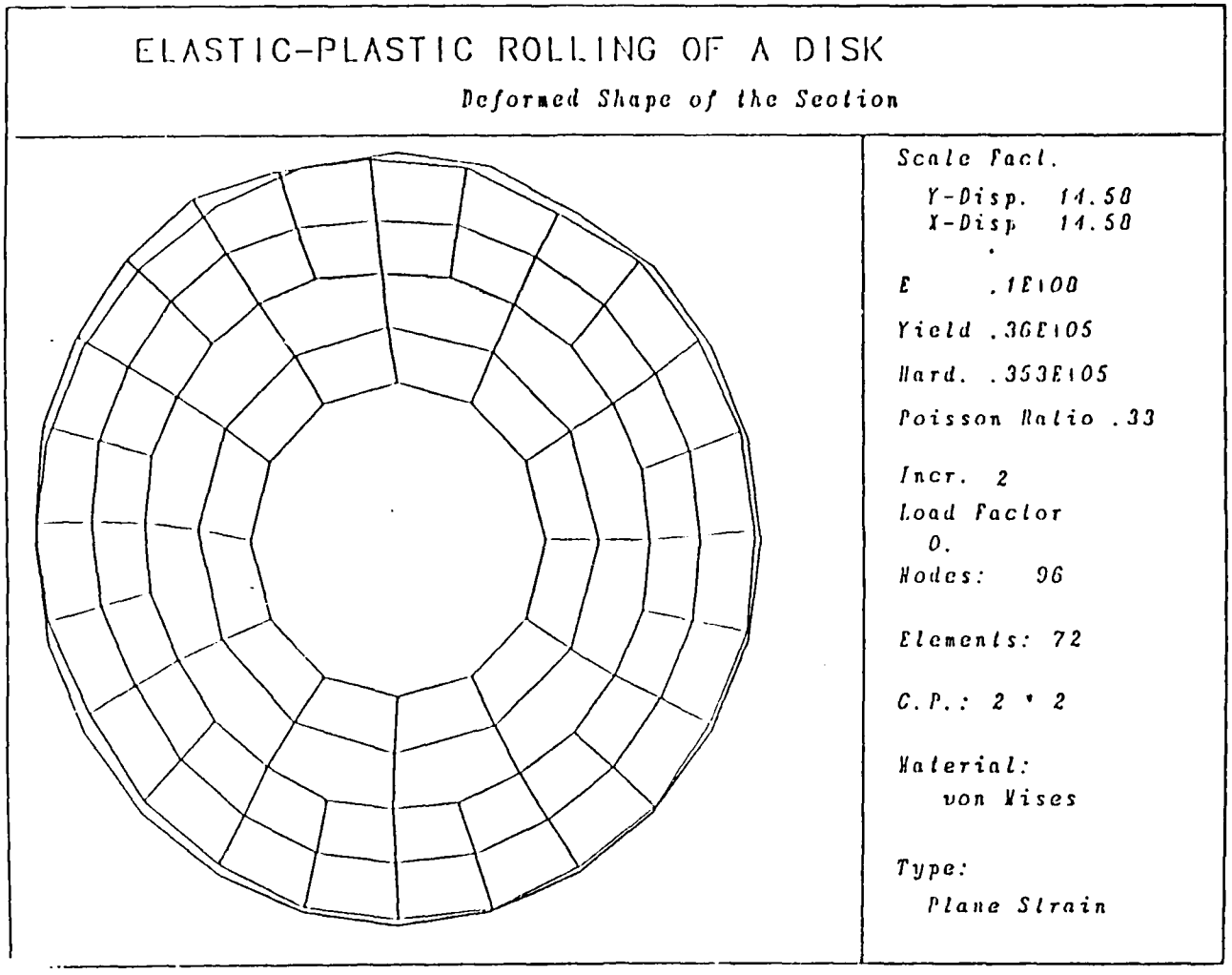

Figure 4.18 ELASTIC-PLASTIC ROLLING OF A DISK:
Deformed Shape of the Section

zone in the numerical plots. However, the tendency of the material, rolled by the die, to flow over the original shape on the side of the workpiece opposite to the rolled side is well represented in the numerical plots.

(2) The agreement is remarkable for the experiment number 1-2 (Figure 4.4) and the simulated results at $172\frac{1}{2}^{\circ}$ (Figure 4.14). The experimental plot is considerably smoother than the numerical one at the end of contact zone due to its continuous nature as against the discreteness of the finite element model. The material overflow is higher for the numerical model but this could be due to some lateral flow in the experiments.

(3) The rolled disk at 230° (Figure 4.9) is stacked against Figure 4.15 (plot at $217\frac{1}{2}^{\circ}$). The notable exceptions of this pair from the earlier ones are that a coarser mesh is employed in the numerical model while the flat die is used in the experiments. Although the displacement patterns are again quite similar, the flat die does not produce as sharply distinguishable rolled zone as brought forth by the round die. The reason for this has been found to be the significant lateral spread of the material in the former case.

(4) The plots in Figures 4.5 (experiment 2-1 at 280°) and 4.16 (numerical result at $262\frac{1}{2}^{\circ}$) compare extremely well with each other in both the indented and the overflowing material zones. The resultant cam shaped object is easily identified in the two plots.

(5) This group, formed by the deformed shapes at $307\frac{1}{2}^{\circ}$ (Figure 4.17), and experiment 2-2 (Figure 4.6) with the round die and number 6-1 (Figure 4.10) with the flat die, both with rolling angle of 320°, makes some interesting points.

The numerical model again predicts a cam shaped object, as also produced by the round die. However, the flat die produces very insignificant amount of overflowing material while causing remarkable indented surface. One reason for this behavior may lie in the deformation measurement, possibly due to the eccentricity of the mounted disk. Since the deformations are of the order of only 0.0005" (0.013 mm), only a slight eccentricity would affect the results. This lack of discernible rolled zone was, however, observed in all other specimens rolled with the flat die. A measurement of the lateral dimensions of the specimen revealed lateral flow of the order of the depth of indentation in these pieces. This contradicts the assumption of plane strain deformation in the specimens. The round die, while indenting only about $\frac{1}{8}$" (3.17 mm) wide material, may have produced plane strain deformation more closely since the deforming material was constrained by surrounding material thus forcing the flow to occur in the plane of rolling. This may explain the semblance of the numerical results with the round die experiments rather than the flat die specimens.

(6) The preceding discussion may also be applied to find a similarity between Figures 4.10 and 4.18.

Although the displacements of the numerical solutions have compared well with the experimental results, a comparison of the forces could not be made. As seen in the Figures 4.4 through 4.10, the forces varied from about 48,000 to 90,000 Lbs (0.2 to 0.4 MN) for the round die and from 100,000 to 200,000 Lbs (0.445 to 0.89 MN) for the flat die. Different force readings were obtained for same settings on the machine thus the reliablity of these values is questionable.

The variation of the total forces with rolling angle for the numerical simulations is plotted in Figure 4.19 for various meshes. The difference between the 15° mesh

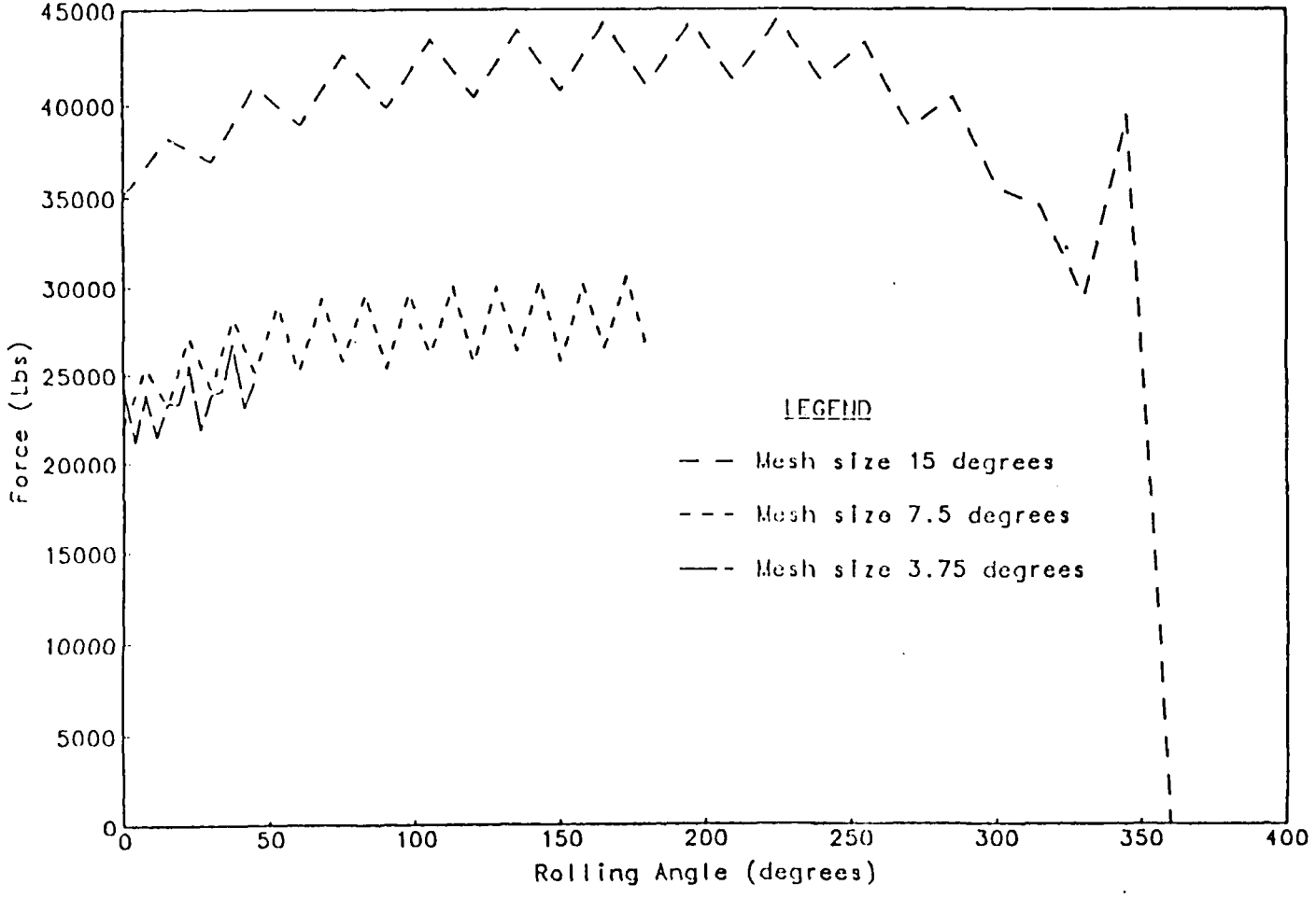

Figure 4.19 VARIATION IN TOTAL FORCE WITH ROLLING ANGLE

and the $7\frac{1}{2}^{\circ}$ mesh is significant and is attributed to the coarseness of the mesh coupled with the stiff behavior of the elements in shear and bending. Refining the mesh to $3\frac{3}{4}^{\circ}$ does not produce further change in the force values indicating the convergence of the solution with the mesh size.

The model of the rolling process in NOFEAP is found to compare satisfactorily with the experimental runs as shown in this section. The applicability of NOFEAP to modelling deformations in a gear tooth when the tooth is subjected to rolling loads is demonstrated in the next section.

4.4 Example of Deformations in Gear Rolling

A gear is only represented here by half of its one tooth (Figure 4.20). The gear is rolled against a hard (rigid) die also modelled by half of a tooth. Two simulation excercises have been performed with clockwise and counterclockwise rotations of the gear (opposite for the die) thus modelling the deformations in the approaching and the trailing sides of the tooth respectively.

The gear tooth is modelled by 167 nodes with 139 elements each containing four or less nodes. The geometric constraints, imposed on the tooth and shown in Figure 4.20, are slightly inaccurate as they do not model the bending of the tooth. In later simulations, some of the constraints on the tooth were released to observe the effect of bending on deformations. This influence was found to be significant. These results, however, are not included here.

The gear and the die dimensions and other relevent details are given next.

Gear		Die	
Number of teeth	= 31	Number of teeth	= 57
Diametral pitch	= 8.5	Diametral pitch	= 8.5
Pressure angle	= 22°	Pressure angle	= 22°
Base diameter	= 3.3816"	Base diameter	= 6.2176"
	= (85.89 mm)		= (157.93 mm)
Pitch diameter	= 3.6471"	Pitch diameter	= 6.7059"
	= (92.64 mm)		= (170.33 mm)
Thickness at PD	= 0.1848"	Outside diameter	= 6.882"
	= (4.69 mm)		= (174.80 mm)

The surface of the teeth have been generated using the definition of the involute. For modelling the trailing side of the tooth, the die is placed with its tip touching the base of the tooth of the gear, then pushed into the gear and rolled in 5° increments. The resulting deformations, stresses and plastic flow patterns are shown in Figures 4.21 through 4.24. The deformations follow the expected pattern shown in Figure 4.25 with the material accumulating towards the tip while forming a slight cavity near the pitch line of the gear. The stress contours of Figure 4.23 indicate the concentration of high compressive stresses near the position of the die. The plastic flow, shown in Figure 4.24, shows the top of the tooth with permanent deformation due to restricting the bending of the tooth.

A similar analysis is made to model the approaching side of the tooth with the gear and the die placed as shown in Figure 4.26. The die is rolled in steps of 3° in the clockwise direction. The deformed shapes, shown in Figures 4.27 and 4.30, again follow the expected patterns (Figure 4.25) with the material now accumulating away from the tip and at the pitch line. Stress contours of Figures 4.28 and 4.29 show the motion of high compressive stress layer as the die rolls over

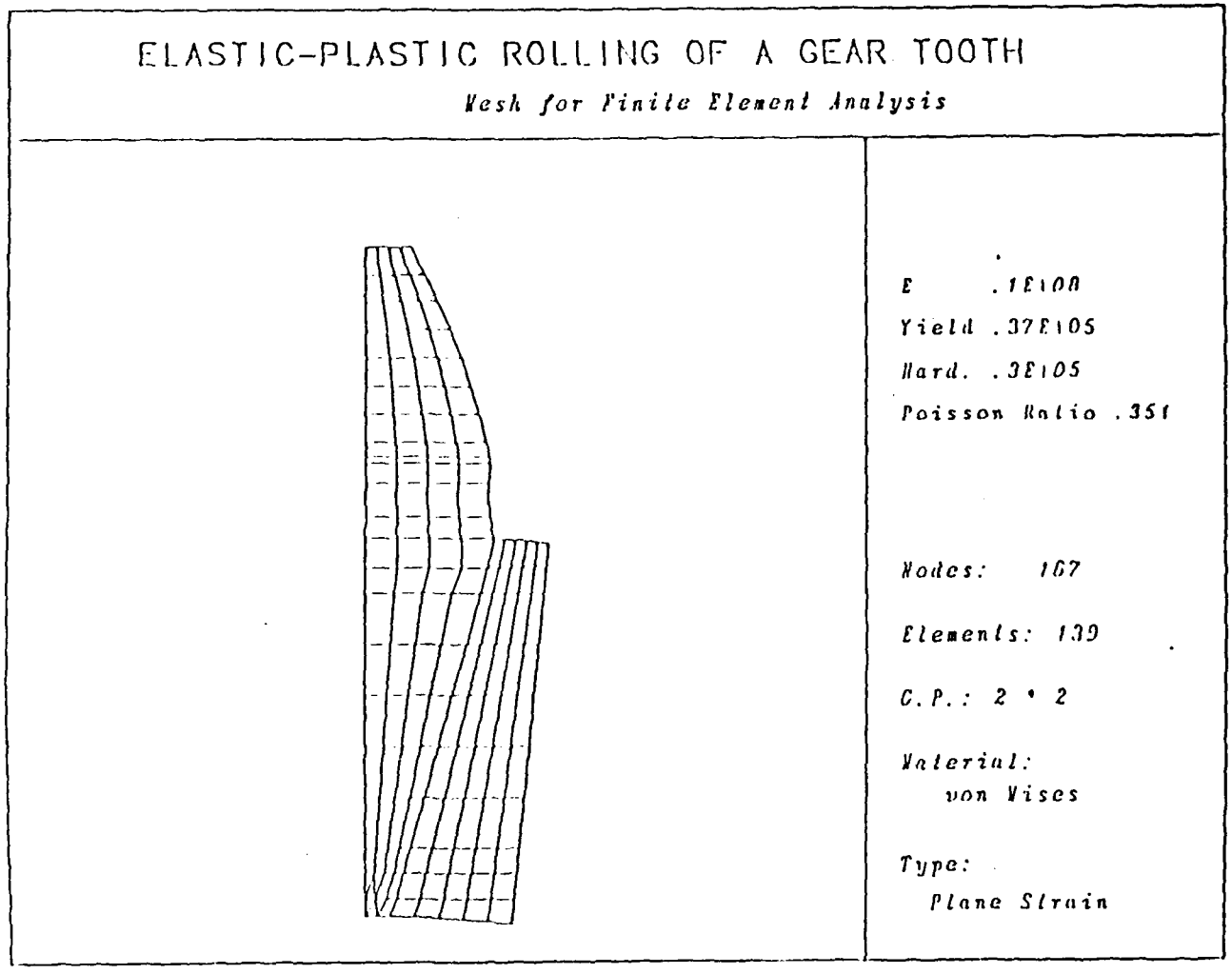

Figure 4.20 ELASTIC-PLASTIC ROLLING OF A GEAR TOOTH:
Mesh for Finite Element Analysis

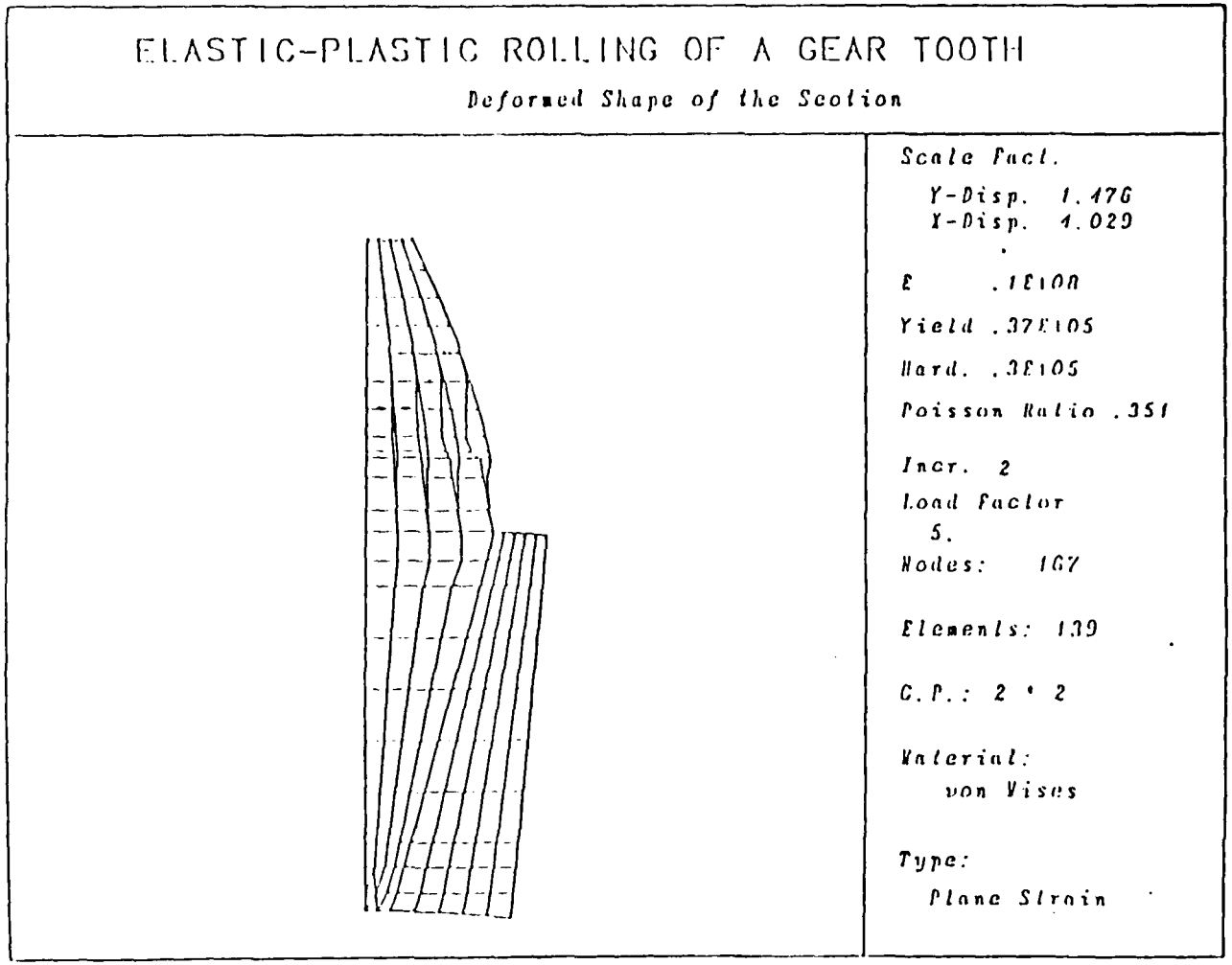

Figure 4.21 ELASTIC-PLASTIC ROLLING OF A GEAR TOOTH: Deformed Shape of the Section at 45°

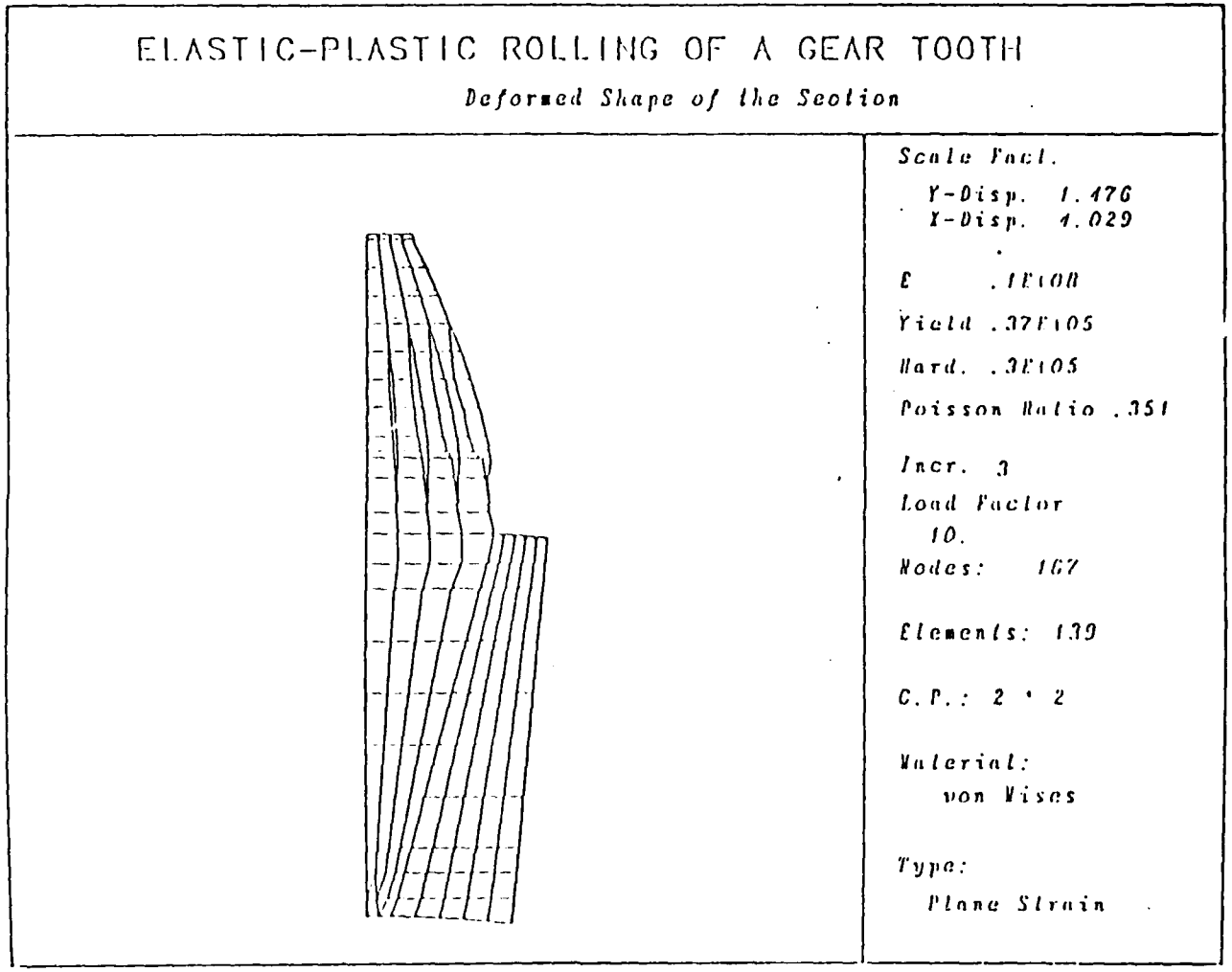

Figure 4.22 ELASTIC-PLASTIC ROLLING OF A GEAR TOOTH: Deformed Shape of the Section at +10°

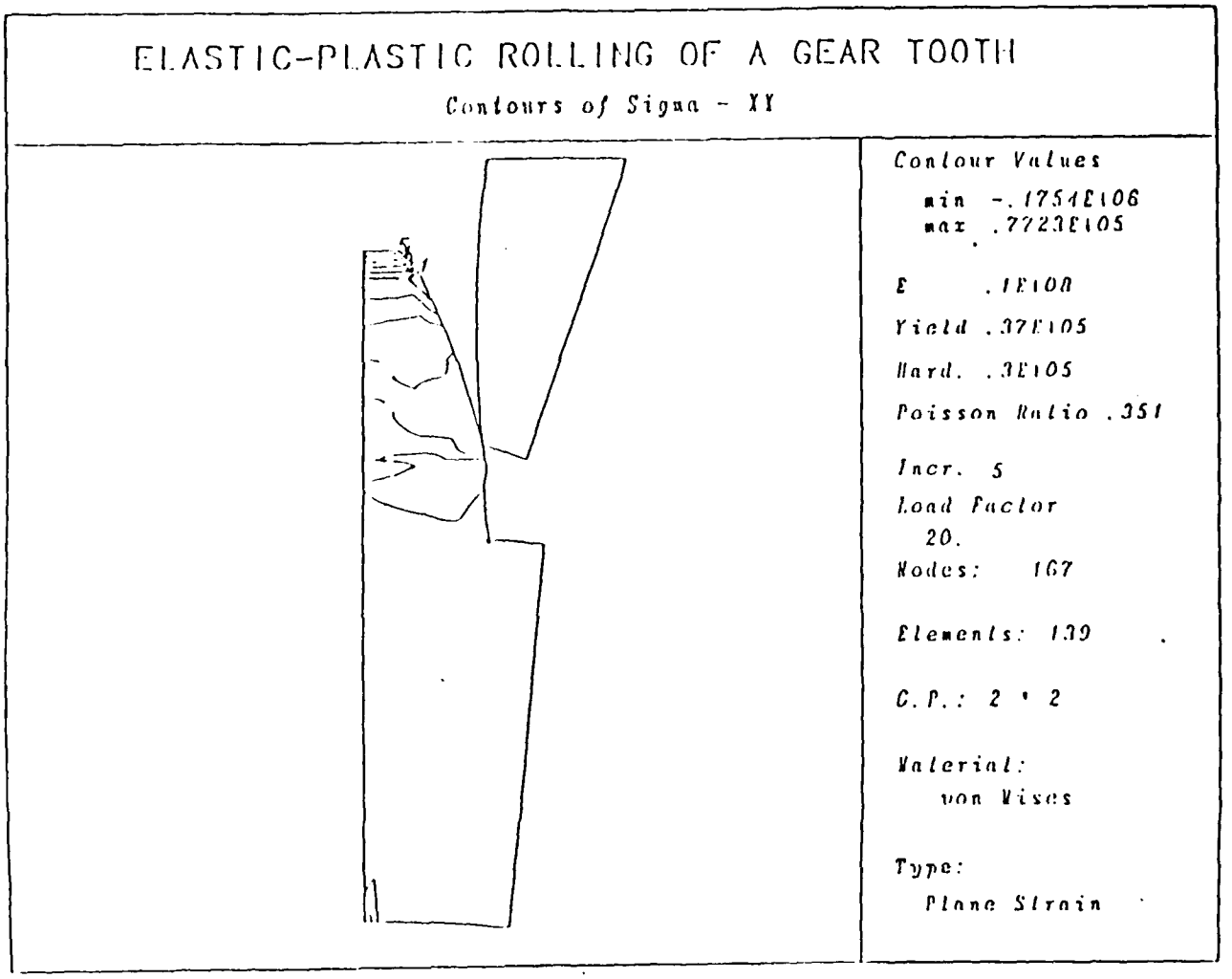

Figure 4.23 ELASTIC-PLASTIC ROLLING OF A GEAR TOOTH: Contours of Sigma-XX at 120°

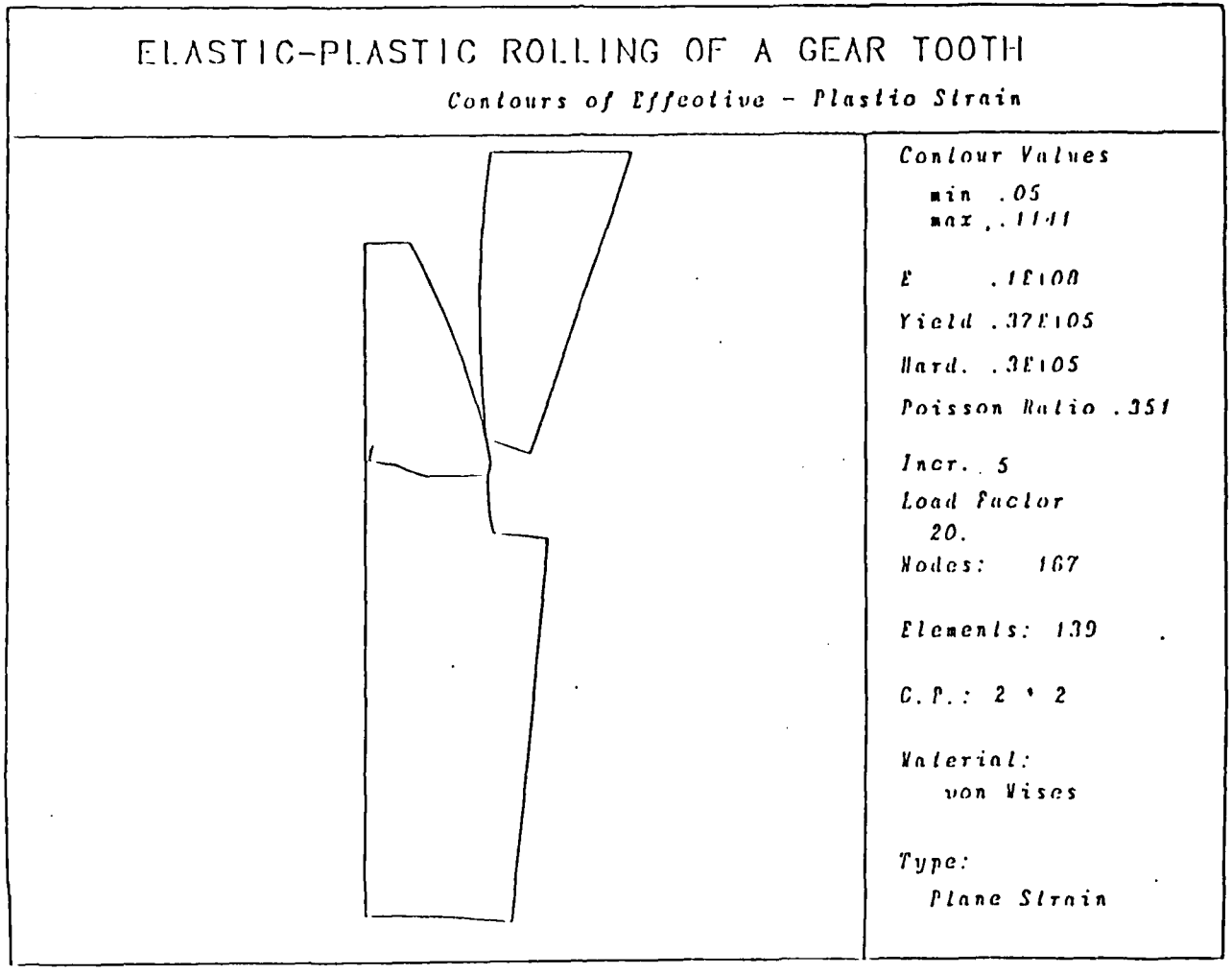

Figure 4.24 ELASTIC-PLASTIC ROLLING OF A GEAR TOOTH: Contours of Effective Plastic Strain at +20°

The plastic zone again dominates the top of the tooth (Figure 4.31) as in the previous case.

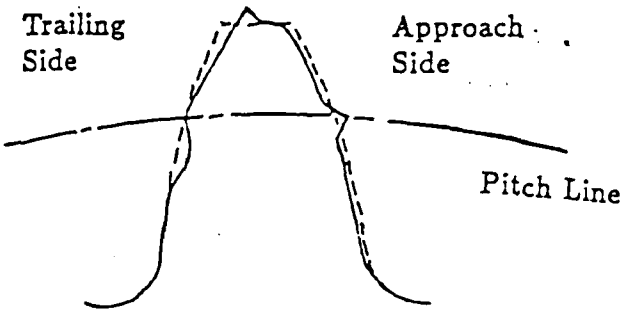

Figure 4.25 EXPECTED DEFORMATIONS IN A GEAR TOOTH DUE TO ROLLING

The preceding examples demonstrate the successful application of NOFEAP to modelling deformations on both sides of a gear tooth as might be expected in ausrolling. The rolling process itself is most satisfactorily modelled in the program as shown in this chapter. This concludes the modelling of essential features of ausroiling. An approximate analysis of the ausrolling process can now be reliably performed using the non-linear finite element analysis program. Further improvements can be made and additional capabilities can be introduced in the program in future. Some of these efforts along with the concluding remarks are included in the next chapter.

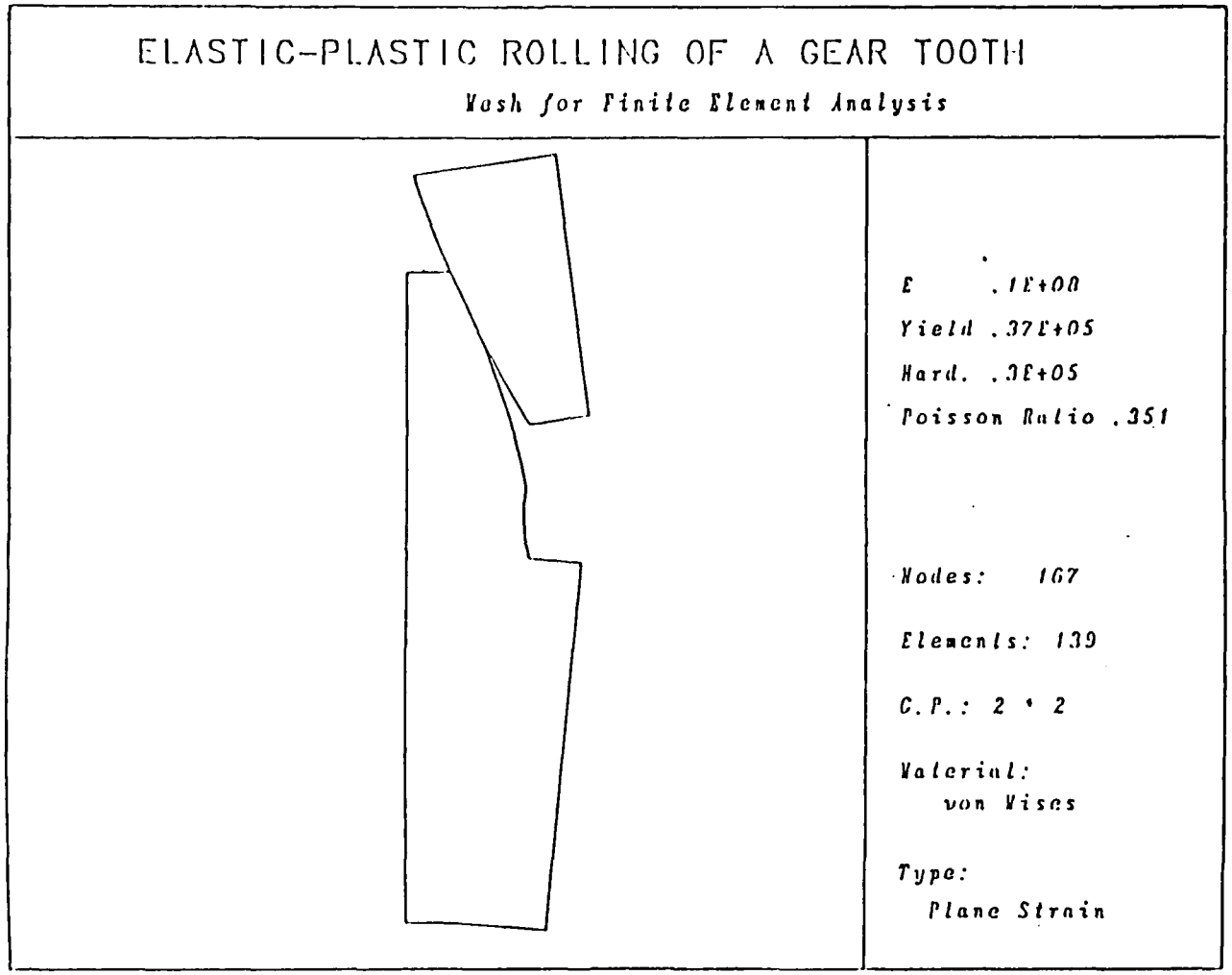

Figure 4.26 ELASTIC-PLASTIC ROLLING OF A GEAR TOOTH:
Surface Contours for Finite Element Analysis

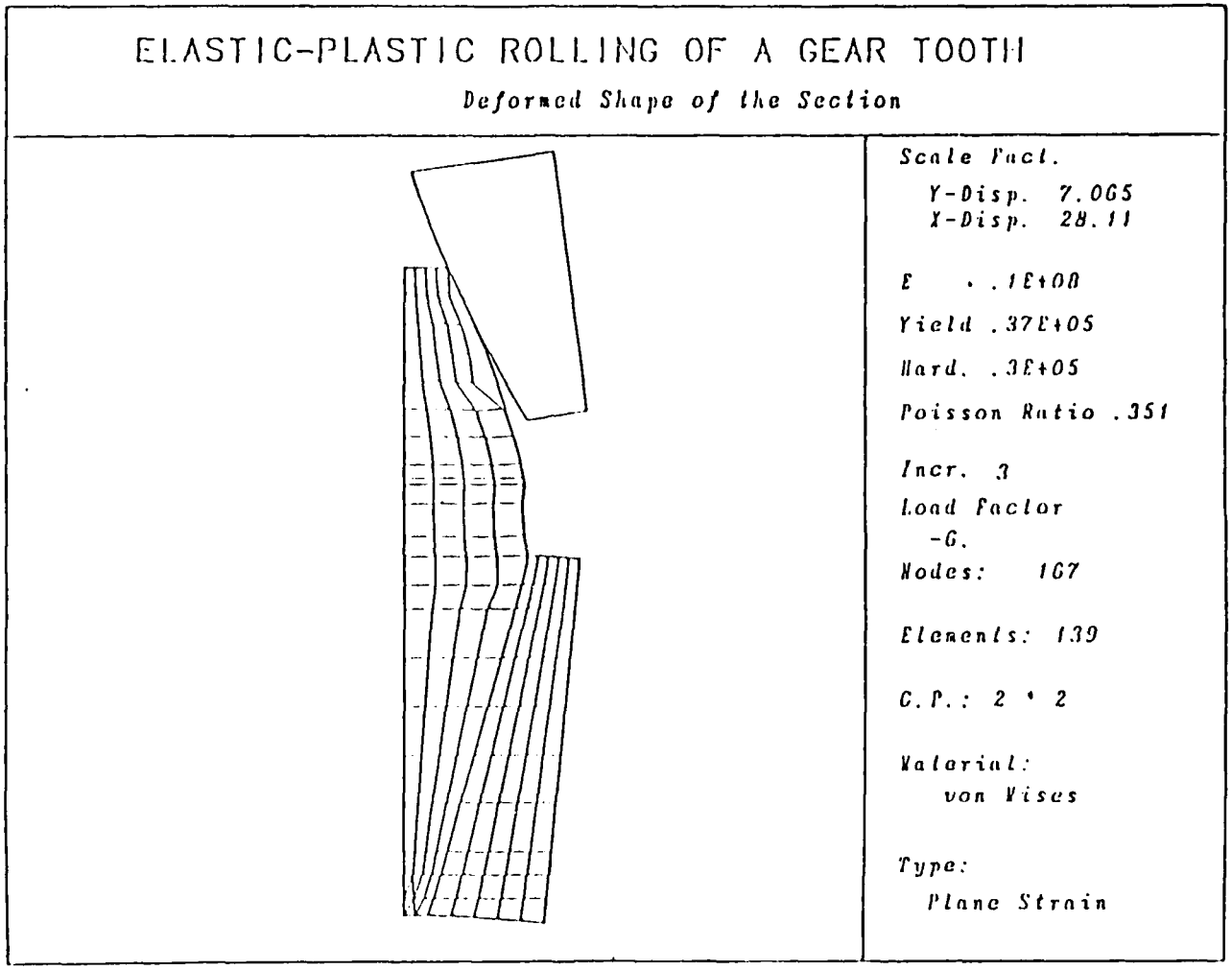

Figure 4.27 ELASTIC-PLASTIC ROLLING OF A GEAR TOOTH: Deformed Shape of the Section at -6°

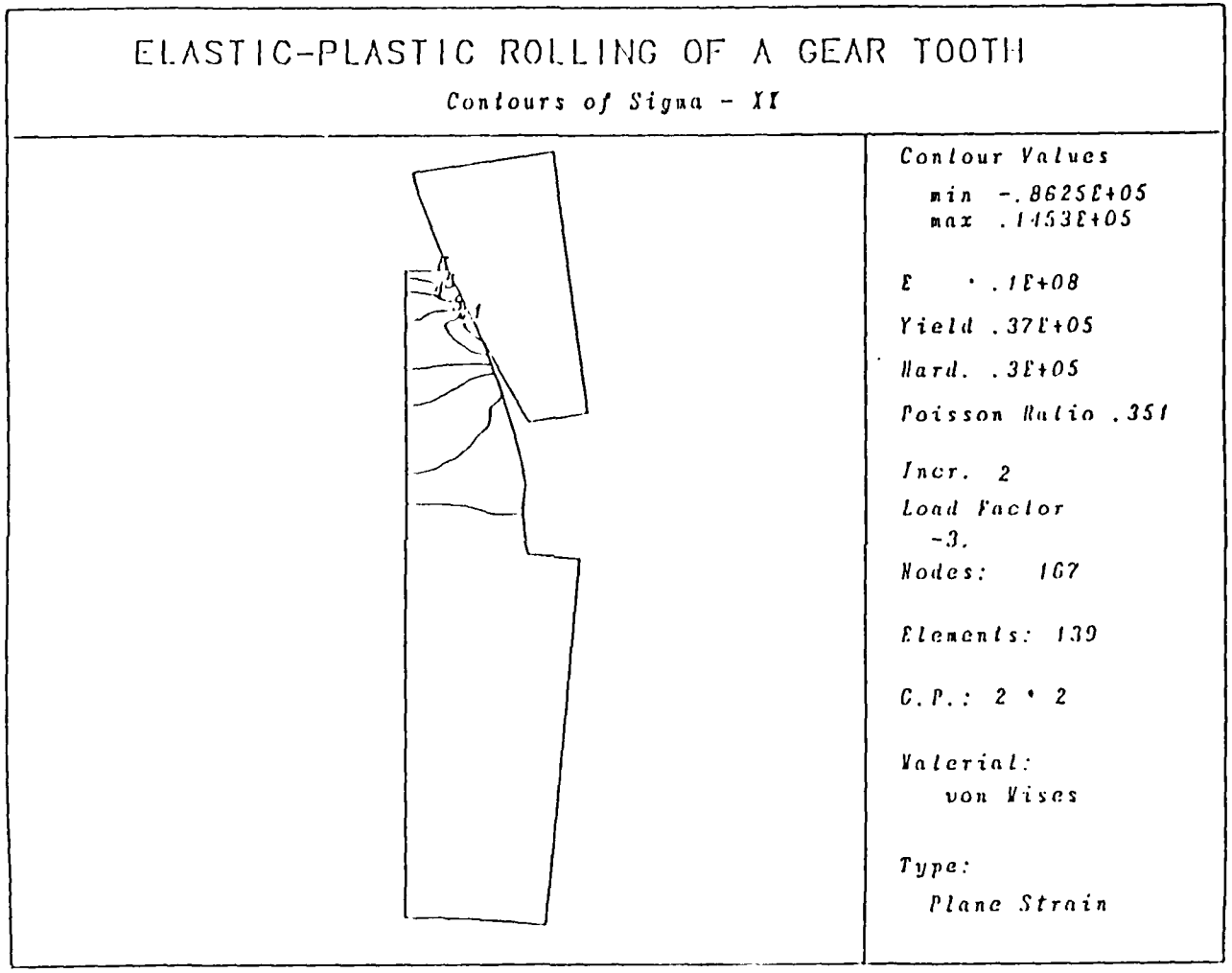

Figure 4.28 ELASTIC-PLASTIC ROLLING OF A GEAR TOOTH: Contours of Sigma-XX at -3°

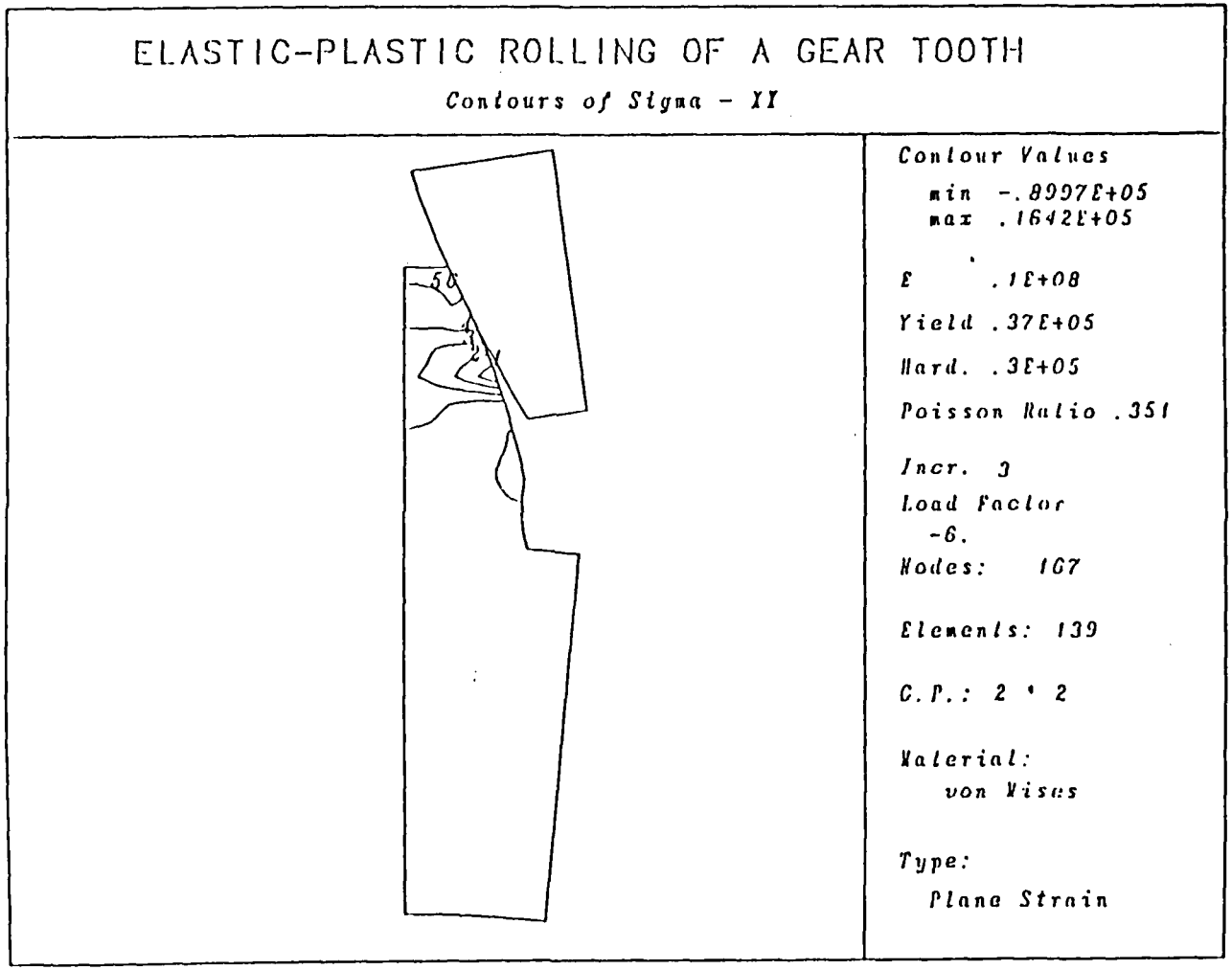

Figure 4.29 ELASTIC-PLASTIC ROLLING OF A GEAR TOOTH: Contours of Sigma-XX at -6°

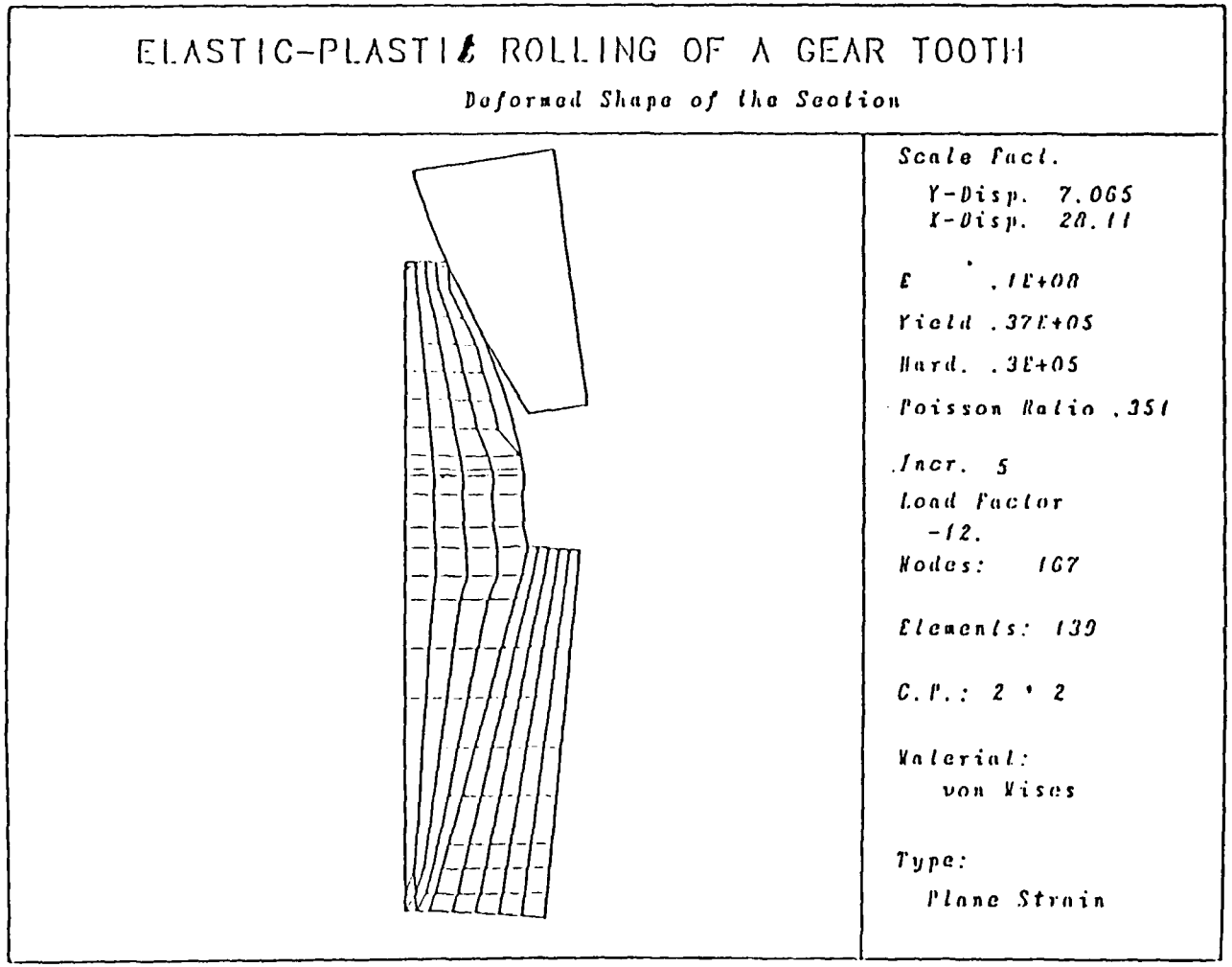

Figure 4.30 ELASTIC-PLASTIC ROLLING OF A GEAR TOOTH: Deformed Shape of the Section at -12°

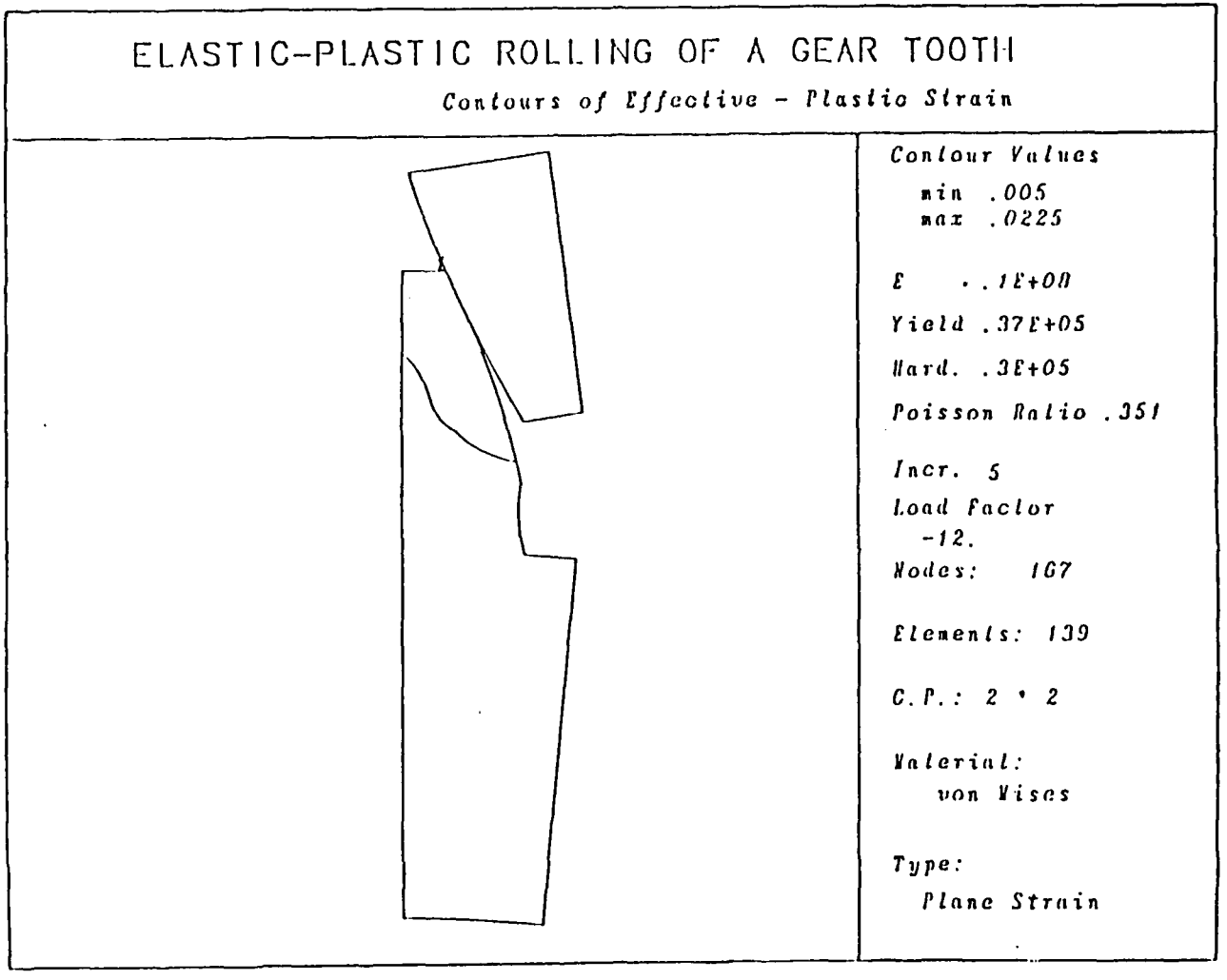

Figure 4.31 ELASTIC-PLASTIC ROLLING OF A GEAR TOOTH: Contours of Effective Plastic Strain at -12°

Chapter 5

CONCLUSIONS AND FUTURE WORK

The main objective of this thesis has been to implement the essential features of the ausrolling process in a computer program to enable approximate simulation of the deformations in a gear following ausrolling. This objective has been successfully achieved with the steps listed in the following concluding remarks.

5.1 Conclusions

1. A non-linear finite element analysis program, NOFEAP, has been developed with capabilities to model non-linear behavior due to elastic-plastic flow with work hardening, large displacements and strains, and frictional contact conditions.

2. Each of these implemented non-linear formulations has been satisfactorily verified by comparing them with existing analytical, numerical and experimental results.

3. A model of the rolling process has been implemented in the computer program NOFEAP.

4. Several rolling experiments have been conducted with aluminum 6061 disks and a round-faced carbon steel die, and a flat-faced tool steel die. The experiments have also been simulated using the NOFEAP program.

5. Deformation patterns obtained experimentally and numerically show excellent similarities. The results of the round-die experiments compare more agreeably with the simulated results than do the results of the flat-die experiments. This

has been attributed to the lateral flow in the specimens rolled with the flat die which violated the assumption of plane strain deformations.

6. The NOFEAP program can be used to model deformations in gear rolling as demonstrated by results of simulated runs on gear teeth.

5.2 Suggestions for Further Developments

As mentioned earlier, only some of the features of ausrolling have been implemented in the program NOFEAP in this research. There is scope for further development of NOFEAP in order to obtain a more accurate representation of ausrolling. Some of these directions are indicated next.

1. Modelling of temperature distributions in the gear and the effect of thermal stresses on the deformations.

2. Representation of the time-temperature-transformation curve of the material in the simulation. This would include changes in the material properties and their gradients as the deformations progresses.

3. Extension of the model to three dimensions to simulate the actions of the swaging and the shearing operations.

4. Miscellaneous improvements in the computation process to reduce the time taken to complete a simulation. This would range from increasing the efficiencies of some algorithms in the program to implementing the program on a supercomputer enabling effective utilization of the vector and parallel processing techniques on these machines.

5.3 Limitations of the Model

The numerical formulations implemented in NOFEAP are restrictive to some extent as pointed out next.

1. The elastic-plastic formulations assumes an isotropically expanding yield surface. For a more accurate analysis, kinematic or mixed hardening conditions may be introduced.

2. The use of additive elastic and plastic strain increments may be objected to by those using the multiplicative decomposition of the deformations gradient. However, the superiority of either theory over the other is yet to be proved. Hence the formulation in the program is considered to be satisfactory.

3. Since the contact conditions are defined at discrete nodes, some error is usually introduced due to relative lateral sliding of the nodal pair. Although these nodal pairs may be updated in NOFEAP at each step by connecting the nodes closest to one another, a separation equal to half the distance between adjacent nodes may still exist. Since these nodes are usually placed in close juxtaposition, this error has not been found to be significant.

REFERENCES

[1] Amateau, M.F., and Cellitti, R.A., Finishing of gears by ausforming, Proceedings of SME Gear Processing and Manufacturing Conference SME, Schaumberg, Illinois, Nov. 1986

[2] Marcal, P.V., and King, I.P., Elastic-plastic analysis of two-dimensional stress systems by the finite element method, Int. J. Mech. Sci., 9, 143-155, 1967

[3] Bathe, K.J., Finite Element Procedures in Engineering Analysis, Prentice-Hall, Englewood Cliffs, N.J., USA, 1982

[4] Chan, S.K., and Tuba, I.S., A finite element method for contact problems of solid bodies — part I, theory and validation, Int. J. Mech. Sci., 13, 615-625, 1971

[5] Owen, D.R.J., and Hinton, E., Finite Elements in Plasticity: Theory and Practice, Pineridge Press, Swansea, U.K., 1981

[6] Okamoto, N., and Nakazawa, M., Finite element incremental contact analysis with various frictional conditions, Int. J. Num. Meth. Eng., 14, 337-357, 1979

[7] Zienkiewicz, O.C., The Finite Element Method, McGraw-Hill, U.K., 1983

[8] Kher, S.N., NOFEAP — Non-linear finite element analysis program, Applied Research Laboratory Technical Memorandum, Number 86-215, State College, PA, Dec. 1986

[9] Mori, K., Osakada, K., and Oda, T., Simulation of plane-strain rolling by rigid-plastic finite element method, Int. J. Mech. Sci., 24, 519-527, 1982

[10] Bhargava, V., Hahn, G.T., and Rubin, C.A., An elastic-plastic finite element model of rolling contact, Part I, J. Appl. Mech., 84-WA/APM-42, 1985

[11] Bhargava, V., Hahn, G.T., and Rubin, C.A., An elastic-plastic finite element model of rolling contact, Part II, J. Appl. Mech., 84-WA/APM-43, 1985

[12] Lee, C.H., and Kobayashi, S., New solutions to rigid-plastic deformation problems using a matrix method, Trans. ASME, J. Eng. Ind., 95, 865-873, 1973

[13] Dung, N.L., and Mahrenholtz, O., Progress in the analysis of unsteady metal forming processes using the finite element method, Proc. Int. Conf. on Num. Meth. in Ind. Forming Processes, 481-490, Swansea, U.K., 1982

[14] Dung, N.L., Mahrenholtz, O., and Westerling, C., Finite element modelling of precise forming, ASME Metals Congress, 8305-008, 1983

[15] Chen, C.C., PLAFOM — A generalized finite element program for metal forming design and analysis, ASM Metals Congress, 8305-033, 1983

[16] Chen, C.C., and Kobayashi, S., Rigid-plastic finite element analysis of ring compression, Application of Numerical Methods to Forming Processes, 163-174, ASME, San Fransisco, 1978

[17] Oh, S.I., Finite element analysis of metal forming processes with arbitrarily shaped dies, Int. J. Mech. Sci., 24, 8, 479-493, 1982

[18] Oh, S.I., Park, J.J., Kobayashi, S., and Altan, T., Application of finite element modelling to simulate metal flow in forging a Titanium alloy engine disk, J. Eng. Ind., 105, 251-258, 1983

[19] Osakada, K., Nakamo, J., and Mori, K., Finite element method for rigid-plastic analysis of metal forming — formulation for finite strain, Int. J. Mech. Sci., 24, 459, 1982

[20] Oh, S.I., Rebelo, N., and Kobayashi, S., Finite element formulation for the analysis of plastic deformation of rate sensitive materials in metal forming, 273-291, Metal Forming Plasticity, IUTAM symposium, Tutzing, Germany 1978

[21] Wifi, A.S., An incremental complete solution of the stretch-forming and deep drawing of a circular blank using a hemispherical punch, Int. J. Mech. Sci., 18, 23-31, 1976

[22] Yamada, Y., Wifi, A.S., and Hirakawa, T., Analysis of large deformation and stresses in metal forming processes by the finite element method, Metal Forming Plasticity, 158-176, IUTAM symposium, Germany 1978

[23] Yamada, Y., and Hirakawa, H., Large deformation and instability analysis in metal forming process, Appl. Num. Meth. to Forming Processes, 27-38, ASME, San Francisco, 1978

[24] Bõer, C.R., Gudmundson, P., and Rebelo, N., Comparison of elasto-plastic FEM, rigid-plastic FEM and experiments for cylinder upsetting, Proc. Int. Conf. on Num. Meth. in Ind. Forming Processes, 217-226, Swansea, U.K., 1982

[25] Nagtegaal, J.C., Parks, D.M., and, Rice J.R., On numerically accurate finite element solutions in the fully plastic range, Comp. Meth. Appl. Mech. Eng., 4, 153-177, 1974

[26] Kikuchi, N., Remarks on 4CST-elements for incompressible materials, Comp. Meth. Appl. Mech. Eng., 37, 109-123, 1983

[27] Hartley, P., Sturgess, C.E.N., and Rowe, G.W., Friction in finite element analysis of metal forming processes, Int. J. Mech. Sci., 21, 301-311, 1979

[28] Kikuchi, N., and Cheng, J-H., Finite element analysis of large deformation problems with unilateral contact and friction, Comp. Meth. for Non-linear Solids and Structural Mechanics, AMD, 54, 121-132, 1983

[29] Fredriksson, B., Finite element solution of surface non-linearities in structural mechanics with special emphasis to contact and fracture mechanics problems, Comp. & Struct., 6, 281-289, 1976

[30] Wertheimer, T.B., Thermal mechanically coupled analysis in metal forming processes, Proc. Int. Conf. on Num. Meth. in Ind. Forming Processes, 425-434, Swansea, U.K., 1982

[31] Cheng, J-H., Finite element simulations of metal forming processes by large deformation thermo-elastic-plastic formulations with grid adaptive and mesh rezoning method, Ph.D. Dissertation, Univ. of Michigan, Ann Arbor, 1985

[32] Lee, E.H., Elastic-plastic deformation at finite strains, J. Appl. Mech., 36, 1-6, 1969

[33] Marcal, P.V., Finite element analysis of combined problems of non-linear material and geometric behavior, Proc. ASME Joint Comp. Conf. on Comp. Approach to Appl. Mech., 133-149, Chicago, 1969

[34] Kleiber, M., Kinematics of deformation processes in materials subjected to finite strain elastic-plastic strains, Int. J. Eng. Sci., 13, 513-525, 1975

[35] Kleiber, M., A note on finite strain theory of elasto-plasticity, Acta Mechanica, 50, 291-297, 1984

[36] Hibbit, H.D., Marcal, P.V., and Rice, J.R., A finite element formulation for problems of large strain and large displacement, Int. J. Sol. Struct., 6, 1069-1086, 1970

[37] Bathe, K.J., Ramm, E., and Wilson, E.L., Finite element formulations for large displacements and large strain analysis, UCSESM, 73-14, Univ. of California, Berkeley, Sept. 1973

[38] McMeeking, R.M., and Rice, J.R., Finite elemtent formulations for problems of large elastic-plastic deformations, Int. J. Sol. Str., 11, 601-616, 1975

[39] Yamada, Y., Hirakawa, T., and Wifi, A.S., Analysis of large deformation and bifurcation in plasticity problems by the finite element method, Finite Elements in Non-linear Mechanics, 393-412, Tapir Publ., 1978

[40] Washizu, K., Variational Methods in Elasticity and Plasticity, Pergamon Press, Oxford, U.K., 1968

[41] Gallagher, R.H., Padlog, J., and Bijlaard, P.P., Stress analysis of heated complex shapes, ARS Journal, 700-707, May 1962

[42] Pope, G., A descrete element method for analysis of plane elastic-plastic stress problems, Royal Aeronautical Establishment, TR 65028, 1965

[43] Marcal, P.V., Finite element analysis with material non-linearities: theory and practice, Recent Advances in Matrix Methods of Structural Analysis and Design, 257-282, Ed. Gallagher, Yamada and Oden, Univ. of Alabama Press, University, Alabama, 1971

[44] Yamada, Y., Recent developments in matrix displacement method for elastic-plastic problems in Japan, Recent Advances in Matrix Methods of Structural Analysis and Design, 283-316, Ed. Gallagher, Yamada and Oden, Univ. of Alabama Press, University, Alabama, 1971

[45] Yamada, Y., and Yosimura, N., Plastic stress-strain matrix and its application for the solution of elastic-plastic problems by the finite element method, Int. J. Mech. Sci., 9, 143-155, 1967

[46] Zienkiewicz, O.C., Valliappan, S., and King, I.P., Elasto-plastic solutions of engineering problems, "initial stress" finite element approach, Int. J. Num. Meth. Eng., 1, 75-100, 1969

[47] Nayak, G.C., and Zienkiewicz, O.C., Elasto-plastic stress analysis, a generalization for various constitutive relations including strain softening, Int. J. Num. Meth. Eng., 3, 113-134, 1972

[48] Nayak, G.C., and Zienkiewicz, O.C., Note on the "ALPHA"-constant stiffness method for the analysis of non-linear problems, Int. J. Num. Meth. Eng., 4, 579-582, 1972

[49] Hill, R., The Mathematical Theory of Plasticity, Oxford University Press, U.K., 1950

[50] Dogui, A., and Sidoroff, F., Kinematic hardening in large elastic-plastic strain, Eng. Fract. Mech., 21, 4, 685-695, 1985

[51] Axelsson, K., Finite element application of mixed and distortional plastic hardening, Finite Elements in Non-linear Mechanics, 191-209, Tapir Publ., 1978

[52] Axelsson, K., and Samuelsson, A., Finite element analysis of elastic-plastic materials displaying mixed hardening, Int. J. Num. Meth. Eng., 14, 211-225, 1979

[53] Lee, E.H., Some comments on elastic-plastic analysis, Int. J. Sol. Struct., 17, 859-872, 1981

[54] Lee, E.H., and McMeeking, R.M., Concerning elastic and plastic components of deformation, Int. J. Sol. Struct., 16, 715-721, 1980

[55] Hofmeister, L.D., Greenbaum, G.A., and Evensen, D.A., Large strain elasto-plastic finite element analysis, AIAA J., 9, 1248-1254, 1971

[56] Gadala, M.S., Dokainish, M.A., and Oravas, G. Ae., Formulation methods in geometric and material non-linearity problems, Int. J. Num. Meth. Eng., 20, 887-914, 1984

[57] Bathe, K.J., Ozdemir, H., and Wilson, E.L., Static and dynamic geometric and material non-linear analysis, UCSESM, 74-4, University of California, Berkeley, 1974

[58] Bathe, K.J., Ramm, E., and Wilson, E.L., Finite element formulation for large deformation dynamic analysis, Int. J. Num. Meth. Eng., 9, 353-386, 1975

[59] Bathe, K.J., and Ozdemir, H., Elastic-plastic large deformation static and dynamic analysis, Comp. & Struct., 6, 2, 81-92, 1976

[60] Osias, J.R., and Swedlow, J.L., Finite elasto-plastic deformation — I: theory and numerical examples, Int. J. Sol. Struct., 10, 321-339, 1974

[61] Liu, C., Hartley, P., Sturgess, C.E.N., and Rowe, G.W., Elastic-plastic finite element modelling of cold rolling of strip, Int. J. Eng. Sci., 27, 7/8, 531-541, 1985

[62] Neale, K.W., On the application of a variational principle for large displacement elastic-plastic problems, Variational Methods in the Mechanics of Solids, Proc. IUTAM Symposium at Northwestern Univ., Ill., 374-377, Ed. S. Nemat-Nasser, Pergamon Press., N.Y., 1980

[63] Haber, R.B., A mixed Eulerian-Lagrangian displacement model for large deformation analysis in solid mechanics, Comp. Meth. Appl. Mech. Eng., 43, 277-292, 1984

[64] Gadala, M.S., Oravas, G. Ae., and Dokainish, M.A., Geometric and material non-linearity problems "formulation aspects," Proc. First Int. Conf. on Numerical Methods for Non-linear Problems, 317-331, Swansea, U.K., 1980

[65] Malvern, L.E., Introduction to the Mechanics of a Continuous Medium, Prentice-Hall, Englewood Cliffs, N.J., 1969

[66] Signorini, A., Questioni di elastostatics linearizzate e semilinearizzata, Rend. di Matem. e Delle Sur. Appl., 18, 1959

[67] Ohte, S., Finite element analysis of elastic contact problems, Bulletin of JSME, 16, 95, 797-804, 1973

[68] Schäfer, H., A contribution to the solution of contact problems with the aid of bond elements, Comp. Meth. Appl. Mech. Eng., 6, 335-354, 1975

[69] Francavilla, A., and Zienkiewicz, O.C., A note on numerical computation of elastic contact problems, Int. J. Num. Meth. Eng., 9, 913-924, 1975

[70] Hughes, T., Taylor, R., Sackman, J., Curnier, A., and Kanoknukalchai, W., A finite element method for a class of contact-impact problems, Comp. Meth. Appl. Mech. Eng., 8, 249-276, 1976

[71] Gaertner, R., Investigation of plane elastic contact allowing for friction, Comp. & Struct., 7, 59-63, 1977

[72] Fredriksson, B., Rydholm, G., and Sjöblom, P., Variational inequalities in structural mechanics with emphasis on contact problems, Finite Elements in Non-linear Mechanics, 863-884, Tapir Publ., 1978

[73] Fredriksson, B., Experimental Determination of Frictional Properties in Araldite B Contacts, Report LiTH-IKP-R-061, Linköping Institute of Technology, Linköping, Sweden, 1975

[74] Wong, C.J., Application of non-linear finite element method to contact problems and paper handling problems, Comp. & Struct., 19, 3, 315-320, 1984

[75] Zeid, I., and Padovan, J., Finite element modelling of rolling contact, Comp. & Struct., 14, 163-170, 1981

[76] Padovan, J., and Zeid, J., On the development of travelling load finite elements, Comp. & Struct., 12, 77-83, 1980

[77] Salamon, N.J., Numerical solution of frictional contact, Final Project Report to NSF, Grant No. MAE-8112535, Dec 1984

[78] Hodge, P.G., and White, G.N., A quantitative comparison of flow and deformation theories of plasticity, J. Appl. Mech., 17, 180-184, 1950

[79] Holden, J.T., On the finite deflections of thin beams, Int. J. Sol. Struct., 8, 1051-1055, 1972

[80] Nagtegaal, J.C., and De Jong, J.E., Some computational aspects of elastic-plastic large strain analysis, Int. J. Num. Meth. Eng., 17, 15-41, 1981

[81] Timoshenko, S., and Goodier, J.N., Theory of Elasticity, McGraw-Hill, N.Y., 1970

[82] Boresi, A.P., and Sidebottom, O.M., Advanced Mechanics of Materials, John Wiley & Sons, N.Y., 1985

Appendix A

LOAD FACTORS IN CONTACT PROBLEM SOLUTION

Assuming the notations in section 2.3.2, the load factors for transitions from one contact state to another are given here. If the contact status of an element does not change, the load factor, α, is equal to one.

1. Open to Sticking Contact:

$$\alpha = \alpha_1 = \frac{Initial \quad Gap \quad (\delta_n)}{Rel. \quad Normal \quad Disp. \quad Inc. \quad (l_n)} \qquad (A-1)$$

2. Open to Sliding Contact: This transition is only permitted if the coefficient of friction is zero, and if there is not relative tangential sliding between the bodies during the load increment. If these conditions are met, the load factor is given by (A-1).

3. Sticking to Open contact: This transition requires special attention. Both Okamoto [6] and Salamon [77] have defined the load factor as

$$\alpha = \alpha_2 = -\frac{R_n}{\Delta R_n} \qquad (A-2)$$

However, for initially sticking contact, the frictional force increment is independent of the normal increment, so that even though using (A-2) for load factor assures that the total normal force given by

$$R_n^{'} = R_n + \alpha \Delta R_n \qquad (A-3)$$

is zero, the total frictional force which is

$$R_t^{'} = R_t + \alpha \Delta R_t \qquad (A-4)$$

may not be zero for certain problems, resulting in a non-zero traction at a free surface. Such a situtation has been encountered in this research. To avoid this problem, further check is essential as given next.

$$s_1 = Signum(R_t + \Delta R_t) \qquad (A-5)$$

$$\alpha_3 = s_1 \frac{(\mu R_n - s_1 R_t)}{(\Delta R_t - s_1 \mu \Delta R_n)} \qquad (A-6)$$

Then $\alpha = \alpha_3$, if α_3 is smaller than α_2, and the new contact status is set to "slip." If this condition is not satisfied, an error message is issued and further computations are terminated.

4. Sticking to Sliding Contact: Letting $s = Signum(R_t + \Delta R_t)$,

$$\alpha = \alpha_4 = s \frac{(\mu R_n - s R_t)}{(\Delta R_t - s \mu \Delta R_n)} \qquad (A-7)$$

All the cases listed by Okamoto [6] and Salamon [77] can be reduced to this simple expression.

5. Sliding to Open Contact: Since the frictional force is a dependent variable, a tractionless free surface is obtained after releasing the contact. The load factor is given by equation (A-2).

6. Sliding to Sticking Contact: The load factor is set to zero [77].

Appendix B

INPUT DATA FILE FOR SIMULATION OF DISK-ROLLING

The following data file has been used to simulate the aluminum 6061 disk-rolling experiments using the non-linear finite element analysis program NOFEAP. The *non-essential entries* (comments) in the file have been printed in lower case characters while all the required commands are in upper case letters. Detailed explanation of each of the following commands can be obtained from the NOFEAP users' manual [8].

```
NOFE ELASTIC-PLASTIC ROLLING OF A DISK\
     2
   144     96     12      2      5      1      2      3      0      2      2
   129      0      0      0
     *      *      *      *      *      *      *      *      *      *      *
  npoi   nele   nvfi   ntyp   nnod   nmat   ncri   nstr   ntil   ndof   ndim
ELEMent listing
     1      1      1      2     14     13
     2      1      2      3     15     14
     3      1      3      4     16     15
     4      1      4      5     17     16
     5      1      5      6     18     17
     6      1      6      7     19     18
     7      1      7      8     20     19
     8      1      8      9     21     20
     9      1      9     10     22     21
    10      1     10     11     23     22
    11      1     11     12     24     23
    12      1     12      1     13     24
    13      1     27     25     13     14     26
    14      1     29     27     14     15     28
    15      1     31     29     15     16     30
    16      1     33     31     16     17     32
    17      1     35     33     17     18     34
    18      1     37     35     18     19     36
    19      1     39     37     19     20     38
    20      1     41     39     20     21     40
    21      1     43     41     21     22     42
```

22	1	45	43	22	23	44
23	1	47	45	23	24	46
24	1	25	47	24	13	48
25	1	50	49	25	26	97
26	1	51	50	26	27	98
27	1	52	51	27	28	99
28	1	53	52	28	29	100
29	1	54	53	29	30	101
30	1	55	54	30	31	102
31	1	56	55	31	32	103
32	1	57	56	32	33	104
33	1	58	57	33	34	105
34	1	59	58	34	35	106
35	1	60	59	35	36	107
36	1	61	60	36	37	108
37	1	62	61	37	38	109
38	1	63	62	38	39	110
39	1	64	63	39	40	111
40	1	65	64	40	41	112
41	1	66	65	41	42	113
42	1	67	66	42	43	114
43	1	68	67	43	44	115
44	1	69	68	44	45	116
45	1	70	69	45	46	117
46	1	71	70	46	47	118
47	1	72	71	47	48	119
48	1	49	72	48	25	120
49	1	49	97	121	73	
50	1	97	50	74	121	
51	1	50	98	122	74	
52	1	98	51	75	122	
53	1	51	99	123	75	
54	1	99	52	76	123	
55	1	52	100	124	76	
56	1	100	53	77	124	
57	1	53	101	125	77	
58	1	101	54	78	125	
59	1	54	102	126	78	
60	1	102	55	79	126	
61	1	55	103	127	79	
62	1	103	56	80	127	
63	1	56	104	128	80	
64	1	104	57	81	128	
65	1	57	105	129	81	
66	1	105	58	82	129	
67	1	58	106	130	82	

68	1	106	59	83	130
69	1	59	107	131	83
70	1	107	60	84	131
71	1	60	108	132	84
72	1	108	61	85	132
73	1	61	109	133	85
74	1	109	62	86	133
75	1	62	110	134	86
76	1	110	63	87	134
77	1	63	111	135	87
78	1	111	64	88	135
79	1	64	112	136	88
80	1	112	65	89	136
81	1	65	113	137	89
82	1	113	66	90	137
83	1	66	114	138	90
84	1	114	67	91	138
85	1	67	115	139	91
86	1	115	68	92	139
87	1	68	116	140	92
88	1	116	69	93	140
89	1	69	117	141	93
90	1	117	70	94	141
91	1	70	118	142	94
92	1	118	71	95	142
93	1	71	119	143	95
94	1	119	72	96	143
95	1	72	120	144	96
96	1	120	49	73	144

*	*	*	*	*	*	*	*	*	*	*
ele	mat	n1	n2	n3	n4	n5	n6	n7	n8	n9

COORdinates of nodes

1	0.00000	0.70100
2	0.35050	0.60708
3	0.60708	0.35050
4	0.70100	0.00000
5	0.60708	-0.35050
6	0.35050	-0.60708
7	0.00000	-0.70100
8	-0.35050	-0.60708
9	-0.60708	-0.35050
10	-0.70100	0.00000
11	-0.60708	0.35050
12	-0.35050	0.60708
13	0.00000	0.95000

14	0.47500	0.82272	
15	0.82272	0.47500	
16	0.95000	0.00000	
17	0.82272	-0.47500	
18	0.47500	-0.82272	
19	0.00000	-0.95000	
20	-0.47500	-0.82272	
21	-0.82272	-0.47500	
22	-0.95000	0.00000	
23	-0.82272	0.47500	
24	-0.45700	0.82272	
25	0.00000	1.20000	
26	0.31058	1.15911	
27	0.60000	1.03923	
28	0.84853	0.84853	
29	1.03923	0.60000	
30	1.15911	0.31058	
31	1.20000	0.00000	
32	1.15911	-0.31058	
33	1.03923	-0.60000	
34	0.84853	-0.84853	
35	0.60000	-1.03923	
36	0.31058	-1.15911	
37	0.00000	-1.20000	
38	-0.31058	-1.15911	
39	-0.60000	-1.03923	
40	-0.84853	-0.84853	
41	-1.03923	-0.60000	
42	-1.15911	-0.31058	
43	-1.20000	0.00000	
44	-1.15911	0.31058	
45	-1.03923	0.60000	
46	-0.84853	0.84853	
47	-0.60000	1.03923	
48	-0.31058	1.15911	
49	0.00000	1.45000	0.00
50	0.37529	1.40059	15.00
51	0.72500	1.25574	30.00
52	1.02530	1.02530	45.00
53	1.25574	0.72500	60.00
54	1.40059	0.37529	75.00
55	1.45000	0.00000	90.00
56	1.40059	-0.37529	105.00
57	1.25574	-0.72500	120.000
58	1.02530	-1.02530	135.000
59	0.72500	-1.25574	150.000

60	0.37529	-1.40059	165.000
61	0.00000	-1.45000	180.000
62	-0.37529	-1.40059	195.000
63	-0.72500	-1.25574	210.000
64	-1.02530	-1.02530	225.000
65	-1.25574	-0.72500	240.000
66	-1.40059	-0.37529	255.000
67	-1.45000	0.00000	270.000
68	-1.40059	0.37529	285.000
69	-1.25574	0.72500	300.000
70	-1.02530	1.02530	315.000
71	-0.72500	1.25574	330.000
72	-0.37529	1.40059	345.000
73	0.00000	1.71450	0.000
74	0.44375	1.65608	15.000
75	0.85725	1.48480	30.000
76	1.21233	1.21233	45.000
77	1.48480	0.85725	60.000
78	1.65608	0.44375	75.000
79	1.71450	0.00000	90.000
80	1.65608	-0.44375	105.000
81	1.48480	-0.85725	120.000
82	1.21233	-1.21233	135.000
83	0.85725	-1.48480	150.000
84	0.44375	-1.65608	165.000
85	0.00000	-1.71450	180.000
86	-0.44375	-1.65608	195.000
87	-0.85725	-1.48480	210.000
88	-1.21233	-1.21233	225.000
89	-1.48480	-0.85725	240.000
90	-1.65608	-0.44375	255.000
91	-1.71450	0.00000	270.000
92	-1.65608	0.44375	285.000
93	-1.48480	0.85725	300.000
94	-1.21233	1.21233	315.000
95	-0.85725	1.48480	330.000
96	-0.44375	1.65608	345.000
97	0.18926	1.43760	7.500
98	0.55489	1.33963	22.500
99	0.88270	1.15036	37.500
100	1.15036	0.88270	52.500
101	1.33963	0.55489	67.500
102	1.43760	0.18926	82.500
103	1.43760	-0.18926	97.500
104	1.33963	-0.55489	112.500
105	1.15036	-0.88270	127.500

106	0.88270	-1.15036	142.500
107	0.55489	-1.33963	157.500
108	0.18926	-1.43760	172.500
109	-0.18926	-1.43760	187.500
110	-0.55489	-1.33963	202.500
111	-0.88270	-1.15036	217.500
112	-1.15036	-0.88270	232.500
113	-1.33963	-0.55489	247.500
114	-1.43760	-0.18926	262.500
115	-1.43760	0.18926	277.500
116	-1.33963	0.55489	292.500
117	-1.15036	0.88270	307.500
118	-0.88270	1.15036	322.500
119	-0.55489	1.33963	337.500
120	-0.18926	1.43760	352.500
121	0.22379	1.69983	7.500
122	0.65611	1.58399	22.500
123	1.04372	1.36020	37.500
124	1.36020	1.04372	52.500
125	1.58399	0.65611	67.500
126	1.69983	0.22379	82.500
127	1.69983	-0.22379	97.500
128	1.58399	-0.65611	112.500
129	1.36020	-1.04372	127.500
130	1.04372	-1.36020	142.500
131	0.65611	-1.58399	157.500
132	0.22379	-1.69983	172.500
133	-0.22379	-1.69983	187.500
134	-0.65611	-1.58399	202.500
135	-1.04372	-1.36020	217.500
136	-1.36020	-1.04372	232.500
137	-1.58399	-0.65611	247.500
138	-1.69983	-0.22379	262.500
139	-1.69983	0.22379	277.500
140	-1.58399	0.65611	292.500
141	-1.36020	1.04372	307.500
142	-1.04372	1.36020	322.500
143	-0.65611	1.58399	337.500
144	-0.22379	1.69983	352.500

n	⟵ x ⟶	⟵ y ⟶	comment

```
MATE
     1
  0.100E+08   0.330E+00                                  0.360E+05   0.353E+05
  0.100E+01   0.200E+01


  nmat*
              e              nu          thick          dense          yield          hard
       el typ              g. p.
BOUN
       1              11          0.00000        0.01500
       2              11          0.00000        0.01500
       3              11          0.00000        0.01500
       4              11          0.00000        0.01500
       5              11          0.00000        0.01500
       6              11          0.00000        0.01500
       7              11          0.00000        0.01500
       8              11          0.00000        0.01500
       9              11          0.00000        0.01500
      10              11          0.00000        0.01500
      11              11          0.00000        0.01500
      12              11          0.00000        0.01500

       n              xy          x - dis        y - dis
END
BODY=2
COORdinates of die
       1         0.00000         1.71450          0.000
       2         0.22424         1.71998          2.800
       3         0.44795         1.73641          5.600
       4         0.67059         1.76375          8.400
       5         0.89163         1.80193         11.200
       6         1.11054         1.85086         14.000
       7         1.32680         1.91042         16.800
       8         1.53989         1.98049         19.600
       9         1.74930         2.06087         22.400
      10         1.95454         2.15139         25.200
      11         2.15511         2.25183         28.000
      12         2.35053         2.36194         30.800
      13         2.54034         2.48148         33.600
      14         2.72409         2.61014         36.400
      15         2.90133         2.74762         39.200
      16         3.07164         2.89359         42.000
      17         3.23462         3.04772         44.800
      18         3.38988         3.20961         47.600
      19         3.53704         3.37891         50.400
```

20	3.67576	3.55518	53.200
21	3.80570	3.73802	56.000
22	3.92655	3.92700	58.800
23	4.03803	4.12165	61.600
24	4.13986	4.32151	64.400
25	4.23181	4.52611	67.200
26	4.31366	4.73496	70.000
27	4.38521	4.94755	72.800
28	4.44628	5.16339	75.600
29	4.49674	5.38195	78.400
30	4.53646	5.60272	81.200
31	4.56535	5.82516	84.000
32	4.58334	6.04875	86.800
33	4.59050	6.30500	90.000
34	4.58502	6.52924	92.800
35	4.56859	6.75295	95.600
36	4.54125	6.97559	98.400
37	4.50307	7.19663	101.200
38	4.45414	7.41554	104.000
39	4.39458	7.63180	106.800
40	4.32451	7.84489	109.600
41	4.24413	8.05430	112.400
42	4.15361	8.25954	115.200
43	4.05317	8.46011	118.000
44	3.94306	8.65553	120.800
45	3.82352	8.84534	123.600
46	3.69486	9.02909	126.400
47	3.55738	9.20633	129.200
48	3.41141	9.37664	132.000
49	3.25728	9.53962	134.800
50	3.09539	9.69488	137.600
51	2.92609	9.84204	140.400
52	2.74982	9.98076	143.200
53	2.56698	10.11070	146.000
54	2.37800	10.23155	148.800
55	2.18335	10.34303	151.600
56	1.98349	10.44486	154.400
57	1.77889	10.53681	157.200
58	1.57004	10.61866	160.000
59	1.35745	10.69021	162.800
60	1.14161	10.75128	165.600
61	0.92305	10.80174	168.400
62	0.70228	10.84146	171.200
63	0.47984	10.87035	174.000
64	0.25625	10.88834	176.800
65	0.00000	10.89550	180.000

66	-0.22424	10.89002	182.800
67	-0.44795	10.87359	185.600
68	-0.67059	10.84625	188.400
69	-0.89163	10.80807	191.200
70	-1.11054	10.75914	194.000
71	-1.32680	10.69958	196.800
72	-1.53989	10.62951	199.600
73	-1.74930	10.54913	202.400
74	-1.95454	10.45861	205.200
75	-2.15511	10.35817	208.000
76	-2.35053	10.24806	210.800
77	-2.54034	10.12852	213.600
78	-2.72409	9.99986	216.400
79	-2.90133	9.86238	219.200
80	-3.07164	9.71641	222.000
81	-3.23462	9.56228	224.800
82	-3.38988	9.40039	227.600
83	-3.53704	9.23109	230.400
84	-3.67576	9.05482	233.200
85	-3.80570	8.87198	236.000
86	-3.92655	8.68300	238.800
87	-4.03803	8.48835	241.600
88	-4.13986	8.28849	244.400
89	-4.23181	8.08389	247.200
90	-4.31366	7.87504	250.000
91	-4.38521	7.66245	252.800
92	-4.44628	7.44661	255.600
93	-4.49674	7.22805	258.400
94	-4.53646	7.00728	261.200
95	-4.56535	6.78484	264.000
96	-4.58334	6.56125	266.800
97	-4.59050	6.30500	270.000
98	-4.58502	6.08076	272.800
99	-4.56859	5.85705	275.600
100	-4.54125	5.63441	278.400
101	-4.50307	5.41337	281.200
102	-4.45414	5.19446	284.000
103	-4.39458	4.97820	286.800
104	-4.32451	4.76511	289.600
105	-4.24413	4.55570	292.400
106	-4.15361	4.35046	295.200
107	-4.05317	4.14989	298.000
108	-3.94306	3.95447	300.800
109	-3.82352	3.76466	303.600
110	-3.69486	3.58091	306.400
111	-3.55738	3.40367	309.200

112	-3.41141	3.23336	312.000
113	-3.25728	3.07038	314.800
114	-3.09539	2.91512	317.600
115	-2.92609	2.76796	320.400
116	-2.74982	2.62924	323.200
117	-2.56698	2.49930	326.000
118	-2.37800	2.37845	328.800
119	-2.18335	2.26697	331.600
120	-1.98349	2.16514	334.400
121	-1.77889	2.07319	337.200
122	-1.57004	1.99134	340.000
123	-1.35745	1.91979	342.800
124	-1.14161	1.85872	345.600
125	-0.92305	1.80826	348.400
126	-0.70228	1.76854	351.200
127	-0.47984	1.73965	354.000
128	-0.25625	1.72166	356.800
129	0.00000	6.30500	center

n	←– x –→	←– y –→	comment

END
CONT

27	65
*	*

number of nodes on contact surface of 'a' and 'b'
NODEs on contact surfaces of workpiece (a), and die (b)

133	85	132	84	131	83	130	82	129	81	! work
128	80	127	79	126	78	125	77	124	76	
123	75	122	74	121	73	144				
1	2	3	4	5	6	7	8	9	10	! die
11	12	13	14	15	16	17	18	19	20	
21	22	23	24	25	26	27	28	29	30	
31	32	33	34	35	36	37	38	39	40	
41	42	43	44	45	46	47	48	49	50	
51	52	53	54	55	56	57	58	59	60	
61	62	63	64	65	66	67	68	69	70	
71	72	73	74	75	76	77	78	79	80	
81	82	83	84	85	86	87	88	89	90	
91	92	93	94	95	96	97	98	99	100	
101	102	103	104	105	106	107	108	109	110	
111	112	113	114	115	116	117	118	119	120	
121	122	123	124	125	126	127	128			
*	*	*	*	*	*	*	*	*	*	

```
MISCellaneous data
NORM=0.250E+00
TANG=0.250E+00
FRIC=0.300000
SMAX=0.10E+14
CHAR=0.2500
END
ANGLe of normals on contact surface of disk
WORK:  1,27, .8250E+02,   1,  .7500E+01
END
PRIN
END
```

MACR				start macro instructions
DATA	TRAN			
FILE	STIF	1.00		open stiffness file
FILE	SOLV	1.00		open solution file
FILE	STAT	1.00		open static condensation file
FILE	NODE	1.00		open nodal file
TOL		1.00	1.00	tolerance value for convergence=1%
INCR		2.00		initial feed=(2.00)(0.0150)
LOOP	FEED	2.00		start feed
DATA	INCR			*input data for increment*
INCR		0.00		default to data incr value
SETL	ROLL	1.00	2.00	set "roll" to 1 when "feed" is 2
LOOP	ROLL	25.0		start rolling – one revolution
FILE	STIF	3.00		rewind stiffness file
SDSS		1.00	1.00	compute stiffnesses
LOOP	ITER	15.0		start iterations
FILE	STIF	3.00		rewind stiffness file
FILE	SOLV	3.00		rewind solution file
FILE	STAT	3.00		rewind static condensation file
STAC		15.0	25.0	reduce dof in system of eqns
ELEM		15.0	25.0	compute norm & tang gaps
comm	....			and generate contact elements
LOOP	CONT	10.0		start contact solution
CONT				generate contact stiffness & loads
USOL				unsymmetric system solution
COVC				convergence check of contact
NEXT	CONT			
BACS		15.0	25.0	back substitute into global system
FORM				compute stresses & equiv. forces
CONV				plasticity convergence check
TIME				update displacements

```
NEXT  ITER
REAC  CONT  1.00                output contact reactions
NODL        6.00                output nodal values
ROLL        -15.0               roll by -15.0 degrees
NEXT  ROLL
NODL        0.00                output final nodal values
NEXT  FEED
END
TRAN        0.00        0.0150
INCR        -1.00                           back off workpiece by 1 unit
ROLL  RAD   1.71450     4.59050             radii of workpiece & die
      NODE              129.0               center of die
      WORK  0.00        0.00                center of workpiece (x-y origin)
      END
INCR        +1.5                            back workpiece off by 1.5
STOP
```

VITA

Shirish N. Kher was born on July 25, 1960, in Indore, India. He received his bachelor's degree in Mechanical Engineering in August 1981 from Birla Institute of Technology and Science, Pilani, India. He was a graduate research assistant from August 1983 to June 1983 in the Mechanical and Aerospace Engineering Department at Case Western Reserve University, Cleveland, Ohio, where he earned his Master's Degree. He enrolled in the graduate program in Engineering Mechanics at the The Pennsylvania State University in August 1983 in pursuit of the Doctor of Philosophy degree. During his stay there, he taught various undergraduate courses and worked as a research assistant at the Applied Research Laboratory at the university.

END

DATE

FILMED

FEB.

1988